Thesis

On

EXPERIMENTAL INVESTIGATION OF MAGNETIC FIELD ASSISTED ELECTRIC DISCHARGE MACHINING PROCESS

Submitted in partial fulfillment of the requirement for the award of the degree of

Master of Engineering

IN

PRODUCTION & INDUSTRIAL ENGINEERING

Submitted By:

GEETA BHATT

Roll No.: 801182008

Under the Guidance of:

Dr. AJAY BATISH

Professor and Head
Mechanical Engineering Department
Thapar University, Patiala

ANIRBAN BHATTACHARYA

Assistant Professor
Mechanical Engineering Department
Thapar University, Patiala

DEPARTMENT OF MECHANICAL ENGINEERING

THAPAR UNIVERSITY

PATIALA-147004, INDIA

JULY - 2013

DECLARATION

I hereby declare that the thesis entitled "**Experimental Investigation of Magnetic field Assisted Electric Discharge Machining process**" is an authentic record of my study carried out as requirements for the award of the degree of **Master of Engineering** in **Production and Industrial Engineering** at **Thapar University, Patiala**, under the guidance of **Dr. Ajay Batish**, Professor and Head of department, Department of Mechanical Engineering, Thapar University, Patiala and **Anirban Bhattacharya**, Assistant Professor, Department of Mechanical Engineering, Thapar University during July 2012 to July 2013. The matter embodied in this report has not been submitted in part or full to any other university or institute for award of any degree.

Date: 15/07/2013

Geeta Bhatt

It is certified that the above statement made by the student is correct to best of my knowledge and belief.

(Dr. AJAY BATISH)
Professor and Head
Mechanical Engineering Department
Thapar University, Patiala-147004

(ANIRBAN BHATTACHARYA)
Assistant Professor
Mechanical Engineering Department
Thapar University, Patiala-147004

Countersigned By:

(Dr. AJAY BATISH)
Professor and Head
Mechanical Engineering Department
Thapar University, Patiala-147004

(Dr. S. K. MOHAPATRA)
Dean of Academic Affairs
Thapar University, Patiala-147004

ACKNOWLEDGEMENTS

I express my deep sense of gratitude and a very sincere thanks to my guide **Dr. Ajay Batish**, Professor and Head, Mechanical Engineering department, Thapar University, Patiala and **Anirban Bhattacharya**, Assistant Professor, Mechanical engineering department, Thapar University, Patiala for their indefatigable guidance and full support which helped me in the accomplishment of this experimental study. I am highly indebted to them for their painstaking efforts and invaluable suggestions during the period of work.

I am thankful to entire faculty and staff members of Mechanical Engineering Department for their direct and indirect cooperation during my thesis work.

I am also thankful to my friends who supported me and constantly encouraged me during the period of work.

At last but most important I am highly indebted to my dear parents for their love, support and trust.

Geeta Bhatt

ABSTRACT

Electrical discharge machining (EDM) is one of the most widely disseminated manufacturing techniques for generation of accurate and complex geometrical shapes on hard metallic components with high dimensional accuracy and good surface finish. Keeping in view different response characteristics, certain modifications in conventional EDM process are proposed and attempted. Mainly focussing on output response parameters like material removal rate (MRR), tool wear rate (TWR), surface roughness (SR), overcut (OC), microhardness (MH) and surface characteristics, a comparison study of magnetic field assisted EDM and magnetic field assisted powder mixed EDM (PMEDM) is performed. Results are analysed using Analysis of Variance (ANOVA) technique. The effect of different input process parameters like current, pulse on time, workpiece (die steels), tool electrodes and powders (at different concentration) under the effect of magnetic field (permanent bar and ring magnet) is studied on the output responses. Scanning Electron Microscope (SEM) and X-Ray Diffraction (XRD) analysis is used to study surface characteristics (phases and composition) and deposition of migrated material in pure or compound form to the machined surface.

ABBREVIATIONS

ANOVA	Analysis of Variance
MRR	Material Removal Rate
TWR	Tool Wear Rate
OC	Overcut
SR	Surface Roughness
MH	Micro-Hardness
EDM	Electric Discharge Machining
PMEDM	Powder mixed EDM
OA	Orthogonal Array
DOF	Degree of freedom
SEM	Scanning Electron Microscope
XRD	X-Ray Diffraction
S/N ratio	Signal to noise ratio
RC	Relaxation Circuit

TABLE OF CONTENTS

LIST OF FIGURES

LIST OF TABLES

CHAPTER 1
INTRODUCTION

1.1 PRODUCTION PROCESS

Production process is the process of converting raw material into the form of a final product (Figure 1.1). Mainly it is divided in three parts:

1) Raw material extraction
2) Transformation Processes
3) Final output

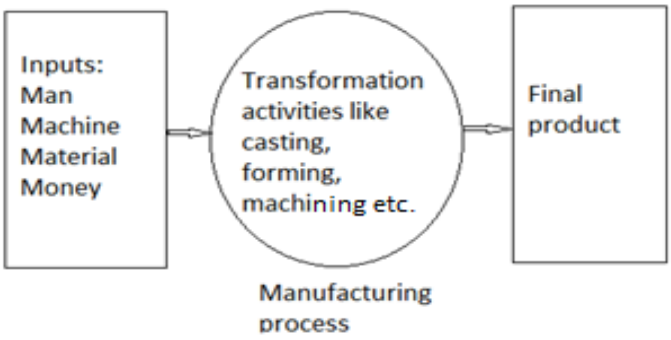

Figure 1.1: Production process

Raw material extraction: Mainly it deals with collecting input materials required for producing desired output. Generally these inputs are man, machine, material and money etc.

Transformation processes: Transformation processes are the main preliminary operations / techniques required for conversion of raw material into final product or some part of the final assembly. These operations are called manufacturing processes. Manufacturing operations are further divided into two main categories (Figure 1.2):

i) *Primary Processes*: The primary processes are those processes which provide basic shape and size to the material as per designer's requirement. Casting, forming, powder metallurgy are such processes to name a few.

ii) *Secondary processes*: Secondary processes are the processes that provide the final shape and size with tighter control on dimension, surface characteristics etc. Material removal processes are mainly the secondary manufacturing processes.

1.2 MATERIAL REMOVAL PROCESS

It is basically a shaping operation in which material is removed in a way to get the finished surface. Depending on the requirements, different material removal techniques are used for different operations. Material removal processes are mainly divided in two types:

i) **Conventional machining**: In conventional machining processes, tool is always in contact with work piece and material is removed in the form of chips. Chips may be continuous or dis-continuous depending on work piece material, like may be ductile or brittle material. Stresses on the work piece are very high in this case and hence it can't be used for machining fragile, delicate materials. As well in this case tool is required to be harder than that of the work piece and hence it can also be not used for very hard materials. Examples are Turning, Drilling, Boring, Shaping and Milling etc.

ii) **Non-conventional machining**: Keeping in view the drawbacks of conventional machining, further advanced techniques were discovered for machining very hard, tough, intricate shape, delicate and fragile materials. In case mechanical energy is not used for machining but different other forms of energies are used for material removal. In this case neither tool is in contact with work piece nor chips are produced but only debris are produced which are very small in size. Depending on different types of energies used for machining, non-conventional machining is divided into different types and classification is shown in flow diagram (Figure 1.2).

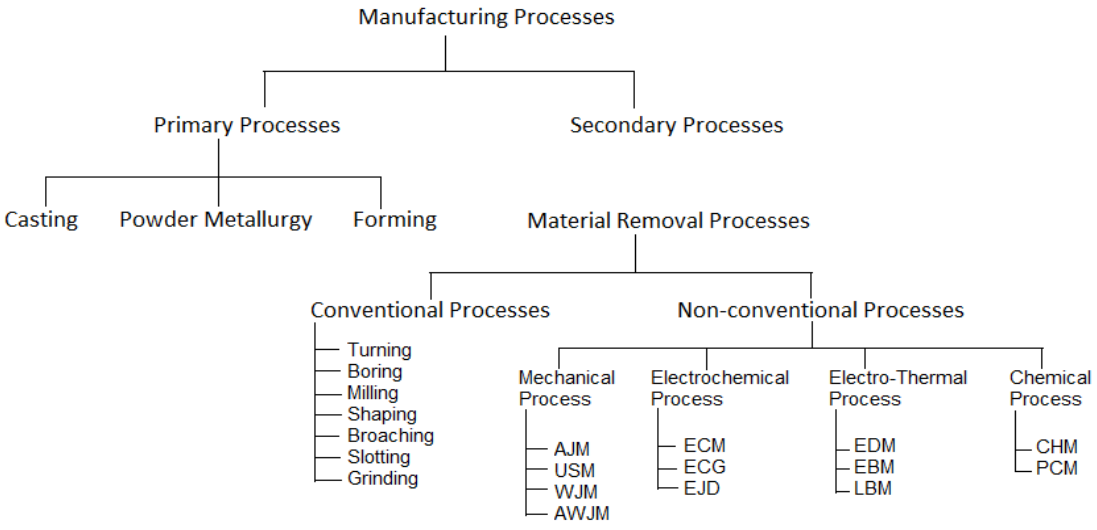

Figure 1.2: Classification of Manufacturing Process

1.3 NEED OF NON TRADITIONAL MACHINING

i) Conventional machining can't be used for drilling intricate shape blind hole. Hence non-traditional machining is required.

ii) Non-conventional machining is used for machining difficult to machine material as in conventional one tool has to be harder than work piece. Hence very hard materials can't be machined satisfactorily by conventional machining.

iii) Stresses are high on work piece in case of conventional machining, hence for low stress grinding, non-traditional machining is used.

iv) To make deep holes with small diameter.

v) For machining of composites.

vi) Where requirement of surface finish and tolerance is too high.

vii) Where residual stresses are undesirable.

viii) Where material is too delicate and not able to withstand high mechanical forces.

1.4 ELECTRICAL DISCHARGE MACHINING

Electrical Discharge Machining (EDM) as a process originated in 1770s when English scientist Joseph Priestly discovered the erosive effect of electrical discharges. The widely accepted principle of material removal in EDM is the conversion of electrical energy into thermal energy through a series of discrete electrical discharges occurring between the electrode and work piece immersed in a dielectric fluid [Tsai and Wang, 2001]. When the discharge takes place between two points of the anode and cathode, the intense heat generated near the zone melts and evaporates the material in sparking zone (Figure 1.3, a). It has been observed that if both the electrodes are made of same material, the electrode connected to positive terminal erodes at a faster rate. For this reason, the work piece is normally made the anode. The insulating effect of the dielectric is important in avoiding electrolysis of the electrodes during the EDM process. The material removal mechanism is shown (Figure 1.3, b).

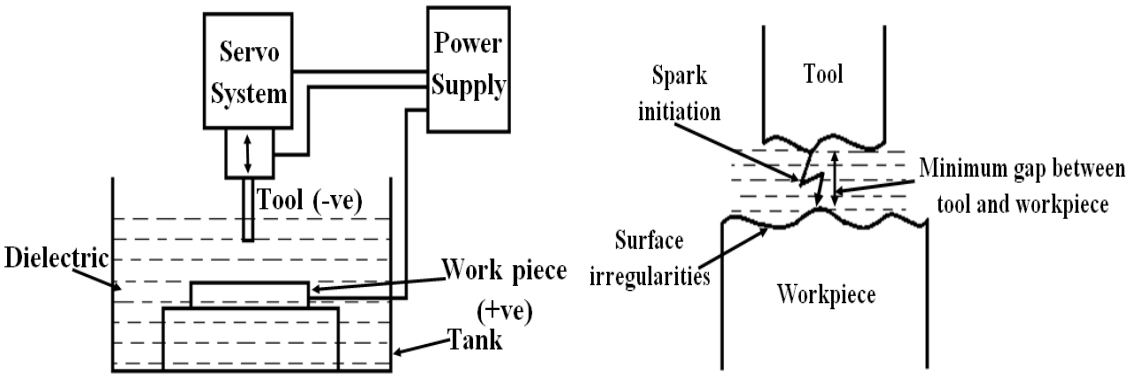

(a) (b)

Figure 1.3: EDM characteristics (a) EDM Set-up; (b) Spark Initiation in EDM

Erosion of metal from both electrodes takes place there. After each discharge, the capacitor is recharged from the DC source through a resistor, relaxation circuit (RC) (Figure 1.4), and the spark that follows is transferred to the next narrowest gap.

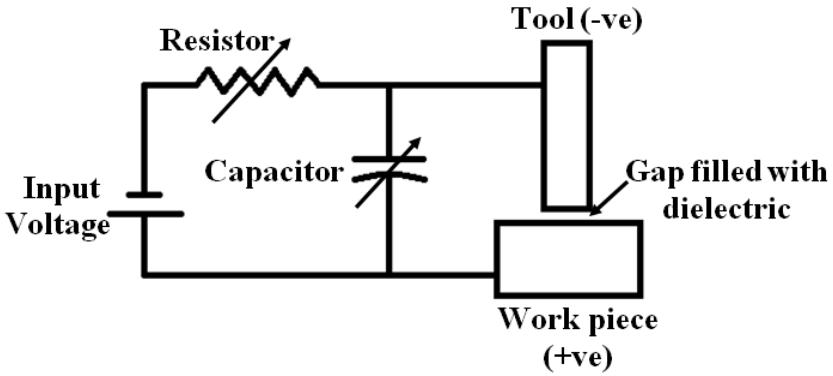

Figure 1.4: Relaxation circuit

Charging and discharging of the capacitors take place in a particular manner (Figure 1.5), which decides the duration for machining to take place. A certain time is utilised in charging the capacitor and after reaching the breakdown voltage, spark generates completing a cycle.

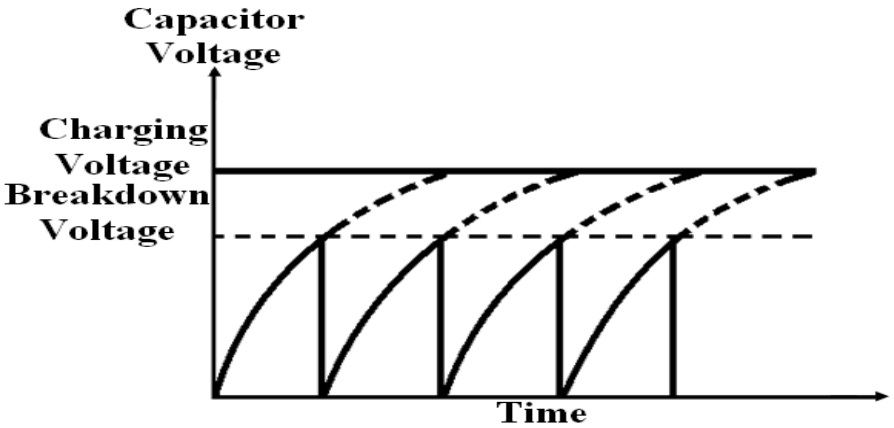

Figure 1.5: Variation of capacitor voltage with time in RC circuit

The cumulative effect of a succession of sparks spread over the entire work piece surface leads to its erosion, or machining to a shape which is approximately complementary to that the tool. Material removal rate (MRR) is the rate at which material removal takes place. It is given by weight of material removed divided by machining time. It is expressed in mm^3/sec and so. Similarly tool wear rate (TWR) is rate at which tool material is removed. It has the same unit and formula as MRR.

The dielectric serves to concentrate the discharge energy into a channel of very small cross-sectional area. It also cools the two electrodes, and flushes away the products of machining from the gap. The electrical resistance of the dielectric influences the discharge energy and the time of spark initiation [Kuneida et al., 2005]. As the work piece is spark-eroded, the tool has to be advanced through the dielectric towards it. A servo system, which compares the gap voltage with a reference value, is employed to ensure that the electrode moves at a proper rate to maintain the right spark gap, and to retract the electrode if short circuiting occurs.

Further to reduce peak current and increase in spark duration in a way to case lesser TWR, which was more in case of RC circuits due to high temperature generation, controlled pulse generator was introduced. Typical waveform is shown in Figure 1.6.

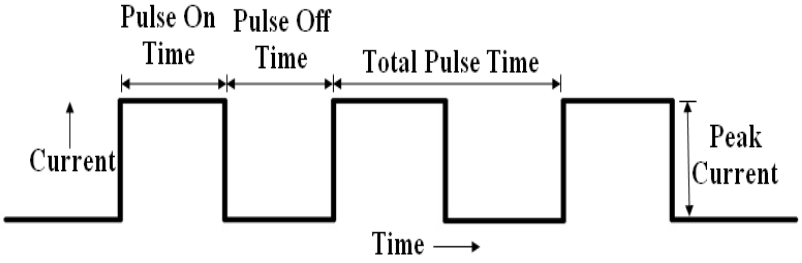

Figure 1.6: Pulse waveform of controlled pulse generator

1.5 PROCESS PARAMETERS

1.5.1 Discharge voltage

Discharge voltage in EDM is related to the spark gap and breakdown strength of the dielectric [Kansal et al., 2005b]. Before current can flow, the open gap voltage increases until it has created an ionization path through the dielectric. Once the current starts to flow, voltage drops and stabilizes at the working gap level. The preset voltage determines the width of the spark gap between the leading edge of the electrode and work piece. Higher voltage settings increase the gap, which improves the flushing conditions and helps to stabilize the cut. MRR, TWR and surface roughness (SR) increases by increasing open circuit voltage, because electric field strength increases.

1.5.2 Peak Current

During each on-time pulse, the current increases until it reaches a preset level, which is expressed as the peak current. In both die-sinking and wire-EDM applications, the maximum amount of amperage is governed by the surface area of the cut. Higher amperage is used in roughing operations and in cavities or details with large surface areas. Higher currents will improve MRR, but at the cost of surface finish and TWR.

1.5.3 Pulse configuration

Metal removal is directly proportional to the amount of energy applied during the on-time [Kansal et al., 2005a]. This energy is controlled by the peak amperage and the length of the on-time. Pulse on-time is commonly referred to as pulse duration and pulse off-time is called pulse interval. With longer pulse duration, more work piece material will be melted away. The resulting crater will be broader and deeper than a crater produced by shorter pulse duration. However, excessive pulse duration can be counter-productive. When the optimum pulse duration for each electrode-work material combination is exceeded, MRR starts to decrease. At the same time, pulse interval must be greater than the deionization time to prevent continued sparking at one point [Fuller, 1996].

The pulse shape is normally rectangular, but generators with other pulse shapes have also been developed. Using a generator which can produce trapezoidal pulses, Bruyn [1968] succeeded in reducing relative TWR to very low values.

1.5.4 Polarity

Polarity plays a very important role in case of EDM. Polarity can be positive (work piece positive, tool negative) or negative (work piece negative and tool positive) depending on the experimental requirement in different machining. Anode and cathode gets eroded by high temperature, but up to different extent depending upon the conditions. Electron will move to anode and positive ions will move towards cathode in EDM. When pulse duration is low, it is easy for electrons to get high speed because of its small quality and high accelerated speed. For positive ions, it is hard to reach the cathode because of their high quality and lower accelerated speed in shorter period of time. So when discharge duration is short (<= 30 μs), energy given by electrons is higher than positive ions and hence erosion is more on anode. In this case it is preferred to make anode as work piece and cathode as tool. When discharge duration is large enough (>= 300 μs), the positive ions are accelerated with high speed and impact is more on cathode. Hence in this case, where higher discharge time is there, negative polarity is preferred [Zhao, 2011].

1.5.5 Electrode gap

As the machining action takes place, the gap between tool and the work piece is increased. For machining process to go good a proper spark gap has to be maintained and this is done by using servomotor. Mostly electro-mechanical (DC or stepper motors) and electro-hydraulic systems are used, and are normally designed to respond to average gap voltage.

1.5.6 Type of Dielectric flushing

Basic characteristics required of a dielectric in EDM are high dielectric strength and quick recovery after breakdown, effective quenching and flushing ability. TWR and MRR are affected by the type of dielectric and the method of its flushing [Wong et al., 1995]. Most dielectric fluids are hydrocarbon compounds or water. Deionised water is used for wire-EDM and high precision die-sinking because of its low viscosity and carbon-free characteristics. The dielectric fluid is flushed through the spark gap to remove gaseous and solid debris during machining and to maintain the dielectric temperature well below its flash point.

1.6 MODIFICATIONS IN EDM

Non-traditional methods are mainly used only when the conventional processes can't work satisfactorily, although their material removal rate is comparatively very low than conventional ones. Hence for improvement in MRR and for achieving better surface finish, different techniques are being implemented on conventional EDM process. Some such techniques are:

i) Magnetic assisted EDM
ii) Dry or near dry EDM
iii) Powder mixed EDM
iv) EDM using ultrasonic vibrations

Here it is broadly discussed about magnetic assisted EDM and powder mixed EDM.

1.6.1 Magnetic force assisted EDM

It is well known that the electrical discharge machining (EDM) process possesses the potential to machine hard, tough, and strong and difficult-to-machine materials. In the EDM process, various sizes of discharge craters are there on the machined surface when the materials is removed, and the surface quality of the machined surface will deteriorate in accordance with the presence of craters. In addition, the machining debris suspended within

the dielectric fluid gets accumulated in the machining gap to induce the abnormal electrical discharge, so the stability of EDM progress is disturbed. Therefore, if the debris in the machining gap can be expelled effectively and completely, the EDM process appears to be a potential candidate to attain high efficiency, high precision, and high-quality surface. Kim et al. [1997] investigated the effect of magnetic field on the electrolytic finishing process concerning the migration of ions. It was reported that using magnetic field the ion migration path is changed from linear to cycloid motion. Results indicated that the motion path of electrolytic ion was changed by the magnetic field and the surface finishing effect was improved to obtain high-quality machined surface effectively and quickly. The contribution for expelling machining debris using the magnetic force assisted EDM is proved to attain a high efficiency and high quality of surface integrity to meet the demand of modern industrial applications. Machine set-up used in some of research works and its effect on debris removal are shown in Figure 1.7.

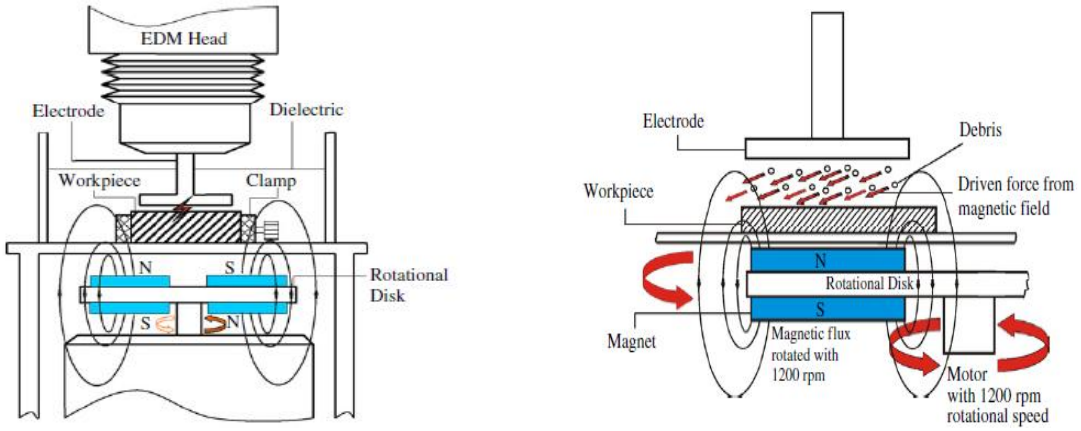

Figure 1.7: Magnetic force set-up and its effect on debris removal [Lin and Lee, 2008]

Brujin et al. [1978] investigated the effects of magnetic field in gap cleaning and indicated that the magnetic field can improve the gap cleaning process. It is clear that magnetic field effects on debris particles. It can be explained that, by applying magnetic field around the gap, debris are affected by the generated Lorentz force. This force can change the debris regular expulsion path to cycloid path. When the magnetic field is applied, the debris traverses longer distance to expel completely. Magnetic field also produces variation in ion path migration from direct motion to curve motion leading to expansion of plasma channel. It causes sparks to occur in the larger area rather than tool face area [Teimouri and Baseri, 2012c].

In EDM process, machining takes place by the action of melting and evaporation, some metal is removed in the form of debris (evaporated) and some metal which is just melted (not

evaporated like debris particles) again settles on the work piece and solidifies. This molten metal is not removed off the gap while machining in normal EDM process. This type of molten metal is some form of ferrofluid when work piece material is ferrous metal. Ferrofluids are suspensions of single domain magnetite particles with average diameters of approximately 10 nm stabilized by surfactants in carrier liquids. When magnetic field is applied, this ferrofluid is affected by magnetic force. In the presence of an external magnetic field, the single-domain colloidal magnetite particles suspended in the carrier liquid of a ferrofluid become magnetized. Figure 1.8 (a) shows randomly oriented north poles of the ferromagnetic particles in ferrofluid in the absence of an external magnetic field (top), and the alignment or polarization of these domains with the magnetic lines of flux emanating from the north pole of a permanent magnet (bottom). The polarization or magnetization of the fluid interacts with the external magnetic field to produce attractive forces on each particle [Oldenburg et al., 2000]. Hence magnetic field assisted EDM provides good results in terms of MRR and SR, by removing both debris as well as molten metal particles (especially in case of ferrous metals) which were not removed in conventional EDM process. Figure 1.8 (b) shows the effect on ferrofluid when kept under the influence of the magnetic field.

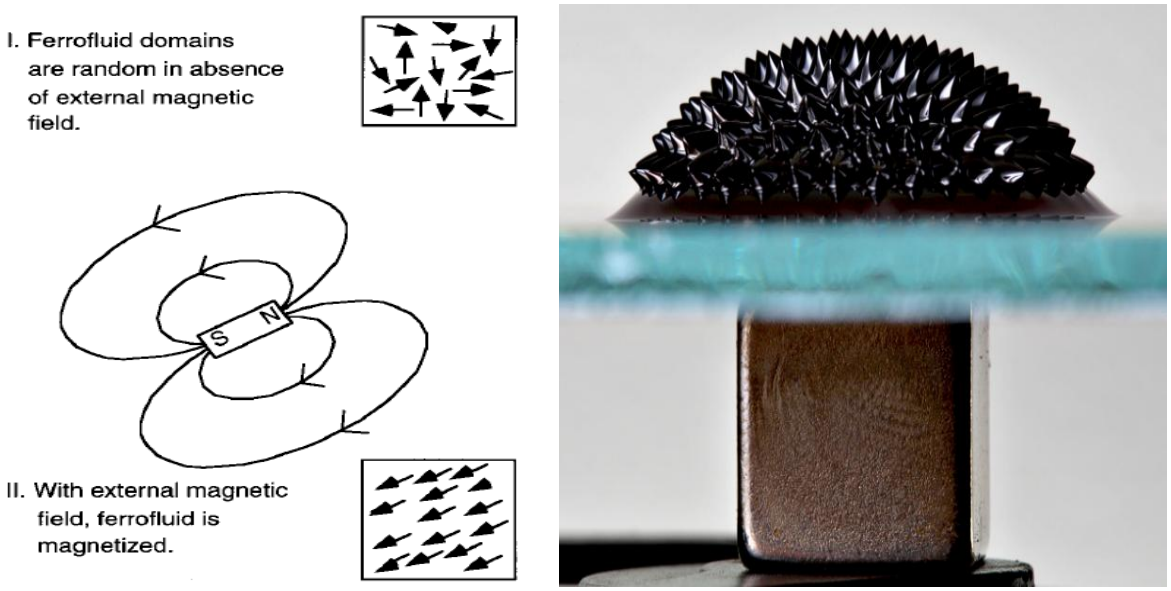

(a) (b)

Figure 1.8: Ferrofluid and Magnetic field (a) Polarization of single-domain ferrofluid particles [Oldenburg et al., 2000]; (b) Ferrofluid under the effect of magnetic field [http://technoccult.net]

1.6.2 Powder mixed Electric Discharge Machining

PMEDM is one of the recent innovations for the enhancement of capabilities of EDM process. In PMEDM, the electrically conductive powder is mixed in the dielectric of EDM, which reduces the insulating strength of the dielectric fluid and increases the spark gap between the tool and work piece. As a result, the process becomes more stable, thereby, improving the MRR and reducing SR, i.e., improving surface finish. Moreover, the surface develops high resistance to corrosion and abrasion. PMEDM also termed as 'Additive EDM' was originally invented during late seventies as a revolutionary technique for achieving mirror like finish relatively at high machining rates on already machined components. The powder particles get energized and behave in a zigzag fashion (Figure 1.9). These charged particles are accelerated by the electric field and act as conductors. The conductive particles promote breakdown in the gap and increase the spark gap between tool and the work piece. Under the sparking area, the particles come closer to each other and arrange themselves in the form of chain like structures between both the electrodes. The interlocking between the different powder particles occurs in the direction of flow of current. The chain formation helps in bridging the discharge gap between both the electrodes. Due to *bridging effect*, the insulating strength of the dielectric fluid decreases. The easy short circuit takes place, which causes early explosion in the gap. As a result, a *series discharge* starts under the electrode area. The faster sparking within a discharge takes place causing faster erosion from the work piece surface and hence the MRR increases. At the same time, the added powder modifies the plasma channel. The plasma channel becomes enlarged and widened [Zhao, 2002]. The sparking is uniformly distributed among the powder particles, hence electric density of the spark decreases. Due to uniform distribution of sparking among the powder particles, shallow craters are produced on the work piece surface. This results in improvement in surface finish.

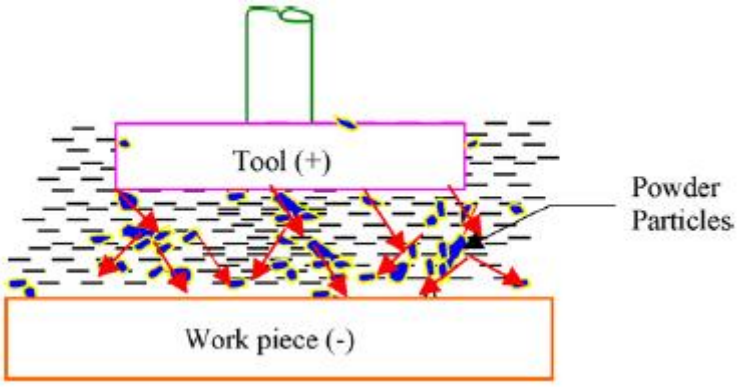

Figure 1.9: Principle of powder mixed EDM [Kansal et al., 2007]

CHAPTER 2
LITERATURE REVIEW

In this report, literature review of two modifications in machining (EDM) is discussed. These two modifications are:

i) Magnetic force assisted EDM
ii) Powder mixed EDM

2.1 MAGNETIC FORCE ASSISTED EDM

Govindan et al. [2013] performed single-spark analysis of removal phenomenon in magnetic field assisted dry EDM by investigating more than 100 single-discharge for dry and liquid EDM trials, with and without magnetic fields at different values of current, voltage, magnetic field, pulse on -time and bi-pulse current. Confinement of plasma due to Lorentz forces is a very important factor in characterizing higher MRR in magnetic field assisted EDM. In case of dry EDM, the magnetic field assistance reduced the diameter of the crater and increased the depth. The maximum observed reduction in crater diameter in dry EDM and liquid dielectric EDM were 81 % and 67 %, respectively. The average increases in the crater depths with application of magnetic field are 27 % and 37 %, for dry EDM and liquid dielectric EDM, respectively. The material removal was observed more uniform with magnetic field assistance in the liquid dielectric EDM. Analysis of composition has shown that alloying of workpiece surface with tool electrode and carbon (from dielectric) increases with the magnetic field assistance. Alloying of surface (with C, Cu and O) increases with discharge energy, which might be the result of good flow of electrons increasing diffusion due to heating and higher field strength. The obtained results were verified by using an analytical model for predicting the effect of Lorentz forces on the crater radius and depth.

Teimouri and Baseri [2012a] studied about the effect of magnetic field and rotary tool on EDM performance with X210Cr12 cold work steel as work piece and copper tool. Experiments were divided in three energy regimes namely low, middle and high depending on the values of peak current, pulse on time and pulse off time. MRR was found to increase with energy (i.e., high current, high pulse on time and high pulse off time situation), while SR was found to increase with the energy.

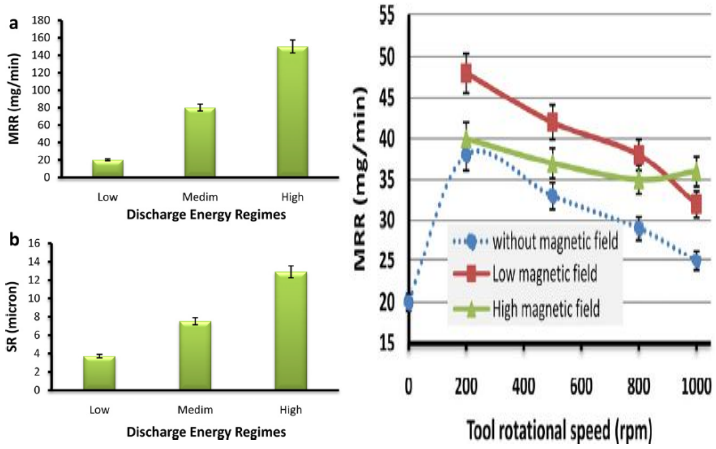

(a) (b)

Figure 2.1: MRR and SR patterns (a) MRR and SR curves at different regime; (b) MRR v/s speed at different field intensities [Teimouri and Baseri, 2012a]

MRR and SR patterns at different energy regimes are shown in Figure 2.1 (a). MRR was found to be higher in case of low magnetic field intensity than high magnetic field intensity but was more than that of no magnetic field. Rotary tools provide centrifugal force as well along with the electromagnetic forces which work well together in clearing the gap and maintaining a proper arc with higher MRR. MRR at different magnetic field strengths is shown in Figure 2.1 (b).

Teimouri and Baseri [2012b] studied about TWR and overcut in EDM with rotary tool and magnetic field assistance with SPK cold work steel (X210Cr12) as work piece and copper tool at three energy regimes namely low, medium and high. It was observed that the TWR increases with increase in discharge energy but at the high energy regime due to deposition of pyrolytic carbon on the surface of the tool, TWR decreases but TWR was found to increase continuously with increase in rotational speed of electrode which avoids deposition of pyrolytic carbon on the electrode by properly clearing the machining gap. Overcut was found to increase with increase in magnetic field strength as in presence of the magnetic field ion travel in cycloid path whose radius increases with increase in magnetic field as well as size of debris also increases with increase in magnetic field, which is responsible for increase in overcut. Overcut was further increased with rotational speed of the electrode.

Teimouri and Baseri [2012c] studied rotary magnetic field-assisted dry EDM with ultrasonic vibration of work piece with SPK cold work steel (X210Cr12) as work piece, brass and copper as electrodes. MRR, TWR, SR and OC were measured. It was observed that brass tools lead to higher MRR condition, because of higher specific resistance of brass than copper which may lead to increase in spark intensity and electrode gap but larger TWR than

copper because of low melting range. MRR was higher with two eccentric holes with low SR and higher TWR. Magnetic field improved process stability, improving MRR and lower SR but higher OC. Also magnetic field decreased the ignition delay time increasing TWR. Ultrasonic vibration of work piece helped in better debris removal, improving stability. Ultrasonic vibration reduced ignition delay time causing increase in TWR and a coarser surface. Also, acoustic cavitations were found responsible for larger overcut.

Heinz et al. [2011] investigated magnetic field assisted material removal in micro-EDM for non-magnetic materials. Micro EDM is used for creating micro sized features irrespective of their hardness. For increasing MRR up to desirable level, i.e., (10 – 15) mm^3/h, from current MRR possible from (0.6 – 6) mm^3/h; experiments were conducted. In this experiment tungsten wire (100 µm diameter) as electrode, grade 5 titanium as work piece, deionised water as dielectric, gap of 1 µm, gap voltage 100 V, power (100 – 150) W and electromagnets with strength 0.33 T, 0.66 T and 1 T were used. Single spark discharge experiments were chosen to study behaviour of melt pool, while erosion efficiency and volume analysis was done to predict MRR. Plasma temperature, electron density, and debris distribution were used to investigate and explain the mechanisms influencing material removal.

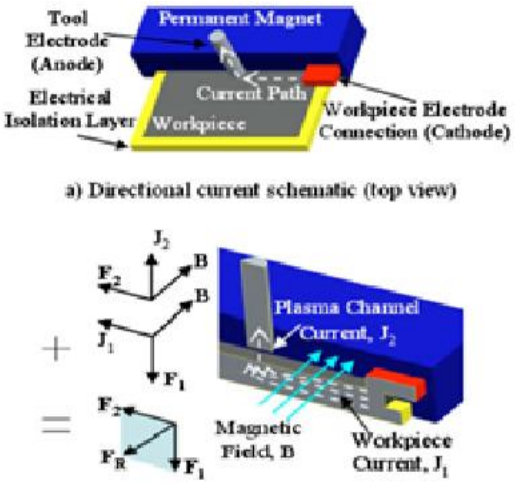

Figure 2.2: Schematic of parallel magnetic field with directional current [Heinz et al., 2011]

Non- magnetic materials generally don't experience any force in the presence of magnetic field, but additionally when current flows in the work piece (Figure 2.2), Lorentz force is generated in the work piece, when current and magnetic field in not normal and it is given by,

$$\vec{F} = \vec{J} \times \vec{B}$$

Where $\vec{F}$ = Force

$\vec{J}$ = Current Density

$\vec{B}$ = Magnetic Field

Maximum force was observed when electric field and magnetic field were perpendicular to each other. An additional Lorentz force F_1 was developed because of current J_1 acting on the work piece in the same way a Lorentz force acts on a current-carrying wire in a magnetic field. The actual direction of the current J_1 in the melt pool was a combination of the overall current direction in the work piece J_1 and the current direction in the plasma channel J_2, thus the resulting force vectors F_1 and F_2 combined to produce a force in the melt pool F_R. Erosion efficiency, η was calculated as,

$$\eta = \frac{E_e}{E_s} = \frac{v_e . \rho . H_m}{E_s}$$

Where E_s = Spark energy, $E_s = V.I.T$

V = Voltage

I = Current

T = Discharge time duration

E_e = Erosion energy

v_e = Erosion volume, v_e = Positive volume - Negative volume (Figure 2.3)

ρ = Density

H_m =Enthalpy of melting

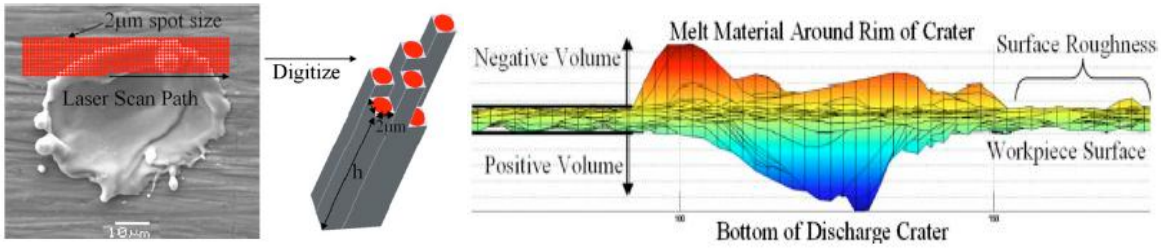

(a) (b)

Figure 2.3: Crater view (a) Digitization of crater surface; (b) Side view of 3D surface map [Heinz et al., 2011]

Then plasma temperature, electron density and Debye length were measured. Using permanent magnet of strength 0.7 T, it was found that positive volume decreases by 23 %, negative volume decreases by 43 % and overall efficiency increase was 25 % from 4.5 % to 5.3 %. Using electromagnets (Lorentz force acting towards work piece), it was seen that erosion efficiency increases by 54 % in increasing field strength from 0.33 T to 0.66 T and 3 % while increasing from 0.66 T to 1 T. In this case it was observed that positive volume increases by 28 % and negative volume decreases by 50 % between the field strength of 0.33

T and 0.66 T. No significant changes were observed in case of plasma temperature with increase in field strength; while electron density was likely to decrease with increase in field strength but they had no significant effect of plasma characteristics and MRR. But field strength showed significant effect on the debris characteristics. It was seen that when the Lorentz force is applied, the discharge debris distance shifts toward values further away from the crater. The average debris distance without the Lorentz force was 164 μm, whereas with the Lorentz force applied, the average increased to 207 μm, as well as the debris with size from 0-50 μm was also cleared from the crater region. Material removal mechanism considered was melting / splashing. With Lorentz force, melt pool experienced an increased pressure above it. This clears away additional melted material from the bottom of the discharge crater, creating a deeper crater. Melted material is transported up the sides of the crater to the crater rim, where it is removed by splashing after the plasma channel collapses.

Joshi et al. [2011] discussed about the effect of pulsating magnetic field on dry EDM. Problems like low stability of arc column, arcing and poor surface quality are seen in the case of dry EDM. In order to prevent these types of problems, effect of pulsating magnetic field on this process was studied. Two stainless steel split work pieces were used with copper pipe electrode and oxygen gas with 99.9 % purity as energy transfer media. Pulsating magnetic field was provided using a triangular configuration of electromagnets energized by (0 – 30) V DC (sequential actuation). Rotating magnetic field produced by sequential actuation influenced electric field and deflected electrons at some angle. By this increased collision was observed with reduced mean free path helping in raising ionization and better transfer of thermal energy to work piece, this helped in increasing the MRR. Better geometric accuracy and better machined surface quality, i.e., lower SR was observed.

Lin et al. [2009] worked towards optimization of machining parameters in magnetic force assisted EDM using Taguchi approach with SKD 61 steel as work piece and copper electrode. In magnetic assisted EDM debris are expelled easily and quickly and hence regular discharge was achieved increasing MRR three times more and $1/3^{rd}$ times lower TWR with better surface finish. Discharge crater obtained in case of magnetic EDM was shallower and smaller than that of conventional EDM as well the micro cracks obtained were less. Optimal combination for high MRR was given as negative machining polarity, 20 A peak current (highest value), 460 μs pulse duration (highest value) and 120 V no-load voltage (lowest voltage value). The optimal combination for lower SR found was positive machining polarity,

5 A peak current (lowest value), 460 µs pulse duration (highest value) and 200 V no-load voltage (highest voltage value).

Lin and Lee [2009] discussed about optimization of machining parameters using magnetic force assisted EDM based on Gray relational analysis on SKD 61 steel with copper electrode. Gray relational coefficient was calculated, higher the value of relational coefficient, stronger the relational degree between reference sequence and comparative sequence. It was obtained that number of effective discharge waveform obtained by magnetic assisted EDM was higher than that of the conventional EDM. MRR was estimated three times more than conventional and SR was 1/3rd of that of the conventional EDM as well as thickness of recast layer and surface cracks were reduced. ANOVA results have shown that peak current, pulse duration and no-load voltage were significantly affecting factors. High peak current, high pulse duration and high no-voltage were preferred along with negative polarity, i.e., negative work piece and positive electrode for achieving high MRR.

Lin and Lee [2008] discussed about effects of magnetic forces on the EDM process with SKD 61 steel as work piece and copper electrode with positive polarity using dielectric kerosene. Different levels of peak current and pulse duration were used. Magnetic force assisted device consisting of rotating disc, driven by electric motor with two magnets under the complete set up of EDM was established for carrying out the experimentation. Magnetic field used helped in gap cleaning and changing the motion path of electrolyte. It resulted mainly in maintaining regular discharge waveforms at prolonged time duration. Using magnetic field, MRR was increased nearly three times as compared to that of conventional EDM, and SR was also less. MRR was high at high peak current and more pulse duration as well as SR was also lower at longer pulse durations. However, the TWR was slightly higher comparatively, but it reduced to even negative at higher pulse duration due to deposition of pyrolytic carbon generated from kerosene on the electrode surface. It helped in expelling debris leading towards improved machining efficiency with lesser surface cracks.

Chattopadhyay et al. [2008] analysed rotary EDM characteristics in reversal magnetic field for EN8 steel with copper electrode and kerosene + therm oil (in 1:1 ratio) as dielectric fluid with the help of Taguchi approach of analysis. Magnetic field strength of range (123 – 617) Gauss was used with field reversal time as 1 s. It was observed that rotary EDM with magnetic field produces higher MRR with less TWR comparatively. Better geometrical accuracy with better gap cleaning was achieved. Further MRR was found to increase with

increase in current and rotating speed but was found to reduce with increase in pulse on time mainly at low currents due to generation of small eroded particles which were not removed effectively but MRR was increased at high current with more pulse on time.

Yeo et al. [2004] studied about the feasibility of application of a magnetic field to obtain higher aspect ratio (Length to Diameter ratio) micro holes on hardened tool steel using the micro electro-discharge machining (micro EDM) process. In this case positive polarity was used with rotating tungsten electrode rod as electrode and hardened tool steel XW 42 as work piece with dielectric HL 25-S. In conventional EDM, pressure flushing and jet flushing are used for debris removal but in case of micro EDM, fragile micro electrodes are used, which can't withstand the flushing forces encountered, so a different technique is required for debris removal in this case. Centrifugal force as a result of rotation of tool and magnetic force as a result of magnetic field are experienced by the debris particles removed and hence a total force is measured on the debris particles by vector addition of two forces. It was observed that at initial stage when aspect ratio is less than 1, centrifugal forces are itself enough to machine but for higher aspect ratio, there was a clear effect of magnetic field. It was observed that 26 % more depth was achieved, there was no as such difference in surface finish of the hole obtained as well as holes were straight as well but in this case TWR was higher.

2.2 POWDER MIXED EDM

Bhattacharya et al. [2013] studied surface characteristics and material migration properties during surface modelling in EDM process, while machining die steels (H11, HCHCr and AISI 1045) with silicon, graphite and tungsten powder. Graphite, tungsten-copper and brass tools are used for machining. Powder mixed in dielectric along with its concentration, current and pulse on time are identified as significant factors for surface finish, while powder and its concentration, current, pulse on time and electrode are found significant for micro hardness (MH). Powder addition improves finish while increase in current and pulse on time decreases finish. Brass as a tool and tungsten as an electrode provide good finish. Tungsten powder and tungsten-copper compliment MH. Scanning Electron Microscope (SEM) and Energy Dispersive Spectroscopy (EDS) are used for analysing microstructure and phases/composition present on the machined surface. Material migration is supposed to take place from powder, tool and dielectric. Silicon is supposed to dissolve in ferrites increasing toughness and strength. Iron carbide formation on the surface increases hardness value.

Syed and Kuppan [2013] studied the effect of aluminium powder mixed in distilled water on white layer thickness in EDM with W300 die steel as workpiece and copper as a tool. Experiments were planned using face centred central composite design procedure and empirical model was developed using response surface methodology. Optical microscopy was used to measure white layer thickness. White layer is found to increase with the increase in the current and pulse on time. White layer thickness is found to decrease with the powder concentration at every current level. Further lowest white layer thickness was observed with negative polarity.

Bhattacharya and Batish [2012] studied the effect of process variables on micro-hardness, grain size and strain during machining of various die steels (HCHCr, H11, H13 and EN31) with PMEDM using dummy treated L27 experiment design. SEM is used to study material transfer during machining, while XRD (X-Ray Diffraction) is used to study grain size and micro-strain developed on the machined surface. Deposition of material is very significant parameter that alters MH. MH is significantly affected by addition of graphite and tungsten powder while aluminium and copper powder are found insignificant. Graphite powder addition and graphite electrode used showed significant MH increase in the machined surface. Grain size was mainly affected by cooling rate and powders used other than the machine process parameters (current and pulse off time). Experiments performed with low melting point powder showed slow cooling rate resulting in the finer grain size. Grain size, temperature factor and antiphase boundary owing rejection of solvent at high rate of cooling tend to enhance micro-strain. HCHCr, H13 and H11 die steels showed higher average strain than EN31 wokpiece.

Batish et al. [2012] studied material transfer mechanism in die steels using powder mixed EDM. The effect of process parameters and mechanism of material deposition in powder mixed EDM on surface properties of EN31, H11, and High Carbon High Chromium (HCHCr) die steel materials was investigated. Samples were analyzed for X-ray diffraction (XRD) followed by microstructure analysis using a Scanning Electron Microscope (SEM). Surface modification was measured in terms of the MH, and results showed that there was almost 80 % increase in MH after powder mixed EDM and the results also showed significant material transfer from the electrode as well as powder, either in free form and / or in compound form. Current, powder and interaction between work piece and electrode affected the MH significantly. Copper electrode was found best for EN31 and H11 die steel, whereas tungsten-copper electrode was better suited for HCHCr steel to achieve higher MH

value. Graphite powder was found to be more suitable compared to aluminium in improving the MH of all three materials. Highly amorphous structure because of high temperature coupled with rapid cooling was observed.

Batish and Bhattacharya [2012] discussed about the mechanism of material deposition from powder, electrode and dielectric for surface modification of H11 and H13 die steels in EDM process, properties measured in terms of the MH of the machined surface. Three different electrode materials (copper, tungsten-copper and graphite), four different powder materials (aluminium, copper, graphite and tungsten) and three different dielectrics (kerosene, EDM oil and refined mineral oil) with other suitable parameters were used. Powder mixed and current was found as significant process parameters. Maximum increase in MH was observed with addition of tungsten powder and with tungsten-copper electrode even at lower current. At relatively higher current settings, it was observed that significant amount of material transfer takes place from the electrode material and breakdown of the dielectric material takes place offering a possibility of material deposition from dielectric. This is definitely attributed to the material migration from powder suspended and / or electrode and / or dielectric. Kerosene was found a superior choice for consistently good machining and surface improvement. Use of graphite electrode provided much possibility of material deposition from electrode and in most of the cases helped in carbide formation thereby increasing the hardness and wear resistance property of the machined surface. Due to rapid cooling amorphous structures formed in the machined surfaces and cracks were observed.

Bhattacharya et al. [2012] investigated about surface modification of HCHCr, EN31 and HDS using powder mixed EDM process with different electrodes (graphite, tungsten-copper), powder (copper, tungsten), dielectric (kerosene, EDM oil) at different pulse on, pulse off time and current values. Current and powder mixed with certain electrode were observed as significant parameters affecting the MH of the work pieces. The mechanism of material deposition was observed from the suspended powder and / or tool electrode as well in either free form or in compound form. Amongst the two electrode materials, copper-tungsten along with tungsten powder had the best MH. Selected samples were analyzed for X-ray Diffraction (XRD) followed by microstructure analysis using a Scanning Electron Microscope (SEM).

Kumar and Batra [2012] studied about surface modification of die steel materials (like OHNS type O2 die steel, HCHCr type D2 steel and H13 steel) with EDM using tungsten powder mixed kerosene dielectric with copper electrode in reverse polarity. X-ray diffraction (XRD)

analysis was used to find out the presence of additional elements and their phases, Scanning Electron Microscopy to analyze the structural features of the machined surfaces and composition testing on Optical Emission Spectrophotometer to confirm material transfer and for quantitative analysis of the changes in the constituents of the machined surfaces. Spectrometric analysis after machining showed that different proportion of tungsten was induced in die steel surfaces (2.89 % in OHNS steel, 2.43 % in HCHCr steel and 3.25 % in H13 steel), while it was negligible in starting. Micro hardness was found to increase with more than 100 % in every case with almost similar optimal settings like low current, low pulse on time and high pulse off time. The presence of tungsten carbide and increase in the percentage of carbon after machining was said to be the result of the suspended powder particles reacting with carbon (from the breakdown of the hydrocarbon dielectric) at high temperatures of the plasma channel to form carbides.

Bhattacharya et al. [2011a] carried out experimentation for setting optimal parameters for rough and finish machining of die steels (EN31, H11 and high carbon high chromium (HCHCr)) in powder mixed EDM. Seven different parameters along with their interactions were evaluated using dummy-treated experimental design and ANOVA (L27 Orthogonal Array). Suspending powder showed surface modification. EN31 showed maximum MRR as compared to the other two materials at similar process settings, then H11 and lowest MRR was observed for HCHCr. Copper electrode with aluminium suspended in the dielectric maximized the MRR, while graphite powder showed low MRR but better finish. The MRR was observed to be dependent upon pulse off, pulse on time and current. The interaction between tool material and suspended powder was observed to be significant. The electrode material independently had no effect on MRR but in combination with the suspended powder affected the MRR significantly. HCHCr required higher current and pulse on settings for initiating a machining cut and worked best in combination with tungsten-copper electrode and graphite powder for improved finish. On the other hand, SR was significantly affected by pulse on time, current and powder and the combined effect of work piece, powder, and electrode.

Bhattacharya et al. [2011b] dealt with optimization of powder mixed electric discharge machining using dummy treated experimental design with analytic hierarchy process with seven different process parameters, i.e., work piece (HCHCr, Hot Die Steel, EN31), dielectric (kerosene and EDM oil), powder (copper, tungsten), electrode, pulse on and pulse off time and current with L_{27} array for optimization of MRR, TWR and SR. The process conditions

that affected the three responses were identified and optimized together using AHP for HCHCr, EN31 and HDS work piece. Addition of powder in the dielectric improved MRR as well as SR. Three factors, current, electrode material, and pulse-on time were found to be the most significant factors affecting MRR. Current, powder, and electrode material significantly affected the TWR. Kerosene as dielectric was observed to be a superior alternative than EDM oil. Graphite electrode worked best for HCHCr and EN31 and tungsten-copper tool electrode worked best for HDS as they globally optimize the three output variables. Also, copper powder suspended in the dielectric resulted in an optimal solution for HCHCr and HDS and tungsten powder was seen to be a better choice for optimizing responses for EN31. Arcing was observed at high current settings with low pulse on time during addition of more electrically conductive copper powder. Current and pulse-on time influenced the SR of the finished work surface.

Jahan et al. [2011] studied the nano-powder-mixed sinking and milling micro-EDM of tungsten copper (WC-Co (10 % Cobalt)) work piece with tungsten electrode and Total FINA ELF EDM 3 oil as dielectric fluid. It was concluded that spark gap increases with increase in powder concentration producing a good surface finish up to a limit but poor surface finish after that, because after a limit when powder is added, it leads to increase in series discharges producing rough surface. MRR was found to increase with increase in powder concentration. For all the concentration levels, powder-mixed milling micro-EDM was found to provide lower SR, higher spark gap and lower TWR compared to powder mixed sinking micro-EDM. The powder-mixed milling micro-EDM was found to suffer from less surface defects and migration of materials compared to sinking, because of improved flushing conditions supposed to assist in some abrasive action of the powder particles in addition to reducing the capacitive effect between electrode and work piece.

Prihandana et al. [2011] studied about accuracy improvement in micro-EDM with nanographite powder-suspended dielectric fluid with silver-tungsten work piece, tungsten electrode and kerosene as dielectric. In pure dielectric fluid, since there are no disturbances at the detection of the first discharge, the machining depth ultimately is accurate. On the other hand, it was observed that the presence of nanographite powder in the dielectric fluid increases the machining gap creating an early detection from discharge pulse. As a result, the machine assumes a bigger first discharge distance; thus, the machining depth becomes inaccurate. In order to observe this phenomenon, the experiments were conducted using position display indicator of micro-EDM together with pulse counting method to fabricate

blind hole with a machining depth of 50 μm. The total number of pulses observed during pure dielectric experiment was used in experiment with nanographite powder to avoid inaccuracy. After experimentation it was observed that introduction of nanographite powder in dielectric reduces machining time by 35 %. The addition of nanopowder to a dielectric fluid also improved surface quality by eliminating micro-cracks in the surface machined and produced a high sparking gap size, which led to reduction of electric discharge power density, hence low in explosion force due to the nanographite powder size.

Prihandana et al. [2009] described about the effect of micro-powder suspension of dielectric fluid in μ-EDM process by using Taguchi Approach. Different dielectrics (pure dielectric, dielectric with 2 gm/l and 5 gm/l concentration of MoS_2 micro powder), tool electrode (copper, tungsten-copper and tungsten-silver) and work piece (copper, brass and tungsten-copper) combinations were analysed in with or without presence of ultrasonic vibration condition. Pareto analysis of variance was used to analyze different machining parameters. Process parameters were optimized using L18 orthogonal array. The results showed that the introduction of MoS_2 in dielectric fluid in ultrasonic vibration significantly increase the MRR and improves surface quality by providing a flat surface free of black carbon spots.

Kung et al. [2009] studied about MRR and TWR in the powder mixed EDM of cobalt-bonded tungsten carbide (94WC-6Co) with copper electrode (negative polarity) and aluminium powder being mixed in mineral oil (TOTAL EDM44) as dielectric. It was observed that by using dielectric fluid with conductive aluminium powder can effectively disperse the discharging energy dispersion in order to improve the machining efficiency. The MRR was found to increase up to a certain maximum value with the increase in amount of aluminium powder and after that MRR reduced. TWR was observed to show exactly the opposite trend to that of the MRR, i.e., TWR value was found to decrease with the aluminium powder concentration down to a minimum value after which it tends to increase. The effect of grain size was somewhat contrary, both MRR and TWR were increased with an increase of the grain size. Both MRR and TWR apparently increased with the increase of the discharge current and pulse on time.

Pecas and Henrique [2008] studied about the effect of addition of powder particles in EDM using AISI H13 steel as work piece with electrolytic copper as electrode in dielectric fluid as Castrol SE fluid 180 with Silicon powder of 99.5 % purity. The analysis was carried out by varying silicon powder concentration and flushing flow rate over a set of different

parameters. With the addition of powder in dielectric, reduction in crater dimension, crater depth, white layer thickness and SR was observed. Better morphology was seen with concentration of range (2 – 3) gm/l.

Wu et al. [2005] discussed about the effect of surfactant (polyoxythylene-20-Sarbitan monooleate) on the powder mixed EDM with aluminium powder mixed in the dielectric and its effect on surface finish. Various parameters like polarity, peak current, peak duration, powder concentration and surfactant concentration were taken. Gap distance between electrode and work piece was found to increase from kerosene to kerosene + aluminium powder and further to Kerosene + aluminium powder + surfactant, uniformly distributing the discharge energy, which was supposed to reduce energy and hence lesser debris and better surface finish with more efficiency. Surfactant retarded agglomeration of aluminium particles and well distributing them reducing the recast layer thickness. For this purpose positive polarity, lower peak current and lesser peak duration were preferred.

Kansal et al. [2005a] optimized powder mixed EDM by response surface methodology using EN-31 tool steel as work piece in kerosene dielectric with silicon mixed powder. Variables like pulse-on time, peak current, duty cycle and concentration of silicon powder in dielectric were selected for measurement of MRR and SR. It was concluded that addition of silicon powder in dielectric increases MRR and gives better surface finish. MRR was found to increase with increase in concentration of silicon powder improving surface finish as well. Concentration and peak current individually affect the MRR and SR as well as their combination was also significant.

Jeswani [1981] investigated the effect of the addition of fine graphite powder into kerosene oil. It was reported that addition of 4 gm/l of fine graphite powder increased the interspaces for electric discharge initiation and lowered the breakdown voltage. The machining process stability was improved, around 60 % increase in MRR and 28 % reduction in TWR was observed.

Erden and Bilgin [1980] reported the experimental and theoretical investigations to determine the effect of impurities in dielectric fluid of EDM. Copper, aluminium, iron and carbon in powder form were mixed into the commercial kerosene oil as artificial impurities and machining was performed on brass – steel and copper – steel pairs. It was found that the added powder improves the breakdown characteristics of the dielectric fluid. It was further observed that the machining rate increases with increase in the concentration of the added

powder. The increase in machining rates was obtained due to the decrease in time lags at high impurity concentrations. It was further observed that the machining becomes unstable at excessive powder concentration due to occurrence of short circuits. Surface quality and the gap size were also improved by the impurity concentrations.

2.3 LITERATURE SUMMARY

From the study of research papers on Electrical discharge machining, it is seen that for improving MRR, TWR and surface finish, different modifications are implemented on conventional EDM and they are found beneficial. Some are:

1) Single discharge crater analysis for magnetic force assisted EDM has shown that magnetic force causes plasma confinement, causing crater diameter to decrease and depth of diameter to increase increasing the MRR in both dry and liquid EDM **[**Govindan et al., 2013].
2) Magnetic force assisted EDM tends to increase MRR by shifting debris distance further from crater, increasing erosion volume and maintaining uniform discharge waves by gap cleaning [Heinz et al., 2011; Chattopadhyay et al., 2008], not only for conventional EDM but also for micro EDM [Yeo et al., 2004] and dry EDM [Joshi et al., 2011].
3) Magnetic force assisted EDM is further complimented by using rotary tool and ultrasonic vibrations to work piece in terms of obtaining better MRR, lower TWR, better surface finish but higher overcut [Teimouri and Baseri, 2012a; 2012b; 2012c).
4) With increase in intensity of magnetic field as compared to lesser magnetic field intensity, MRR is reduced, which was although higher than no magnetic field condition [Teimouri and Baseri, 2012a].
5) MRR can be increased up to three times more and surface roughness can be reduced to 1/3rd using magnetic force, further MRR was found higher with reverse polarity [Lin et al., 2009; Lin and Lee, 2009; Lin and Lee, 2008].
6) Another modification powder mixed EDM can enhance MRR by increasing discharge strength while larger and shallower craters produced as a result of high discharge energy reduces SR [Bhattacharya et al., 2011a; 2011b; Pecas and Henrique, 2008; Jeswani, 1981].
7) MRR is mainly influenced by powder concentration (MRR increases with increase in concentration up to a certain limit) and current (MRR linearly increases with current)

in powder mixed EDM [Kung et al., 2009; Kansal et al., 2005a; Erden and Bilgin, 1980].

8) In powder mixed EDM material transfer is from electrode as well as powder in free or compound form, which is used for estimating micro hardness of the work piece [Batish et al., 2012; Batish and Bhattacharya, 2012; Bhattacharya et al., 2012; Kumar and Batra, 2012; Bhattacharya et al., 2013].
9) Average grain size and micro-strain calculation are done for PMEDM using XRD analysis [Bhattacharya and Batish, 2012] concluding that finer grain size can be obtained using lower melting point powders.
10) Syed and Kuppan [2013] studied white layer thickness in PMEDM and reported that white layer thickness increases with increase in current and pulse on time while it decreases with powder concentration.
11) Addition of surfactant retards agglomeration of powder particles maintaining uniform gap improving MRR in powder mixed EDM [Wu et al., 2005].
12) Addition of nano-particle powders [Prihandana et al., 2011] and micro-powders [Prihandana et al., 2009] improves surface quality removing micro cracks too. Better effects are observed for milling than sinking process [Jahan et al., 2011] in case of nano-particle powders.

2.4 GAP IN LITERATURE REVIEW

It is been identified that insufficient amount of work has been done in the field of magnetic force assisted EDM, hence magnetic force assisted EDM along with some other modifications can be carried out:

i) Magnetic field assisted EDM with powder mixed dielectric.
ii) Magnetic field assisted EDM with ring magnets or some other form of magnets that can enhance magnetic force characteristics.
iii) Effect of magnetic force on machined surface characteristics.

Hence depending upon the gaps identified, a comparison study of magnetic field assisted and magnetic field assisted PMEDM is planned with different types of magnets (bar and ring magnets) at different magnetic strengths.

CHAPTER 3
DESIGN OF STUDY

3.1 INTRODUCTION

This experimental work is aimed at studying the magnetic force assisted EDM with and without powder mixed in dielectric with different configuration of magnets like bar and ring magnet with different strengths. Different input parameters are taken in account with some machine input parameters and some process parameters. For ferrous metals magnetic forces act well and assist in removal of debris particles from the gap and lead to gap cleaning. The effect of magnetic forces on non ferrous metal powders mixed in the dielectric medium will be studied and their effect in improving the performance of the process would be studied. Individually both powder mixed EDM and magnetic force assisted EDM work well. In this study it is proposed to evaluate the effect of magnetic field on machining characteristics with the combination of magnetic field assisted EDM and powder mixed EDM. The present research work is mainly aimed at studying the effect of magnetic field on:

i) Conventional and powder mixed EDM and their comparison
ii) MRR and TWR during machining of ferrous work material using non-ferrous powders mixed in dielectric
iii) Surface roughness
iv) Micro hardness
v) Overcut
vi) Metallurgical Analysis

3.2 EXPERIMENTAL DESIGN

Designing an experiment is the foremost need of experimentation plan. In present study, Taguchi Method is used for preparing experimental design. Main steps of designing an experiment are listed below. All the steps are discussed in detail except last two steps which are further characterized as chapters.

- Defining Objective Function
- Selecting an appropriate OA
    - Selection of factors and their interactions
    - Calculation of DOF

- Experimentation
- Analysis of results using ANOVA technique
- Results and Discussions
- Conclusions

3.2.1 Defining Objective Function

The main objective of this study is to study the effect input process parameters for conventional EDM and powder mixed EDM for different configurations of magnets like ring and bar magnet to quantify different output parameters like MRR, TWR, OC, SR and MH. For conventional EDM, input process parameters like current, pulse on time, tool electrode and workpiece material for different magnetic strength levels of bar magnets. For powder mixed EDM, input parameters like current, pulse on time, tool electrode, workpiece material, powder type and powder concentration are studied with bar magnets as well as ring magnet.

3.2.2 Selecting an appropriate OA

The Taguchi method involves reducing the variation in a process through robust design of experiments by using a selected set of experimentation plan. The overall objective of this method is to determine which factors affect the most with a minimum amount of experimentation, thus saving time and resources. Designing an OA is the most fundamental need of applying Taguchi Method and processing with analysis. OA is designed from factorial design of experiments using mathematical algorithms including combinatorics, finite field theories, geometry and error-correcting codes. The arrays are designed to handle as many factors as possible in the least possible number of runs as compared to those dictated by full factorial design, just a small fraction of full factorial design. The algorithms ensure that the OA constructed is in such a statistically independent manner that each column of the array is orthogonal to each other. Each factor is assigned column (s) depending on its DOF. Each level of a factor has an equal number of occurrences within each column; and for each level within one column, each level within any other column will occur an equal number of times as well. A variety of OA's (2-level or 3-level) are available with a number of combinations of factors and their levels in the Taguchi method. Since each column is orthogonal to others, if the results associated with one level of a specific factor are much different at another level, it is because changing that factor from one level to the next has strong impact on the quality characteristic being measured. Since the levels of the other

factors are present an equal number of times for each level of the strong factor, any effect by these other factors will be ruled out. Orthogonal designs allow estimating the effect of each factor on the response independently of all other factors. The Taguchi method is proved best with the intermediate number of variables (3 to 50), few interactions and when only a few variables contribute significantly. The Taguchi method apparently has the following strengths:

- Consistency in experimental design and analysis.
- Most appropriate utilisation of time and resources.
- Robustness of performance without removing the noise factors.

The selection of orthogonal array is mainly based on total DOF, calculated by considering

- Factors and their interactions
- Calculation of DOF

Selection of factors and their interactions

Selection of factors is a crucial task which is to be done carefully to prepare the most effective design of experiment. Brainstorming and pilot experimentations are conducted to decide the factors and their levels.

Calculation of DOF

DOF denotes the number of the independent comparisons that can be made in any experiment. The number of factors considered for experimentation, their respective levels and considered interactions determine the total degree of freedom required for designing OA. Mathematically, DOF for each factor is calculated as,
DOF= n-1, where n is the level of each factor.
DOF for interactions is calculated as,
DOF= (n_A-1) × (n_B-1), where n_A and n_B are the levels of factor A and B respectively.

Once the DOF are known, OA is selected as the number of rows in the OA must be equal to or greater than the DOF. The interactions to be evaluated will require an even larger OA. Once the appropriate OA has been selected, the factors and interactions can be assigned to various columns.

3.2.3 Selection of OA for magnetic field assisted EDM

Different factors considered for magnetic field assisted EDM (with bar magnets) and their levels are listed in Table 3.1.

Table 3.1: Factors and their levels for magnetic assisted EDM

Factors (unit)	Designation	Levels					
		Level 1	Level 2	Level 3	Level 4	Level 5	Level 6
Current (A)	A	3	4	5	6	7	8
Magnetic field (T)	B	0	0.09	0.36	--	--	--
Work piece	C	AISI D2	AISI D3	AISI H13	--	--	--
Tool	D	Cu	W-Cu	C18000	--	--	--
Pulse On Time (µs)	E	50	100	200	--	--	--

Table 3.2 tabulates total DOF calculation for magnetic field assisted EDM.

Table 3.2: DOF for magnetic field assisted EDM

Factors	A	B	C	D	E	Total
DOF	5	2	2	2	2	13

In this case total DOF comes out to be 13. Hence, an OA with a minimum of 13 DOF is to be considered. From the available Taguchi OA designs, L18 OA is selected for this experimentation. L18 OA designed for experimentation is shown in Table 3.3.

Table 3.3: L18 OA for magnetic field assisted EDM

S. No.	Current (A)	Magnetic Field (T)	Workpiece	Tool	Pulse On Time (µs)
1	3	0	D2	Cu	50
2	3	0.09	D3	W-Cu	100
3	3	0.36	H13	C18000	200
4	4	0	D2	W-Cu	100
5	4	0.09	D3	C18000	200
6	4	0.36	H13	Cu	50
7	5	0	D3	Cu	200
8	5	0.09	H13	W-Cu	50
9	5	0.36	D2	C18000	100
10	6	0	H13	C18000	100
11	6	0.09	D2	Cu	200
12	6	0.36	D3	W-Cu	50
13	7	0	D3	C18000	50
14	7	0.09	H13	Cu	100
15	7	0.36	D2	W-Cu	200
16	8	0	H13	W-Cu	200
17	8	0.09	D2	C18000	50
18	8	0.36	D3	Cu	100

Magnetic field is this case is produced by using bar magnets, with '0' designating no field. Tool electrodes namely copper (Cu), tungsten-copper (W-Cu) and copper chromium nickel silicon (beryllium free) copper alloy (C18000) with diameter 10 mm are used. No interaction is considered in this case.

3.2.4 Selection of OA for magnetic field assisted PMEDM

Different factors considered for magnetic field assisted PMEDM and their levels are listed in Table 3.4. Same factors and their respective levels are utilised for bar as well as ring magnet excluding their magnetic strengths, which are 1 as '0 T', 2 as '0.09 T' and 3 as '0.36 T' in case of bar magnets and 1 as '0 T', 2 as '0.075 T' and 3 as '0.17 T' in case of ring magnet.

Table 3.4: Factors and their levels for magnetic assisted PMEDM

Factors (unit)	Designation	Levels		
		Level 1	Level 2	Level 3
Magnetic Field	A	1	2	3
Current (A)	B	3	5	7
Powder Concentration (gm/l)	C	3	6	9
Work piece	D	AISI D2	AISI D3	H13
Tool	E	Cu	W-Cu	C18000
Powder	F	Gr	W	Ti
Pulse On Time (µs)	G	20	50	100

Powders (graphite (Gr), tungsten (W) and titanium (Ti)) with grit size of 320 are used. For magnetic field assisted PMEDM, two interactions are considered. One is magnetic field and current (A×B) and other is current and powder concentration (B×C). DOF for the considered set of factors and their levels including interactions are listed below in Table 3.5.

Table 3.5: DOF for magnetic field assisted PMEDM

Factors	A	B	C	D	E	F	G	A×B	B×C	Total
DOF	2	2	2	2	2	2	2	2×2=4	2×2=4	22

In magnetic field assisted PMEDM, total DOF comes out to be 22. Hence an OA has to be selected with a minimum DOF as 22. Hence with detailed analysis, L27 OA is selected.

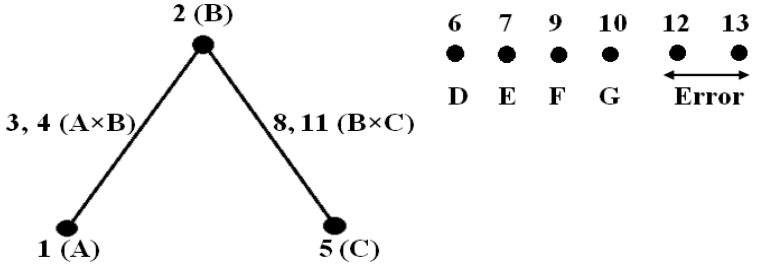

Figure 3.1: Linear graph used in L27 OA

The linear graph used for assignment of factors in L27 array is shown below in Figure 3.1. The linear graph shows the assignment of factors and their assignment of interactions to columns. L27 OA has 13 columns, each with DOF associated with it as two. Hence a column can allocate a factor with DOF as two. In linear graph, each vertex represents a column in the OA. In the defined OA, factor A is assigned to the column 1, factor B is assigned to the column 2 and factor C is assigned to column 5 as shown by the graph. Each vertex connected by the line represents the interaction defined. In the defined OA, two interactions are taken into account, A×B and B×C, being represented by the connected lines. Interaction A×B, with DOF four is assigned to column 3 and 4, while interaction B×C is assigned to columns 8 and 11. Other remaining factors, D, E, F and G are assigned to the columns 6, 7, 9 and 10 respectively.

Table 3.6: L27 OA for magnetic field assisted PMEDM

S. No.	Magnetic Field	Current (A)	Powder Conc. (gm/l)	Work piece	Tool	Powder	Pulse On Time (μs)
1	1	3	3	D2	Cu	Gr	20
2	1	3	6	D3	W-Cu	W	50
3	1	3	9	H13	C18000	Ti	100
4	1	5	3	D2	Cu	W	50
5	1	5	6	D3	W-Cu	Ti	100
6	1	5	9	H13	C18000	Gr	20
7	1	7	3	D2	Cu	Ti	100
8	1	7	6	D3	W-Cu	Gr	20
9	1	7	9	H13	C18000	W	50
10	2	3	3	D3	C18000	W	100
11	2	3	6	H13	Cu	Ti	20
12	2	3	9	D2	W-Cu	Gr	50
13	2	5	3	D3	C18000	Ti	20
14	2	5	6	H13	Cu	Gr	50
15	2	5	9	D2	W-Cu	W	100
16	2	7	3	D3	C18000	Gr	50
17	2	7	6	H13	Cu	W	100
18	2	7	9	D2	W-Cu	Ti	20
19	3	3	3	H13	W-Cu	Ti	50
20	3	3	6	D2	C18000	Gr	100
21	3	3	9	D3	Cu	W	20
22	3	5	3	H13	W-Cu	Gr	100
23	3	5	6	D2	C18000	W	20
24	3	5	9	D3	Cu	Ti	50
25	3	7	3	H13	W-Cu	W	20
26	3	7	6	D2	C18000	Ti	50
27	3	7	9	D3	Cu	Gr	100

As the total DOF of the OA design selected is 22, while DOF of standard L27 OA is 26, hence there are four DOF assigned to error. Error has been assigned two remaining columns that are 12 and 13. Table 3.6 shows the L27 OA designed for PMEDM with magnetic field assistance for both the configuration of magnets i.e., bar magnets and ring magnet.

3.2.5 Experimentation

Experimentation is conducted for L18 OA and L27 OA. Single trial is conducted for L18 OA, while two trials are conducted for L27 OA with bar as well as ring magnet.

3.2.6 Analysis of results

Analysis is to be done by using Analysis of Variance (ANOVA) for Mean & Signal to Noise ratio (S/N ratio).

Analysis of Variance

ANOVA is a statistical technique which can infer some important conclusions based on analysis of the experimental data. The method is very useful for revealing the level of significance of influence of factor(s) or interaction of factors on a particular response. It separates the total variability of the response (sum of squared deviations about the grand mean) into contributions rendered by each of the parameter/ factor and the error. A brief description of ANOVA analysis is given as following.

The Sum of squares (SS) is a measure of the deviation of the experimental data from the mean value of the data. Let A be the factor taken in account for investigation. Thus

$$\boldsymbol{SS_T = SS_A + SS_E}$$

Where SS_T = Total Sum of squared deviations about the mean

SS_A = Sum of squared deviations due to factor A

SS_E = Sum of squared deviation due to error

$$SS_T = \sum_{j=1}^{N} \left(\gamma_j - \gamma_m\right)^2$$

Where N = Number of response observations

γ_j = Mean response for j^{th} experiment

γ_m = Grand mean of the response = $\frac{\gamma}{N}$

$$SS_A = \left[\sum_{j=1}^{k_A} \left(\frac{{A_j}^2}{n_{Aj}}\right)\right] - \frac{\gamma^2}{N}$$

Where A_j = Average of all the observations under factor A_j level

γ = Sum of all the observations

n_{Aj} = Number of observations under A_j level

$SS_E = \sum_{k=1}^{k_A} \sum_{j=1}^{n_{Aj}} \left(\gamma_j - A_{km}\right)^2$

Sum of squares for interaction (suppose A × B) is given by

$SS_{A\times B} = \left[\sum_{j=1}^{c} \left(\frac{(A\times B)_j^2}{n_{(A\times B)j}}\right)\right] - \frac{\gamma^2}{N} - SS_A - SS_B$

In ANOVA analysis technique, mean square deviation is defined as:

MS = Mean Squared deviation

$MS = \frac{\text{SS (Sum of squared deviation)}}{\text{DOF (Degree of Freedom)}}$

F-value of Fisher's *F* ratio (Variance ratio) is defined as:

$F\text{-ratio} = \frac{\text{MS for a term}}{\text{MS for the error term}}$

Calculated *F*-ratio is compared with tabulated *F*-ratio and on the basis of the comparison of calculated and tabulated *F* value, final decision is taken means whether it is significant or non-significant, means whether hypothesis is accepted or rejected.

S/N ratio

In the Taguchi method, there are three categories of performance characteristic in the analysis of the signal-to-noise ratio, that is, the lower-the-better (Equation 3.2), the higher-the-better (Equation 3.1), and the nominal the better (Equation 3.3). The change in quality characteristic of a product under investigation in response to a factor introduced in the experimental design is the 'signal' of the desired effect. The effect of the external factors (uncontrollable factors) on the outcome of quality characteristic is termed as 'noise'. The objective of any experiment is to achieve the best possible S/N ratio.

Finding a correct objective function to maximize in an engineering design problem is very important. Depending upon the type of response, the following three types of S/N ratios are employed in practice:

- ***Higher the Better***

$(S/N)_{HB} = -10 \log (MSD_{HB})$ (3.1)

Where $MSD_{HB} = \frac{1}{R}\sum_{j=1}^{R}\left(\frac{1}{y_j^2}\right)$

MSD_{HB} = Mean Square Deviation for higher-the-better response

- ***Lower the Better***

$(S/N)_{LB} = -10 \log (MSD_{LB})$ (3.2)

Where $MSD_{LB} = \frac{1}{R}\sum_{j=1}^{R}(y_j^2)$

MSD_{LB} = Mean Square Deviation for Lower-the-better response

- ***Nominal the Best***

$(S/N)_{NB} = -10 \log (MSD_{NB})$ (3.3)

Where $MSD_{NB} = \frac{1}{R}\sum_{j=1}^{R}(y_j - y_0)^2$

MSD_{NB} = Mean Square Deviation for Nominal-the-best response

y_j = Observed value of the response characteristic

y_0 = nominal or target value of the results

R = Number of repetitions

S/N ratio for response characteristics

The parameters that influence the output can be categorized in two categories, controllable factors and uncontrollable factors. The control factors that may contribute to reduced variation can be quickly identified by looking at the amount of variation present in response. The uncontrollable factors are the sources of variation often associated with operational environment. For present experimental work, response characteristics are listed in Table 3.7.

Table 3.7: Response Characteristics

Response Name	Response Type	Units
Material Removal Rate (MRR)	Higher the better	mm^3/min
Tool Wear Rate (TWR)	Lower the better	mm^3/min
Overcut (OC)	Lower the better	mm
Surface Roughness (SR)	Lower the better	µm
Micro Hardness (MH)	Higher the better	VHN

3.3 EXPERIMENTAL SET UP

3.3.1 Machine Set Up

The experimentation work is performed on T-3822 M Electric Discharge Machine of Victory Electromech placed in non-traditional machining lab at Thapar University, Patiala. A separate arrangement is added for performing powder mixed EDM, a mild steel tank with inside dimensions as length 330 mm, breadth 180 mm, height 187 mm and plate thickness 3 mm. Capacity of the used tank is 9 L. A stirrer with the maximum speed of 1400 rpm is used to properly mix the powder in the dielectric medium. Figure 3.2 shows a view of machine with arrangement for powder mixed EDM with properly visible control panel and machining arrangement.

Figure 3.2: Electric Discharge Machine (Courtesy: NTM lab, Thapar University, Patiala)

Various input parameters varied on the EDM machine for present study are current and pulse on time. Levels of the input parameters are decided on the basis of pilot experimentation. Some parameters that are kept constant during the study are listed in Table 3.8.

Table 3.8: Constant input parameters

S. No.	Parameter	Value
1	Voltage	135±5% V
2	Polarity	Positive
3	Machining Time	10 min
4	Pulse off time	57 µs
5	Dielectric Medium	EDM oil

Schematic arrangement of EDM machine and machining arrangement is shown in Figure 3.3.

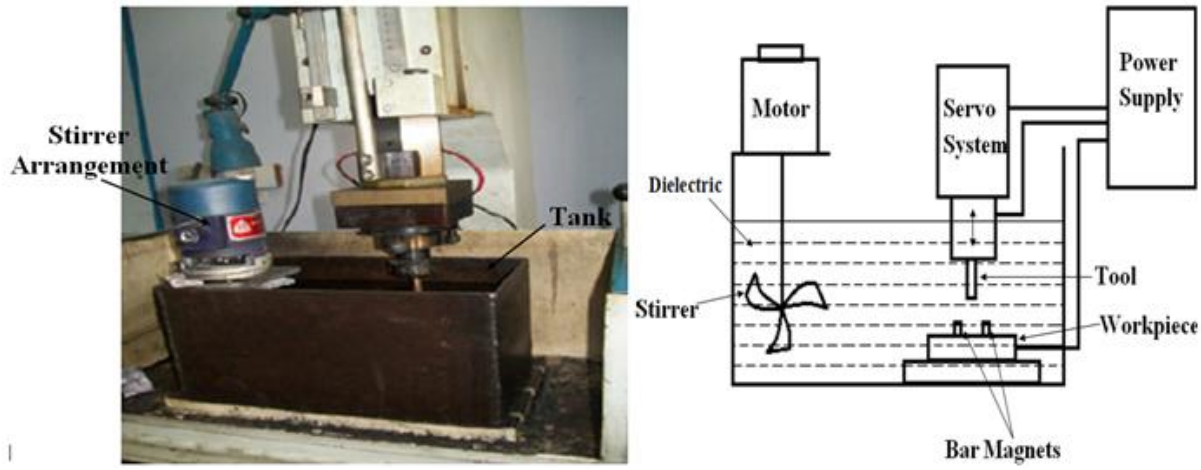

(a) (b)

Figure 3.3: EDM machine (a) Dielectric tank with stirrer arrangement; (b) Schematic arrangement with bar magnets

3.3.2 Workpiece and Tool electrode details

For experimentation, die steel material is used as workpiece with three different grades namely AISI H13, AISI D2 and AISI D3. Before machining, workpiece is properly grinded from both the sides for maintaining perfect alignment of workpiece with the tool electrode during machining. Three tool electrode materials are used for machining purpose, namely copper, tungsten-copper and C18000 (copper chromium nickel silicon (beryllium free) copper alloy), all with the diameter of 10 mm. Workpiece materials before machining and tool electrodes are shown in Figure 3.4.

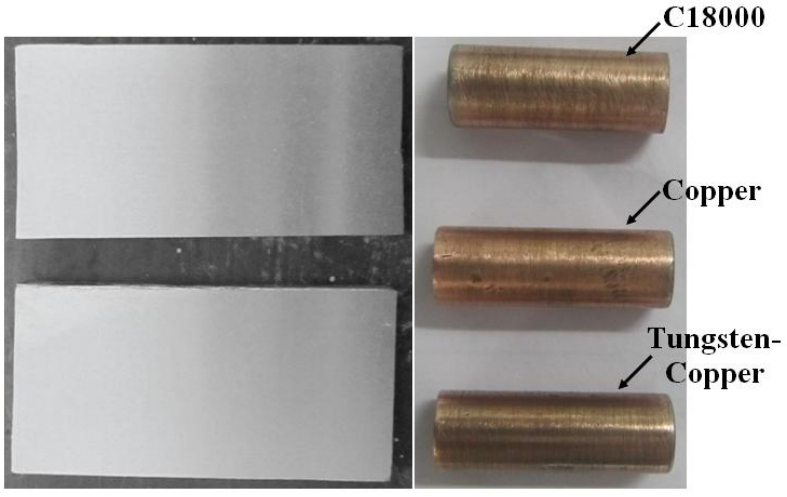

(a) (b)

Figure 3.4: Workpiece and tool material used for machining (a) Workpiece; (b) Tool

Composition of workpiece is measured on an Optical Emission Spectrometer DV-6. The percentage composition of workpiece material is listed in Table 3.9.

Table 3.9: Chemical Composition of workpiece materials

Workpiece		D2	D3	H13
% Composition	Fe	84.1000	86.1000	90.7000
	C	1.5100	1.5400	0.3680
	Si	0.0408	0.2910	0.9100
	Mn	0.2630	0.4650	0.3450
	P	0.0224	0.0213	0.0219
	S	<0.0050	0.0232	0.0118
	Cr	11.8000	11.2000	5.0400
	Mo	0.0560	0.0701	1.2800
	Ni	0.2020	0.0648	0.1620
	Co	0.0164	0.0256	0.0206
	Cu	0.0788	0.0098	0.0909
	Nb	0.0105	0.0134	0.0185
	Ti	0.0116	0.0172	0.0055
	V	0.0634	0.0077	0.9150
	W	<0.0200	0.0606	0.0389

Micro Hardness of base material is listed in Table 3.10.

Table 3.10: Micro Hardness of workpiece material

Workpiece	H13	D2	D3
Micro Hardness (VHN)	75.3181	85.8118	95.0286

Workpiece material after being machined is shown in Figure 3.5.

Figure 3.5: Workpiece material after machining (D2 die steel)

3.3.3 Magnets Configurations and details

For providing magnetic field assistance, two different types of magnet configuration are used, bar magnet and ring magnet, both with two strengths (0.09 T and 0.36 T for bar magnets while 0.075 T and 0.17 T for ring magnets). No separate fixture is designed for placing magnets. Magnets are kept directly on workpiece material dipped in the dielectric medium as shown in Figure 3.3 (b). Ring magnet is also kept in the same way around machining zone. Bar magnets are kept in such a way that, two bar magnets are kept 20 mm apart from each other facing opposite poles to each other. Ring magnets with the internal diameter of 20 mm are taken, and are kept in a way that North Pole is in upward direction. Figure 3.6 shows the bar magnets and ring magnets that are used in the experimentation purpose.

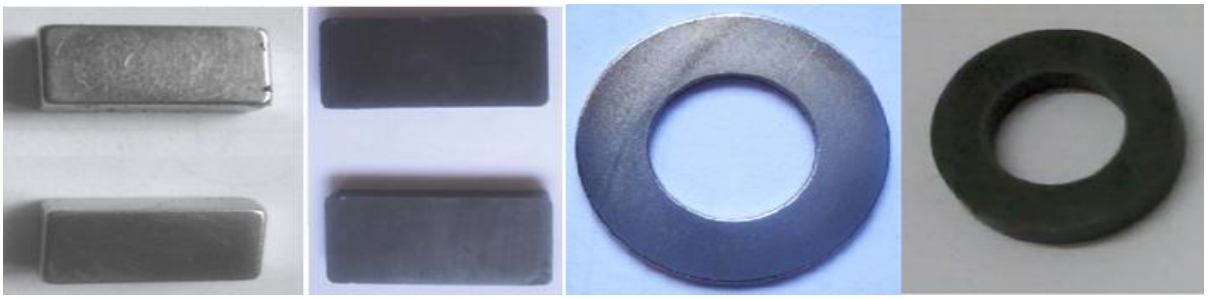

(a) (b) (c) (d)

Figure 3.6: Magnets (a) 0.36 T bar magnets (NdFeB magnets); (b) 0.09 T bar magnets (ferrite magnets); (c) 0.17 T ring magnet (NdFeB magnet); (d) 0.075 T ring magnet (ferrite magnet)

3.4 MEASURING AND TEST EQUIPMENTS USED

Measuring and test equipment that are used in the present work are:

- Surface Grinder for grinding workpiece material
- Weighing machine with 0.001 gm least count for weighing workpiece and tool material during experimentation for MRR and TWR measurement
- Profile Projector (Figure 3.7, a)
- Surface Roughness Tester (Figure 3.7, b)
- Digital Gauss meter (Figure 3.7, c)
- Optical Emission Spectrometer (Figure 3.7, d)
- Micro Hardness Tester (Figure 3.7, e)
- Metallurgical microscope (Figure 3.7, f)
- Scanning Electron Microscope (Figure 3.7, g)
- X-Ray Diffraction machine (Figure 3.7, h)

(a) (b) (c)

(d) (e) (f)

(g) (h)

Figure 3.7: Measuring and test equipments (a) Profile projector; (b) Surface roughness tester; (c) Digital Gauss meter; (d) Optical emission spectroscope; (e) Metallurgical microscope; (f) Micro hardness tester; (g) X-Ray Diffraction machine; (h) Scanning Electron Microscope

The details of important test equipments used are listed below:

3.4.1 Profile projector

Measurement of overcut size was investigated on Nikon Profile Projector (Model: V-10A) of Japan available in Metrology Lab of Thapar University, Patiala. The voltage requirement is 220 V / 230 V / 240 V and current requirement is 0.6 A. Its least count is 0.001 mm.

3.4.2 Surface Roughness Tester

Surface roughness was measured using Mitutoyo Surface Roughness Tester (Model: SJ-400). The equipment uses the stylus method of measurement, has profile resolution of 12 nm and

measures roughness up to 100 µm. A tracing length of 4.8 mm was used for analysis. Surface Roughness values were taken two times for each trial and average was used for analysis.

3.4.3 Digital Gauss meter

Magnetic strength of the magnets used in the experimentation is measured using Digital Gauss meter (Model: ESC18B), Eastwest Engineering Electronics Pvt. Ltd., Mumbai, India. It can be used to measure magnetic strength up to 2000 Gauss on ×1 range and 20000 Gauss on ×10 ranges.

3.4.4 Optical Emission Spectrometer

Chemical composition of the workpiece base materials and the composition of machined surfaces is measured using Optical Emission Spectrometer (Model: DV-6), Baird, USA. An accuracy of 0.0001 % is achieved in the measurement. Argon gas is used for composition measurement process.

3.4.5 Micro Hardness Tester

Micro hardness was measured on a computer interfaced Micro Hardness Tester (Model: MVH-2), Metatech industries, Pune, India available at Thapar University, Patiala. The micro hardness measurement is dependent on the diameter of indentation produced on the samples. The indents formed by the pyramid shaped indenter using a load of 1 kg for 20 s and were measured with Quantimet software. 40 MP Camera was used for observing / focussing images.

3.4.6 Scanning Electron Microscope (SEM)

Microstructure of some selected samples was investigated using SEM (Model-LEO 435 VP), SEMTech Solutions, USA. SEM is used mainly for imaging of surfaces and analysis of small surface features. It provides magnification up to 240,000 and high spatial resolution. For the present experimentation work, SEM of samples was investigated on three magnification ranges, namely, 200×, 500× and 1000×.

3.4.7 X-Ray Diffraction machine

X-ray diffraction (XRD) is a rapid analytical technique primarily used for phase identification of a crystalline material and can provide information on unit cell dimensions. XRD analysis of some selected samples was done using X-ray diffraction machine (Model-D8 ADVANCE), Bruker Corporation, USA with Copper radiation. For present study, the range of 2θ used is from 5^o to 120^o at a scan speed of 5^o/min for every sample.

CHAPTER 4
RESULTS AND ANALYSIS

4.1 RESULTS AND ANALYSIS OF MRR

4.1.1 Introduction

The effect of current, pulse on time, workpiece, tool electrode under the effect of three magnetic field conditions is analysed with and without powder mixed in dielectric medium using ring and bar magnets. Following Taguchi experimental design, 27 trials are conducted using powder mixed dielectric with ring and bar magnets. A separate L18 orthogonal array (OA) is planned for experiments using bar magnet without powder being mixed in dielectric medium. MRR is calculated measuring the difference between initial and final weight of workpiece using a weighing machine with least count as 0.001 gm. For each trial MRR is calculated using Equation 4.1.

$$MRR = \frac{(w_i - w_f)\times 1000}{\rho \times t} \ (\mathrm{mm}^3/\mathrm{min}) \qquad (4.1)$$

Where w_i =Initial weight of the workpiece (in gm),

w_f =Final weight of workpiece after experimentation (in gm),

ρ =Density of workpiece (in gm/cm^3) and

t =Machining time (in min).

4.1.2 Result and analysis of MRR using bar magnets with conventional EDM

Results for MRR

Results for mean MRR are given in Table 4.1 for each trial of L18 OA.

Table 4.1: MRR Results (L18 OA)

S. No.	Current (A)	Magnetic Field (T)	Work piece	Tool	Pulse On Time (μs)	MRR (mm^3/min)
1	3	0	D2	Cu	50	2.632
2	3	0.09	D3	W-Cu	100	2.926
3	3	0.36	H13	C18000	200	2.179
4	4	0	D2	W-Cu	100	2.3689
5	4	0.09	D3	C18000	200	3.053
6	4	0.36	H13	Cu	50	2.6923
7	5	0	D3	Cu	200	3.5623
8	5	0.09	H13	W-Cu	50	3.5897
9	5	0.36	D2	C18000	100	3.8165
10	6	0	H13	C18000	100	4.6153
11	6	0.09	D2	Cu	200	6.3171
12	6	0.36	D3	W-Cu	50	6.743
13	7	0	D3	C18000	50	9.54
14	7	0.09	H13	Cu	100	7.4358
15	7	0.36	D2	W-Cu	200	8.5544
16	8	0	H13	W-Cu	200	7.692
17	8	0.09	D2	C18000	50	11.186
18	8	0.36	D3	Cu	100	11.57

Analysis of Variance of MRR

The results for MRR are analysed using analysis of variance (ANOVA) for identifying the significant process parameters which affect the output parameter i.e., MRR. ANOVA for the mean MRR at 95 % confidence level is given in Table 4.2. *F*-test is utilised for testing variance data corresponding to each input parameter to find their significance. The principle of *F*-test is that the larger the *F* value for a particular input parameter, the greater is its effect on the output parameter. ANOVA table shows the analysis of MRR values using bar magnets without powder being mixed in dielectric medium. For such conditions, current is identified to be the most significant parameter affecting the MRR with the highest value of *F*, 78.06 corresponding to it. With increase in current, MRR increases as the energy available is more and hence more material is melted and evaporated. Next higher value of *F* is corresponding to workpiece material with *F* value of 9.68. D3 die steel as workpiece has shown maximum MRR while H13 shows least MRR value. Taking other factors in account, MRR is shown high with C18000 as tool material and low pulse on time. MRR increases with the field strength, higher MRR is observed with high magnetic strength field as compared to no magnetic field. Table 4.3 shows the response table with the ranks of various input parameters in terms of their relative significance. Current is assigned rank 1 making it the most

significant parameter while tool is assigned the rank of 6 proving it the most insignificant parameter. Plots segregated on the basis of current have shown that MRR is higher for magnetic field assisted EDM as compared to that of the without magnetic field assistance for almost all the current conditions. As with the increase in field strength the debris are expelled effectively leading to clear gap between electrode and workpiece, hence increasing the MRR.

Table 4.2: ANOVA Table for MRR (L18 OA)

Parameter	DOF	SS	MS	*F* (calculated)
Current (A)	5	151.607	30.3214	78.06
Magnetic Field (T)	2	2.464	1.232	3.17
Workpiece	2	7.517	3.7585	9.68
Tool	2	0.656	0.3282	0.85
Pulse On Time (µs)	2	2.248	1.1241	2.89
Error	4	1.554	0.3884	
Total	17	166.046		
e pooled	10	6.922	0.6922	

Table 4.3: Response Table for MRR (L18 OA)

Level	Current (A)	Magnetic Field (T)	Workpiece	Tool	Pulse On Time (µs)
1	2.579	5.068	5.812	5.702	6.064
2	2.705	5.751	6.232	5.312	5.455
3	3.656	5.926	4.701	5.732	5.226
4	5.892				
5	8.510				
6	10.149				
Delta	7.570	0.857	1.532	0.419	0.838
Rank	1	3	2	5	4

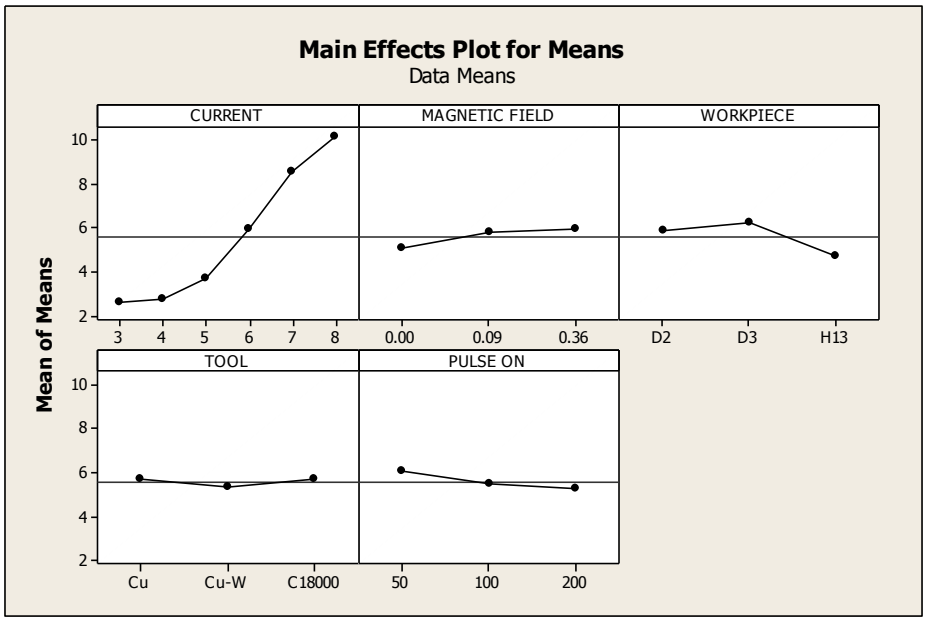

Figure 4.1: Main Effect plots of MRR (L18 OA)

Figure 4.1 shows the ANOVA plot for MRR corresponding to input parameters and Figure 4.2 shows MRR plots on the basis of segregated current values.

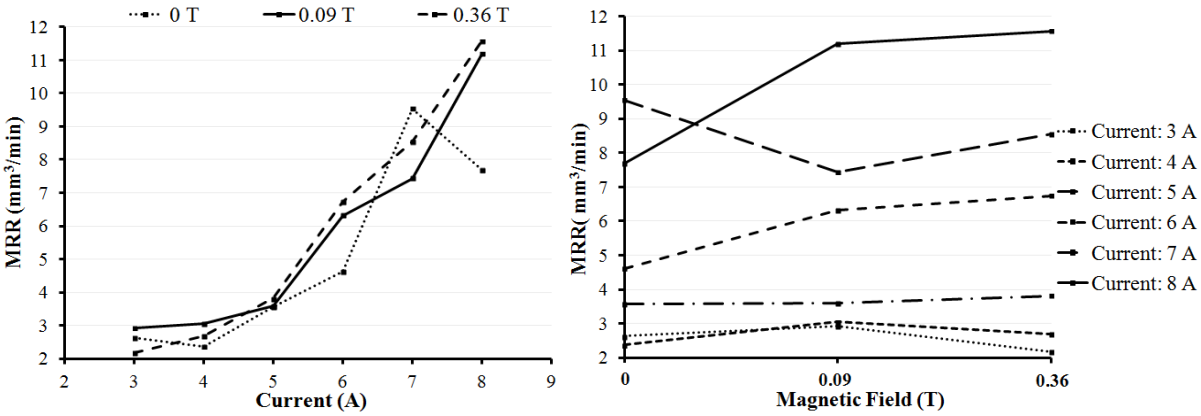

(a) (b)

Figure 4.2: MRR plots for segregated current values (a) MRR v/s current; (b) MRR v/s magnetic field (L18 OA)

Optimal Design (Estimation of mean value)

In the experimental analysis, the mean effect plots (Figure 4.1) are used to estimate the mean MRR with optimal design conditions. Mean values of MRR are calculated to give an optimum MRR value. MRR is 'Higher the better' type response. Desired mean in this case is estimated as:

$\mu_{A_6,C_2} = \bar{A}_6 + \bar{C}_2 - \bar{T}$ = 10.149 + 6.232 – 5.58185 = 10.799 mm^3/min

The estimate of μ is only a point estimate based on the average of results calculated on the basis of experiments. Mean value signifies that there are 50 % chances of averages being less than μ and 50 % chances of average being greater than μ. Hence confidence interval is calculated to decide the maximum and the minimum value between which the true average fall at some stated percentage of confidence. Confidence interval around the estimated MRR:

$$CI = \sqrt{\frac{F_{\alpha,v_1,v_2} V_e}{n_{eff}}}$$

Where F_{α,v_1,v_2} = F ratio

α = 0.05 (risk)

Confidence = 1 – α

v_1 = DOF for mean (always 1)

v_2 = DOF for error (pooled)

n_{eff} = Number of tests under that condition using the participating factors

$$n_{eff} = \frac{N}{1 + DOF_{A,C}} = \frac{18}{1+7} = 2.25$$

N = Number of trials in the experiments

$V_e = MS$ (pooled error) = MS (e (pooled)) = $\frac{\text{SS (e (pooled))}}{DOF\ (e\ (pooled))}$

$$CI = \sqrt{\frac{4.96 \times 0.6922}{2.25}} = \pm 1.2352$$

Thus the optimum value of MRR is given by (10.799 ± 1.2352) mm^3/min.

4.1.3 Result and analysis of MRR using bar magnets with PMEDM

Results for MRR

MRR results including their corresponding S/N ratio values are given in Table 4.4 for L27 OA.

Table 4.4: MRR Results (L27 OA-Bar magnet)

S. No.	Magnetic Field (T)	Current (A)	Powder Conc. (gm/l)	Work piece	Tool	Powder	Pulse On Time (µs)	MRR (mm^3/min)			
								Trial 1	Trial 2	Mean	S/N (dB)
1	0	3	3	D2	Cu	Gr	20	5.71	5.84	5.775	15.2294
2	0	3	6	D3	W-Cu	W	50	5.36	6.23	5.795	15.1876
3	0	3	9	H13	C18000	Ti	100	3.157	3.157	3.157	9.9855
4	0	5	3	D2	Cu	W	50	10.923	11.84	11.3815	21.10284
5	0	5	6	D3	W-Cu	Ti	100	10.79	10.658	10.724	20.60664
6	0	5	9	H13	C18000	Gr	20	9.09	7.27	8.18	18.09348
7	0	7	3	D2	Cu	Ti	100	11.31	10.26	10.785	20.62552
8	0	7	6	D3	W-Cu	Gr	20	17.764	17.764	17.764	24.99082
9	0	7	9	H13	C18000	W	50	12.471	13.38	12.9255	22.21283
10	0.09	3	3	D3	C18000	W	100	6.44	6.711	6.5755	16.35304
11	0.09	3	6	H13	Cu	Ti	20	6.1	6.495	6.2975	15.97055
12	0.09	3	9	D2	W-Cu	Gr	50	2.764	3.422	3.093	9.659901
13	0.09	5	3	D3	C18000	Ti	20	13.422	14.21	13.816	22.79705
14	0.09	5	6	H13	Cu	Gr	50	7.534	7.794	7.664	17.68536
15	0.09	5	9	D2	W-Cu	W	100	10.265	9.475	9.87	19.86547
16	0.09	7	3	D3	C18000	Gr	50	18.159	18.291	18.225	25.21318
17	0.09	7	6	H13	Cu	W	100	12.471	13.12	12.7955	22.13276
18	0.09	7	9	D2	W-Cu	Ti	20	11.713	12.502	12.1075	21.64725
19	0.36	3	3	H13	W-Cu	Ti	50	5.236	5.326	5.281	14.45338
20	0.36	3	6	D2	C18000	Gr	100	4.738	4.474	4.606	13.25578
21	0.36	3	9	D3	Cu	W	20	8.553	8.29	8.4215	18.50461
22	0.36	5	3	H13	W-Cu	Gr	100	7.794	8.184	7.989	18.04209
23	0.36	5	6	D2	C18000	W	20	13.292	12.634	12.963	22.24572
24	0.36	5	9	D3	Cu	Ti	50	13.422	12.764	13.093	22.33256
25	0.36	7	3	H13	W-Cu	W	20	12.861	11.951	12.406	21.85511
26	0.36	7	6	D2	C18000	Ti	50	14.61	13.82	14.215	23.04488
27	0.36	7	9	D3	Cu	Gr	100	13.422	11.185	12.3035	12.3035

Analysis of Variance of MRR

ANOVA results for MRR is given in Table 4.5 and response table is given in Table 4.6. ANOVA results for MRR show that current is the most significant parameter for which higher current leads to higher MRR. Workpiece is second important parameter that affects MRR. Out of all the workpiece materials used, D3 die steel shows maximum MRR value as compared to all other workpiece material. Taking other parameters in account, C18000 as tool, concentration up to 6 gm/l, low pulse on time and powder as tungsten have reported high value of MRR. Taking effect of magnetic field in account, very marginal increase in MRR is reported as a combined effect but interaction of current v/s magnetic field has shown important results. MRR is found to increase with increase in field strength as compared to no magnetic field strength for low and moderate current values while contrary results are shown for high current value. About 20 % increase in MRR is observed for lowest current value, which decreases with increase in current. Interaction of current and powder concentration has reported that the best combination for high MRR of current and concentration is highest current with moderate concentration. Figure 4.3 shows the MRR plots corresponding to input parameters along with the interaction plots.

Table 4.5: ANOVA Table for MRR (L27 OA-Bar magnet)

Parameter	DOF	SS	MS	*F* (calculated)
Magnetic Field (T)	2	1.456	0.728	0.16
Current (A)	2	315.126	157.563	34.29
Powder Conc. (gm/l)	2	6.534	3.267	0.71
Workpiece	2	53.611	26.805	5.83
Tool	2	5.287	2.643	0.58
Powder	2	3.154	1.577	0.34
Pulse On Time (µs)	2	20.756	10.378	2.26
Magnetic Field × Current	4	6.243	1.561	0.34
Current × Powder Conc.	4	5.085	1.271	0.26
Error	4	18.38	4.595	
Total	26	435.632		
e (pooled)	22	66.895	3.040	

Table 4.6: Response Table for MRR (L27 OA-Bar magnet)

Level	Magnetic Field (T)	Current (A)	Powder Conc. (gm/l)	Workpiece	Tool	Powder	Pulse On Time (µs)
1	9.610	5.445	10.248	9.422	9.835	9.511	10.859
2	10.049	10.631	10.314	11.858	9.448	10.348	10.186
3	10.142	13.725	9.239	8.522	10.518	9.942	8.756
Delta	0.532	8.281	1.075	3.336	1.070	0.837	2.103
Rank	7	1	4	2	5	6	3

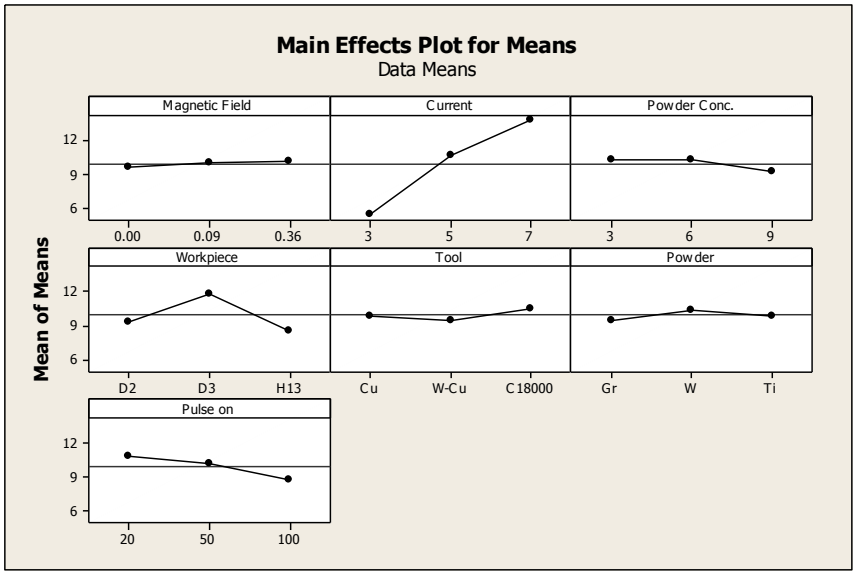

(a)

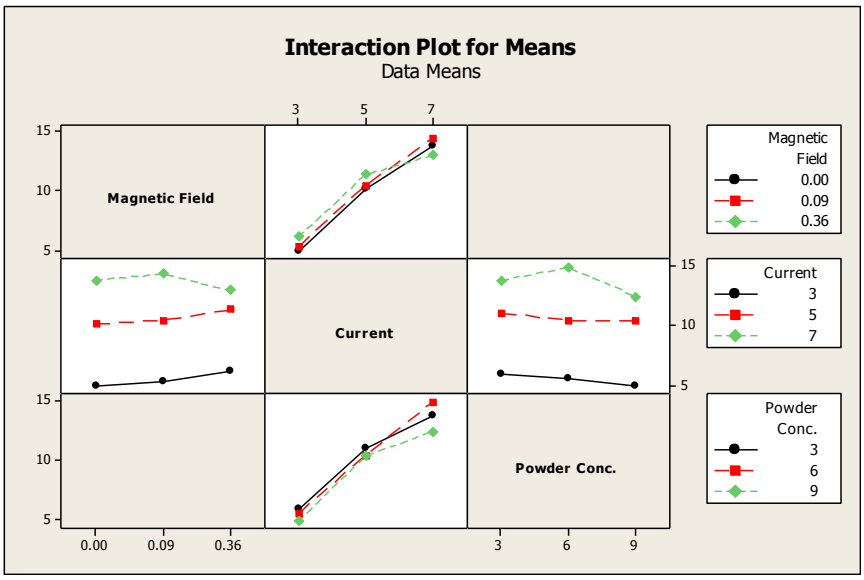

(b)

Figure 4.3: MRR plots (a) Main effect plots; (b) Interaction Plots (L27 OA-Bar magnet)

Analysis of variance of S/N ratio

For calculating S/N ratio for MRR, higher the better criterion is used identifying major contributing input parameters that cause the variation in the MRR using Equation 3.1. Current is the most significant parameter, then workpiece and then pulse on time. Table 4.7 shows ANOVA table for S/N ratio and Table 4.8 shows response table for S/N ratio. Figure 4.4 shows main effect plots and interaction plots for S/N ratio.

Table 4.7: ANOVA Table for S/N ratio for MRR (L27 OA-Bar magnet)

Parameter	DOF	SS	MS	*F* (calculated)
Magnetic Field (T)	2	3.048	1.524	0.58
Current (A)	2	331.780	165.890	58.73
Powder Conc. (gm/l)	2	9.646	4.823	1.71
Workpiece	2	45.277	22.639	8.01
Tool	2	4.898	2.449	0.87
Powder	2	13.518	6.759	2.39
Pulse On Time (µs)	2	19.665	9.832	3.48
Magnetic Field × Current	4	5.420	1.355	0.48
Current × Powder Conc.	4	6.001	1.500	0.53
Error	4	11.299	2.825	
Total	26	450.552		

Table 4.8: Response Table for S/N ratio for MRR (L27 OA-Bar magnet)

Level	Magnetic Field (T)	Current (A)	Powder Conc. (gm/l)	Workpiece	Tool	Powder	Pulse On Time (µs)
1	18.67	14.29	19.52	18.52	19.48	18.21	20.15
2	19.04	20.31	19.46	20.85	18.48	19.94	18.99
3	19.49	22.60	18.22	17.83	19.24	19.05	18.06
Delta	0.82	8.31	1.30	3.03	1.00	1.73	2.09
Rank	7	1	5	2	6	4	3

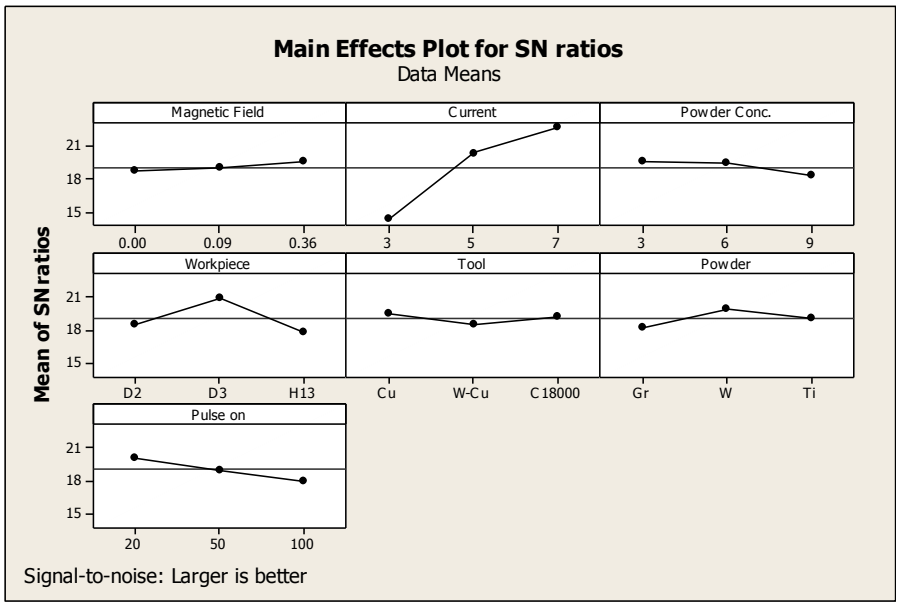

(a)

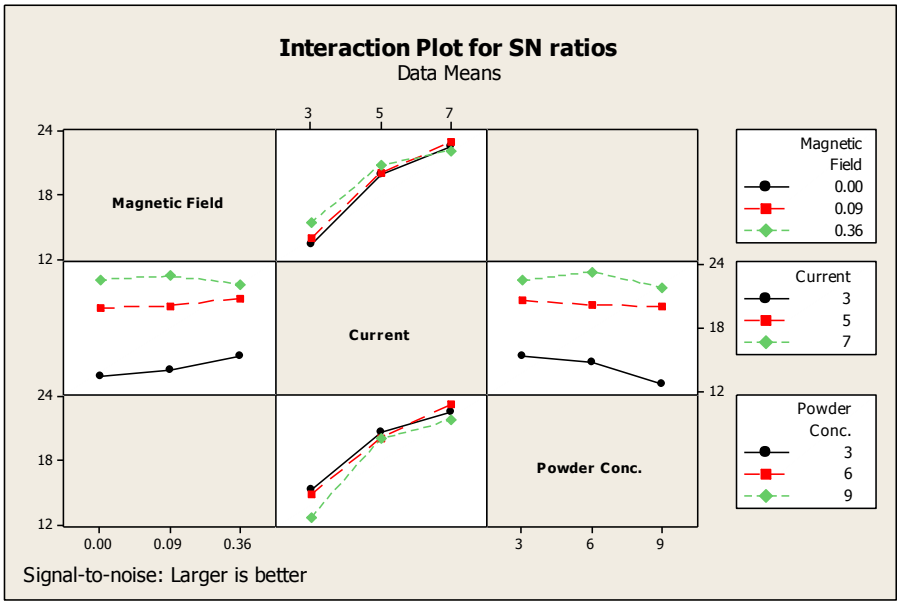

(b)

Figure 4.4: S/N ratio plots for MRR (a) Main effect plots; (b) Interaction plots (L27 OA-Bar magnet)

Optimal Design (Estimation of mean value)

In the experimental analysis, the mean effect plots corresponding to PMEDM (bar magnets assisted) (Figure 4.3) are used to estimate the mean MRR with optimal design conditions. Mean values of MRR are calculated to give an optimum MRR value. MRR is 'Higher the better' type response. Desired mean in this case is estimated as:

$\mu_{B_3,D_2} = \bar{B}_3 + \bar{D}_2 - \bar{T}$ = 13.725 + 11.858 – 9.9336 = 15.629 mm^3/min

Confidence interval around the estimated MRR:

$$CI = \sqrt{\frac{F_{\alpha,v_1,v_2} V_e}{n_{eff}}} = \sqrt{\frac{4.3 \times 3.0406}{5.4}} = \pm 1.556$$

Where $n_{eff} = \frac{N}{1 + DOF_{B,D}} = \frac{27}{1+4} = 5.4$

Thus the optimum value of MRR is given by (15.629 ± 1.556) mm^3/min.

4.1.4 Result and analysis of MRR using ring magnet with PMEDM

Results for MRR

MRR results with its calculated S/N ratio value for magnetic field assisted PMEDM using ring magnet are tabulated in Table 4.9.

Table 4.9: MRR Results (L27 OA-Ring magnet)

S. No.	Magnetic Field (T)	Current (A)	Powder Conc. (gm/l)	Work piece	Tool	Powder	Pulse On time (µs)	MRR (mm^3/min)			
								Trial 1	Trial 2	Mean	S/N (dB)
1	0	3	3	D2	Cu	Gr	20	6.396	5.87	6.133	15.7295
2	0	3	6	D3	W-Cu	W	50	5.869	5.869	5.869	15.3713
3	0	3	9	H13	C18000	Ti	100	2.786	3.306	3.046	9.5796
4	0	5	3	D2	Cu	W	50	10.379	11.449	10.914	20.72836
5	0	5	6	D3	W-Cu	Ti	100	10.79	10.658	10.724	20.60664
6	0	5	9	H13	C18000	Gr	20	8.314	8.054	8.184	18.25602
7	0	7	3	D2	Cu	Ti	100	11.055	9.212	10.1335	20.0073
8	0	7	6	D3	W-Cu	Gr	20	20.659	19.08	19.8695	25.94316
9	0	7	9	H13	C18000	W	50	13.64	14.419	14.0295	22.9308
10	0.075	3	3	D3	C18000	W	100	6.053	7.105	6.579	16.27982
11	0.075	3	6	H13	Cu	Ti	20	6.625	5.196	5.9105	15.24161
12	0.075	3	9	D2	W-Cu	Gr	50	4.737	4.474	4.6055	13.25491
13	0.075	5	3	D3	C18000	Ti	20	14.211	14.606	14.4085	23.16993
14	0.075	5	6	H13	Cu	Gr	50	8.184	8.184	8.184	18.25931
15	0.075	5	9	D2	W-Cu	W	100	10.265	10.396	10.3305	20.2819
16	0.075	7	3	D3	C18000	Gr	50	15.568	16.448	16.008	24.0769
17	0.075	7	6	H13	Cu	W	100	13.64	12.471	13.0555	22.28975
18	0.075	7	9	D2	W-Cu	Ti	20	10.791	11.45	11.1205	20.91105
19	0.17	3	3	H13	W-Cu	Ti	50	4.676	5.585	5.1305	14.10081
20	0.17	3	6	D2	C18000	Gr	100	4.737	4.343	4.54	13.11658
21	0.17	3	9	D3	Cu	W	20	9.342	9.342	9.342	19.4088
22	0.17	5	3	H13	W-Cu	Gr	100	7.794	7.664	7.729	17.76154
23	0.17	5	6	D2	C18000	W	20	11.844	12.502	12.173	21.69843
24	0.17	5	9	D3	Cu	Ti	50	12.632	12.5	12.566	21.98358
25	0.17	7	3	H13	W-Cu	W	20	12.211	13.25	12.7305	22.07521
26	0.17	7	6	D2	C18000	Ti	50	12.765	13.818	13.2915	22.45103
27	0.17	7	9	D3	Cu	Gr	100	12.5	12.764	12.632	22.02802

Analysis of Variance of MRR

Table 4.10 and 4.11 represent ANOVA and response table for MRR using ring magnet. As a result of ANOVA analysis, it is observed that current is the most significant parameter while workpiece material is the second most important process parameter. Higher the current, higher is the MRR, while maximum MRR is observed for D3 workpiece. Taking other parameters in account, optimum parameters for MRR are moderate powder concentration, tungsten powder and C18000 tool. Interactions show that maximum current and moderate powder concentration are desired parameters, while interaction plots of current v/s magnetic field shows that for different current values, MRR curve shows continuous increase with increase in field strength except for maximum current value for which MRR reduces for

maximum field strength. For minimum current value almost 25 % increase in MRR is observed while for moderate current about 11 % improvements are noticed. Main plots and interaction plots for MRR are shown in Figure 4.5.

Table 4.10: ANOVA Table for MRR (L27 OA-Ring magnet)

Parameter	DOF	SS	MS	*F* (calculated)
Magnetic Field (T)	2	0.119	0.059	0.01
Current (A)	2	290.705	145.353	32.29
Powder Conc. (gm/l)	2	3.346	1.673	0.37
Workpiece	2	57.047	28.524	6.34
Tool	2	1.085	0.542	0.12
Powder	2	4.775	2.387	0.53
Pulse On Time (µs)	2	24.859	12.430	2.76
Magnetic Field × Current	4	9.491	2.373	0.53
Current × Powder Conc.	4	11.935	2.984	0.66
Error	4	18.007	4.502	
Total	26	382.767		
e (pooled)	20	10.156	0.508	

Table 4.11: Response Table for MRR (L27 OA-Ring magnet)

Level	Magnetic Field (T)	Current (A)	Powder Conc. (gm/l)	Workpiece	Tool	Powder	Pulse On Time (µs)
1	9.878	5.684	9.974	9.249	9.875	9.765	11.097
2	10.022	10.579	10.402	12.000	9.790	10.559	10.066
3	10.015	13.652	9.540	8.667	10.251	9.592	8.752
Delta	0.144	7.968	0.862	3.333	0.461	0.966	2.345
Rank	7	1	5	2	6	4	3

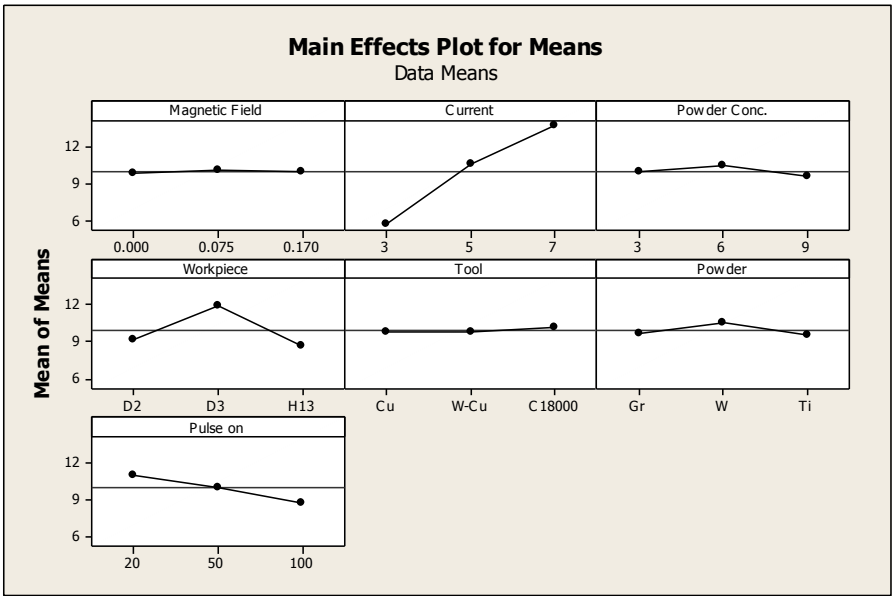

(a)

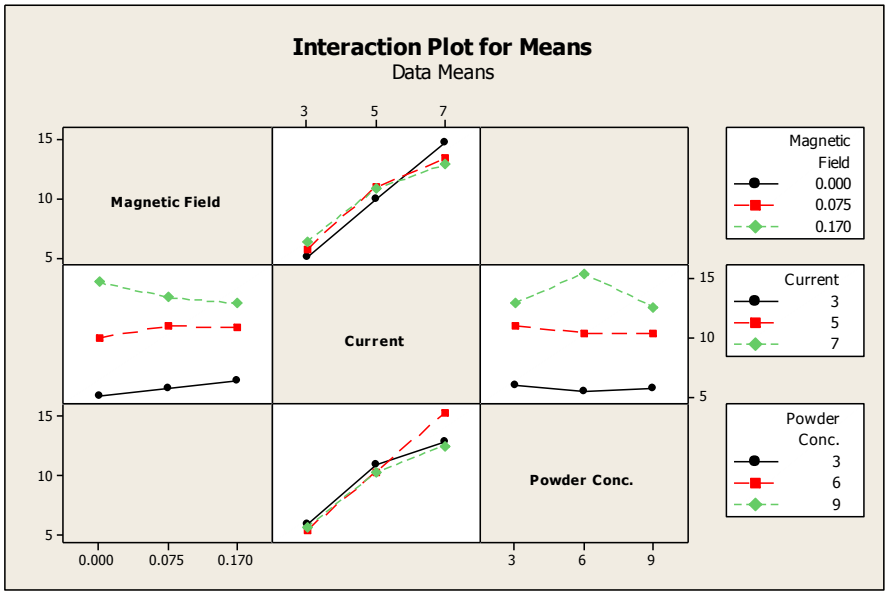

(b)

Figure 4.5: MRR plots (a) Main effect plots; (b) Interaction plots (L27 OA-Ring magnet)

Analysis of variance of S/N ratio

S/N ratio for MRR results with higher the better constraint (using Equation 3.1) is considered. Table 4.12 and 4.13 show ANOVA for S/N ratio and Response table for S/N ratio respectively. Figure 4.6 shows the main effect plots and interaction plots for S/N ratio. Response table shows that current is most significant parameter while tool is found to be the least effecting parameter.

Table 4.12: ANOVA Table for S/N ratio for MRR (L27 OA-Ring magnet)

Parameter	DOF	SS	MS	*F* (calculated)
Magnetic Field (T)	2	1.924	0.962	0.45
Current (A)	2	294.595	147.298	68.66
Powder Conc. (gm/l)	2	2.569	1.285	0.60
Workpiece	2	47.857	23.929	11.15
Tool	2	1.754	0.877	0.41
Powder	2	12.193	6.096	2.84
Pulse On Time (µs)	2	23.377	11.688	5.45
Magnetic Field × Current	4	6.083	1.521	0.71
Current × Powder Conc.	4	5.104	1.276	0.59
Error	4	8.581	2.145	
Total	26	404.037		

Table 4.13: Response Table for S/N ratio for MRR (L27 OA-Ring magnet)

Level	Magnetic Field (T)	Current (A)	Powder Conc. (gm/l)	Workpiece	Tool	Powder	Pulse On Time (µs)
1	18.79	14.68	19.33	18.69	19.52	18.71	20.27
2	19.31	20.31	19.44	20.99	18.92	20.12	19.24
3	19.40	22.52	18.74	17.83	19.06	18.67	17.99
Delta	0.61	7.85	0.70	3.15	0.60	1.45	2.28
Rank	6	1	5	2	7	4	3

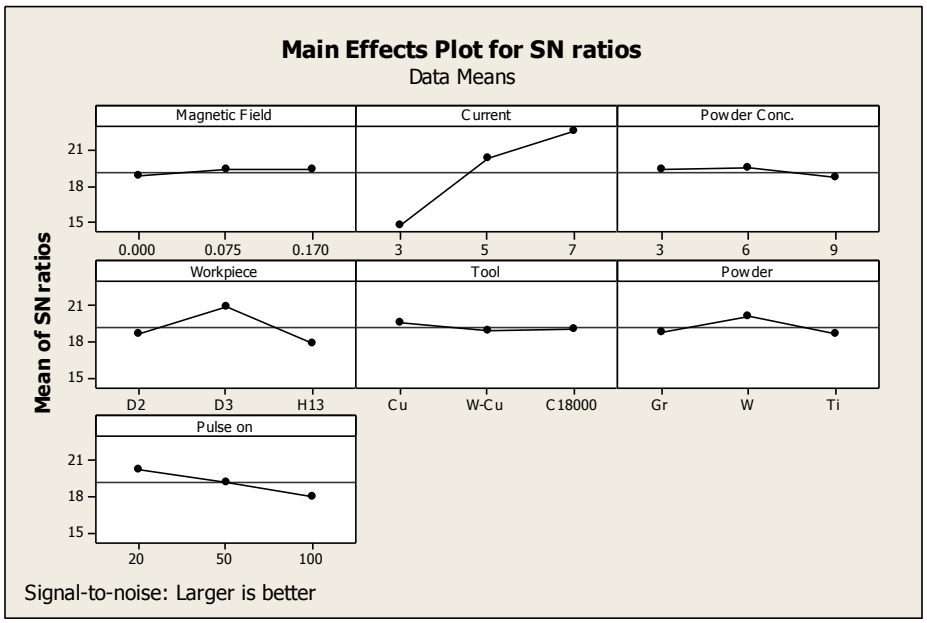

(a)

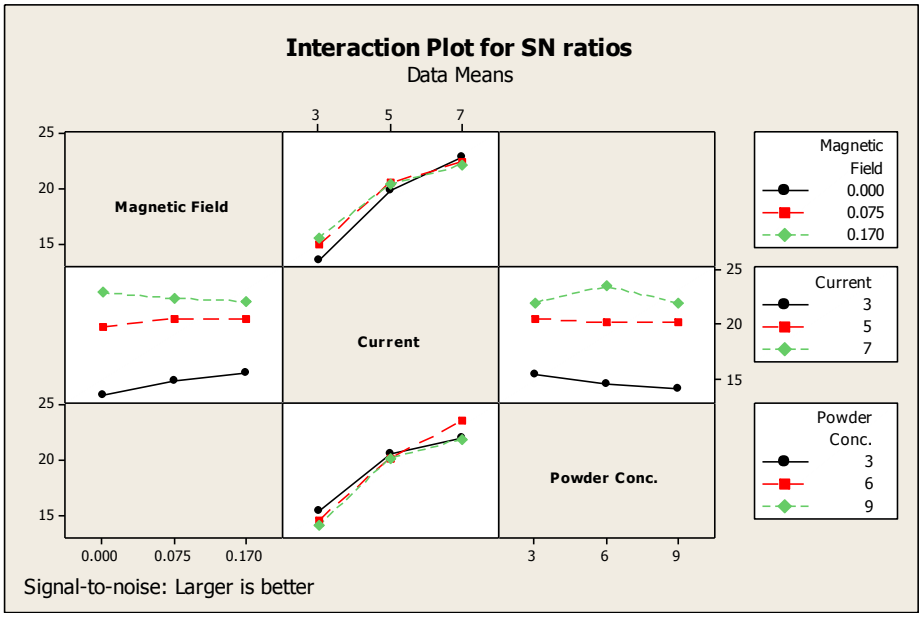

(b)

Figure 4.6: S/N ratio plots for MRR (a) Main effect plots; (b) Interaction plots (L27 OA-Ring magnet)

Optimal Design (Estimation of mean value)

In the experimental analysis, the mean effect plots corresponding to PMEDM (ring magnet assisted) (Figure 4.5) are used to estimate the mean MRR with optimal design conditions. Mean values of MRR are calculated to give an optimum MRR value. MRR is 'Higher the better' type response. Desired mean in this case is estimated as:

$\mu_{B_3,D_2,G_1} = \bar{B}_3 + \bar{D}_2 + \bar{G}_1 - 2\bar{T}$ = 13.652 + 12 + 11.097 – 2 × 9.972 = 16.805 mm^3/min

Confidence interval around the estimated MRR:

$$CI = \sqrt{\frac{F_{\alpha,v_1,v_2} V_e}{n_{eff}}} = \sqrt{\frac{4.35 \times 0.508}{5.4}} = \pm 0.64$$

Where $n_{eff} = \frac{N}{1 + DOF_{B,D}} = \frac{27}{1+6} = 3.85$

Thus the optimum value of MRR is given by (16.805 ± 0.64) mm^3/min.

4.2 RESULTS AND ANALYSIS OF TWR

4.2.1 Introduction

TWR is calculated measuring the difference between initial and final weight of tool electrode using a weighing machine with least count as 0.001 gm. For each trial TWR is calculated using Equation 4.2.

$$TWR = \frac{(w_{it} - w_{ft}) \times 1000}{\rho_t \times t} \ (\text{mm}^3/\text{min}) \qquad (4.2)$$

Where w_{it} =Initial weight of the tool material (in gm),

w_{ft} =Final weight of tool material after experimentation (in gm),

ρ_t =Density of tool material (in gm/cm^3) and

t =Machining time (in min).

4.2.2 Result and analysis of TWR using bar magnets with conventional EDM

Results for TWR

TWR results of mean value are shown in Table 4.14 for L18 OA.

Table 4.14: TWR Results (L18 OA)

S. No.	Current (A)	Magnetic Field (T)	Work piece	Tool	Pulse On Time (μs)	TWR (mm^3/min)
1	3	0	D2	Cu	50	0.0561
2	3	0.09	D3	W-Cu	100	0.0285
3	3	0.36	H13	C18000	200	0.0568
4	4	0	D2	W-Cu	100	0.1142
5	4	0.09	D3	C18000	200	0.1136
6	4	0.36	H13	Cu	50	0.1123
7	5	0	D3	Cu	200	0.1123
8	5	0.09	H13	W-Cu	50	0.1142
9	5	0.36	D2	C18000	100	0.1136
10	6	0	H13	C18000	100	0.2272
11	6	0.09	D2	Cu	200	0.2246
12	6	0.36	D3	W-Cu	50	0.1143
13	7	0	D3	C18000	50	0.4543
14	7	0.09	H13	Cu	100	0.2245
15	7	0.36	D2	W-Cu	200	0.1143
16	8	0	H13	W-Cu	200	0.2286
17	8	0.09	D2	C18000	50	0.4543
18	8	0.36	D3	Cu	100	0.3368

Analysis of Variance of TWR

ANOVA is applied to find the significant parameters and their respective effect on the performance parameter. Table 4.15 and 4.16 show the ANOVA and response table for TWR for L18 trials conducted with bar magnet without powder mixed in dielectric medium. From ANOVA table it is observed that most significant factor for TWR is current and tool material. With increase in current, TWR increases and reaches maximum with maximum level of current. Further TWR is supposed to be inversely proportional to the hardness of the tool. Harder the tool, lower is the TWR. Hence minimum TWR is observed with tungsten-copper tool, while maximum TWR is observed for C18000, copper alloy. Further TWR reduces with increase in pulse on time. In this case also magnetic field is insignificant as compared to current, but it reduces TWR as observed at individual level. TWR plots drawn on the basis of segregated results corresponding to current show that TWR for magnetic assisted EDM show reduced TWR values as compared to that of the no magnetic field assisted strength. Hence magnetic field is also helpful in reducing TWR up to a limit. Response table shows that current is the most significant parameter while workpiece is least significant. Figure 4.7 and 4.8 show main effect plots and segregated current value plots for TWR.

Table 4.15: ANOVA Table for TWR (L18 OA)

Parameter	DOF	SS	MS	*F* (calculated)
Current (A)	5	0.177798	0.035560	7.00
Magnetic Field (T)	2	0.012052	0.006026	1.19
Workpiece	2	0.003234	0.001617	0.32
Tool	2	0.041501	0.020751	4.09
Pulse On Time (µs)	2	0.017396	0.008698	1.71
Error	4	0.020317	0.005079	
Total	17	0.272298		
e (pooled)	10	0.052992	0.005299	

Table 4.16: Response Table for TWR (L18 OA)

Level	Current (A)	Magnetic Field (T)	Workpiece	Tool	Pulse On Time (µs)
1	0.04763	0.19878	0.17952	0.17777	0.21758
2	0.11337	0.19328	0.19330	0.11902	0.17413
3	0.11337	0.14135	0.16060	0.23663	0.14170
4	0.18870				
5	0.26437				
6	0.33990				
Delta	0.29277	0.05743	0.03270	0.11762	0.07588
Rank	1	4	5	2	3

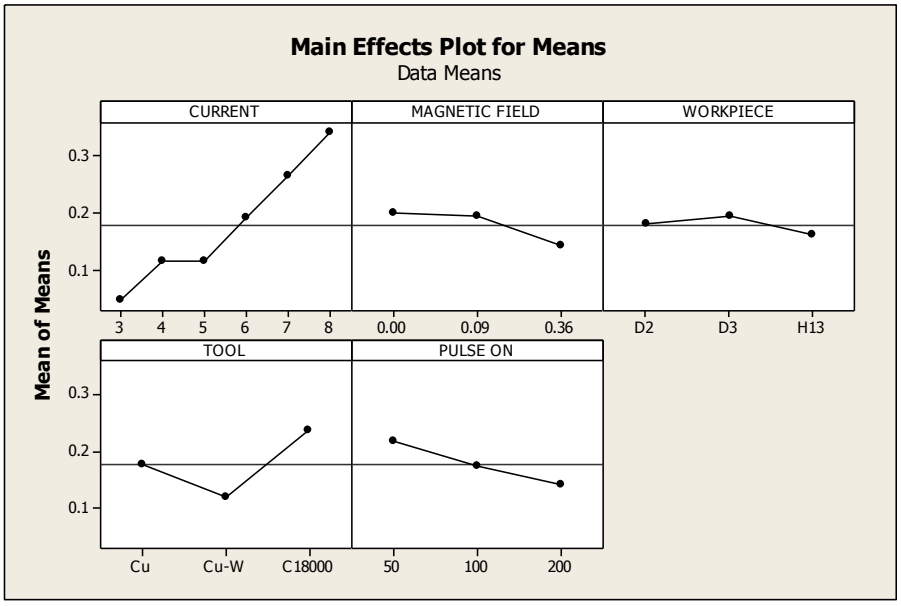

Figure 4.7: Main Effect plots for TWR (L18 OA)

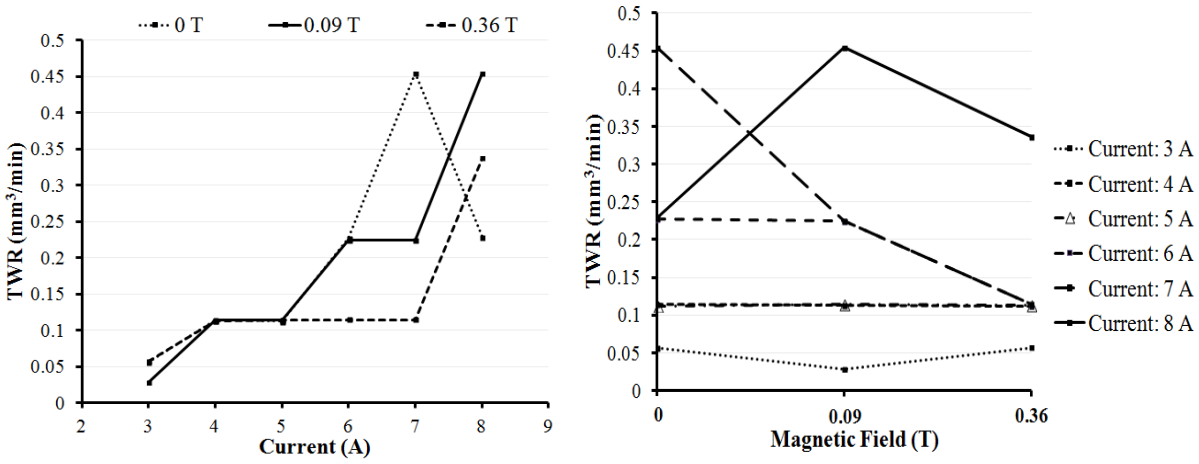

(a) (b)

Figure 4.8: TWR plots for segregated current values (a) TWR v/s Current; (b) TWR v/s magnetic field (L18 OA)

Optimal design (Estimation of mean value)

In the experimental analysis, the mean effect plots (Figure 4.7) are used to estimate the mean TWR values with optimal design conditions. Mean values of TWR are calculated to give an optimum TWR value. TWR is 'Lower the better' type response. Desired mean in this case is estimated as:

$\mu_{A_2,D_2} = \bar{A}_2 + \bar{D}_2 - \bar{T}$ = 0.11337 + 0.119 – 0.1762 = 0.056 mm^3/min

Confidence interval around the estimated TWR:

$$n_{eff} = \frac{N}{1+ DOF_{A,D}} = \frac{18}{1+7} = 2.25$$

$$CI = \sqrt{\frac{F_{\alpha,v_1,v_2} V_e}{n_{eff}}} = \sqrt{\frac{4.96 \times 0.00529}{2.25}} = \pm 0.108$$

Thus the optimum value of TWR is given by (0.056 ± 0.108) mm^3/min.

4.2.3 Result and analysis of TWR using bar magnets with PMEDM

Results for TWR

Results corresponding to TWR values for both the trials including their calculated S/N ratio values are shown in Table 4.17 for L27 trials.

Table 4.17: TWR Results (L27 OA-Bar magnet)

S. No.	Magnetic Field (T)	Current (A)	Powder Conc. (gm/l)	Work piece	Tool	Powder	Pulse On Time (µs)	TWR (mm^3/min)			
								Trial 1	Trial 2	Mean	S/N (dB)
1	0	3	3	D2	Cu	Gr	20	0.2245	0.3368	0.28065	10.86625
2	0	3	6	D3	W-Cu	W	50	0.2285	0.1143	0.1714	14.86272
3	0	3	9	H13	C18000	Ti	100	0.1136	0.1136	0.1136	18.89243
4	0	5	3	D2	Cu	W	50	0.3368	0.2245	0.28065	10.86625
5	0	5	6	D3	W-Cu	Ti	100	0.1143	0.1143	0.1143	18.83908
6	0	5	9	H13	C18000	Gr	20	0.4543	0.3407	0.3975	7.925474
7	0	7	3	D2	Cu	Ti	100	0.2245	0.1122	0.16835	15.01765
8	0	7	6	D3	W-Cu	Gr	20	0.4571	0.4571	0.4571	6.799776
9	0	7	9	H13	C18000	W	50	0.6815	0.4543	0.5679	4.74417
10	0.09	3	3	D3	C18000	W	100	0.2271	0.1136	0.17035	14.91609
11	0.09	3	6	H13	Cu	Ti	20	0.2245	0.2245	0.2245	12.97567
12	0.09	3	9	D2	W-Cu	Gr	50	0	0.1143	0.05715	21.84938
13	0.09	5	3	D3	C18000	Ti	20	0.4543	0.4543	0.4543	6.853145
14	0.09	5	6	H13	Cu	Gr	50	0.3368	0.2245	0.28065	10.86625
15	0.09	5	9	D2	W-Cu	W	100	0.1143	0.1143	0.1143	18.83908
16	0.09	7	3	D3	C18000	Gr	50	0.4543	0.6815	0.5679	4.74417
17	0.09	7	6	H13	Cu	W	100	0.2245	0.3368	0.28065	10.86625
18	0.09	7	9	D2	W-Cu	Ti	20	0.2285	0.2285	0.2285	12.82228
19	0.36	3	3	H13	W-Cu	Ti	50	0.1143	0.1143	0.1143	18.83908
20	0.36	3	6	D2	C18000	Gr	100	0.1136	0.1136	0.1136	18.89243
21	0.36	3	9	D3	Cu	W	20	0.2245	0.1122	0.16835	15.01765
22	0.36	5	3	H13	W-Cu	Gr	100	0.2285	0.1143	0.1714	14.86272
23	0.36	5	6	D2	C18000	W	20	0.4543	0.6815	0.5679	4.74417
24	0.36	5	9	D3	Cu	Ti	50	0.1122	0.2245	0.16835	15.01765
25	0.36	7	3	H13	W-Cu	W	20	0.3428	0.2285	0.28565	10.71287
26	0.36	7	6	D2	C18000	Ti	50	0.5679	0.4543	0.5111	5.776573
27	0.36	7	9	D3	Cu	Gr	100	0.3368	0.3368	0.3368	9.452558

Analysis of Variance of TWR

TWR results for powder mixed EDM with bar magnet analysed with ANOVA techniques are reported in Table 4.18 and their response table is provided in Table 4.19. Main effect plot and interaction plots are provided in Figure 4.9. ANOVA results have reported that the most significant parameter is current, which increases TWR. TWR is found maximum with maximum current value. After current, tool is the next significant parameter affecting TWR; maximum TWR is observed for C18000 electrode, then for copper and least for tungsten-copper. Increase in pulse on time reduces TWR while titanium as powder reported minimum TWR value amongst all the used powders. Maximum powder concentration results in minimum TWR. Taking interactions in account, interaction of magnetic field and current has shown that for most of the current values, TWR decreases with increase in field strengths.

Interaction of current and powder concentration shows that TWR attains maximum value at moderate concentration and reduces afterwards for all the current values.

Table 4.18: ANOVA Table for TWR (L27 OA-Bar magnet)

Parameter	DOF	SS	MS	*F* (calculated)
Magnetic Field (T)	2	0.001721	0.000861	0.09
Current (A)	2	0.221477	0.110739	10.99
Powder Conc. (gm/l)	2	0.018209	0.009105	0.90
Workpiece	2	0.004629	0.002314	0.23
Tool	2	0.182011	0.091005	s9.03
Powder	2	0.021584	0.010792	1.07
Pulse On Time (µs)	2	0.133457	0.066728	6.62
Magnetic Field × Current	4	0.007715	0.001929	0.19
Current × Powder Conc.	4	0.014553	0.003638	0.36
Error	4	0.040295	0.010074	
Total	26	0.645651		
e (pooled)	20	0.108706	0.005435	

Table 4.19: Response Table for TWR (L27 OA-Bar magnet)

Level	Magnetic Field (T)	Current (A)	Powder Conc. (gm/l)	Workpiece	Tool	Powder	Pulse On Time (µs)
1	0.2835	0.1571	0.2771	0.2580	0.2432	0.2959	0.3405
2	0.2643	0.2833	0.3024	0.2899	0.1905	0.2897	0.3022
3	0.2708	0.3742	0.2392	0.2707	0.3849	0.2330	0.1759
Delta	0.0192	0.2211	0.0632	0.0319	0.1944	0.0628	0.1646
Rank	7	1	4	6	2	5	3

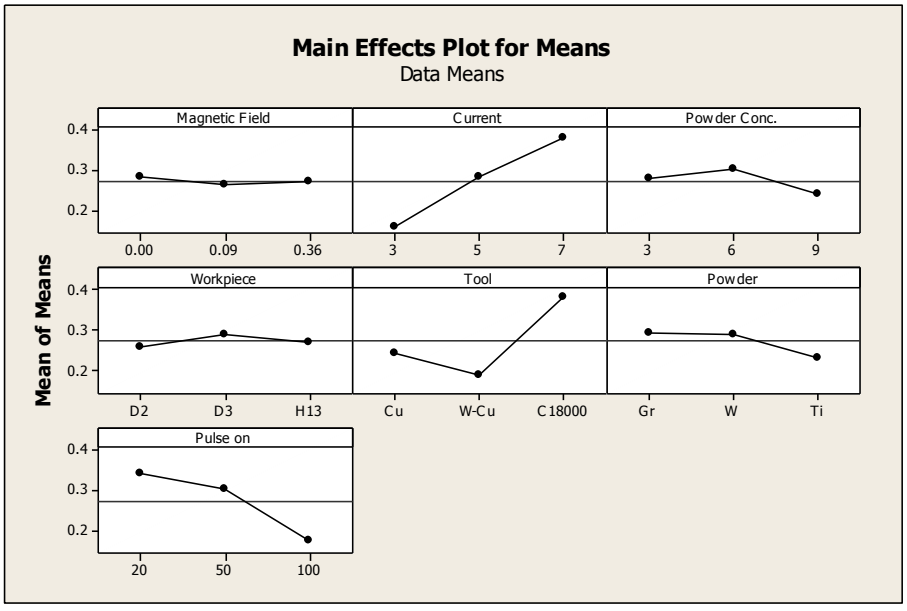

(a)

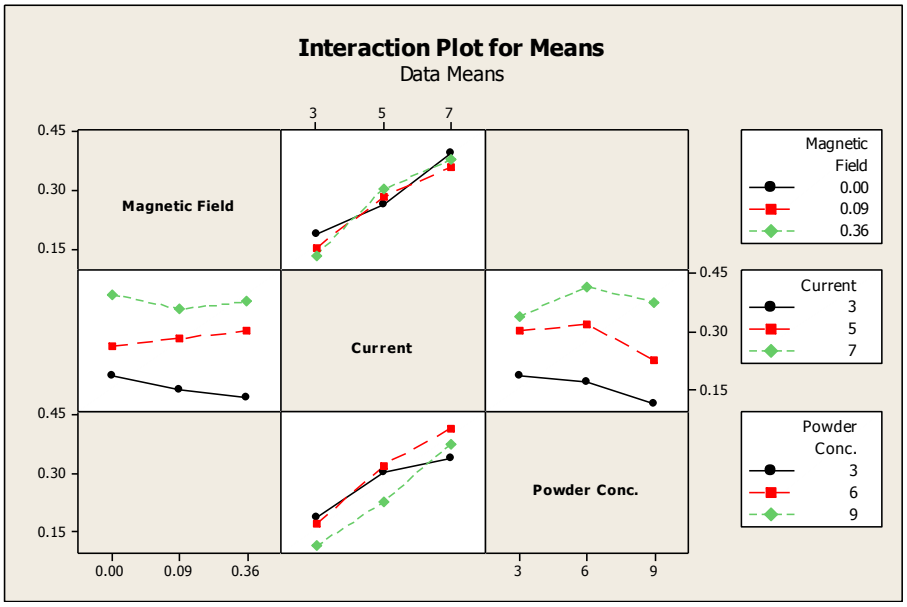

(b)

Figure 4.9: TWR plots (a) Main effect plots; (b) Interaction plots (L27 OA-Bar magnet)

Analysis of variance of S/N ratio

For TWR, lower the better criterion is followed for calculation of S/N ratio (using Equation 3.2). From S/N ratio values it is observed that current is observed to be the most significant parameter, then pulse on time and then the tool material. Lowest contributing factor towards S/N ratio is magnetic field. Table 4.20 shows ANOVA table for S/N ratio values and Table 4.21 shows response table for S/N ratio. Main effect plots and interaction plots are shown in Figure 4.10.

Table 4.20: ANOVA Table for S/N ratio for TWR (L27 OA-Bar magnet)

Parameter	DOF	SS	MS	*F* (calculated)
Magnetic Field (T)	2	2.122	1.061	0.23
Current (A)	2	245.299	122.649	26.06
Powder Conc. (gm/l)	2	25.625	12.812	2.72
Workpiece	2	10.066	5.033	1.07
Tool	2	144.45	72.225	15.35
Powder	2	27.104	13.552	2.88
Pulse On Time (µs)	2	153.135	76.567	16.27
Magnetic Field × Current	4	11.804	2.951	0.63
Current × Powder Conc.	4	21.720	5.430	1.15
Error	4	18.823	4.706	
Total	26	660.148		

Table 4.21: Response Table for S/N ratio for TWR (L27 OA-Bar magnet)

Level	Magnetic Field (T)	Current (A)	Powder Conc. (gm/l)	Workpiece	Tool	Powder	Pulse On Time (µs)
1	12.090	16.346	11.964	13.297	12.327	11.807	9.857
2	12.748	12.090	11.625	11.834	15.381	11.730	11.952
3	12.591	8.993	13.840	12.298	9.721	13.893	15.620
Delta	0.658	7.353	2.215	1.463	5.660	2.163	5.762
Rank	7	1	4	6	3	5	2

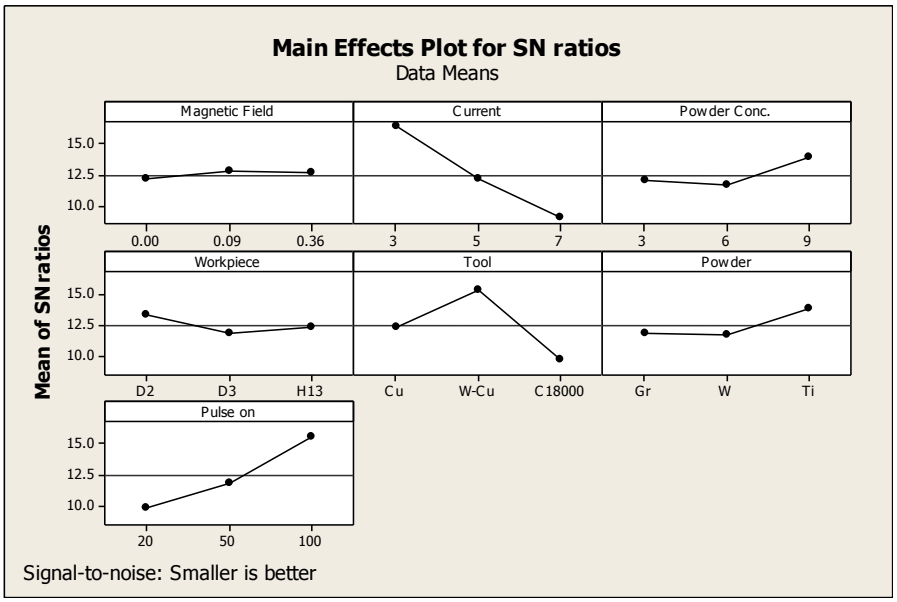

(a)

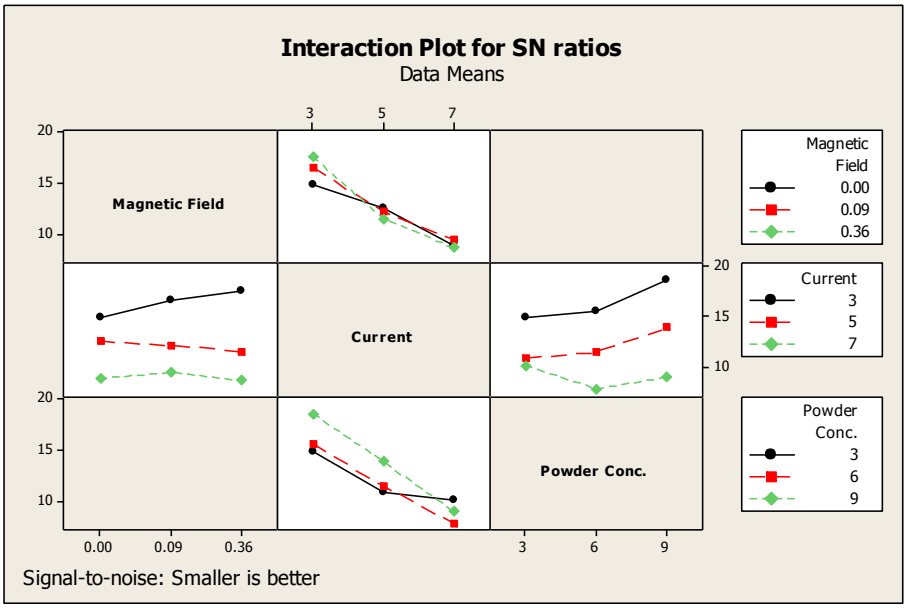

(b)

Figure 4.10: S/N ratio plots for TWR (a) Main Effect plot; (b) Interaction Plot (L27 OA-Bar magnet)

Optimal Design (Estimation of mean value)

In the experimental analysis, the mean effect plots corresponding to PMEDM (bar magnets assisted) (Figure 4.9) are used to estimate the mean TWR with optimal design conditions. Mean values of TWR are calculated to give an optimum TWR value. TWR is 'Lower the better' type response. Desired mean in this case is estimated as:

$\mu_{B_2,E_2,G_3} = \bar{B}_2 + \bar{E}_2 + \bar{G}_3 - 2\bar{T}$ = 0.2833 + 0.1905 + 0.1759 – 2 × 0.2728 = 0.1041 mm^3/min

Confidence interval around the estimated TWR:

$$CI = \sqrt{\frac{F_{\alpha,v_1,v_2} V_e}{n_{eff}}}$$

$$n_{eff} = \frac{N}{1 + DOF_{B,E,G}} = \frac{27}{1+6} = 3.857$$

$$CI = \sqrt{\frac{4.35 \times 0.005435}{3.857}} = \pm 0.0783$$

Thus the optimum value of TWR is given by (0.1041 ± 0.0783) mm^3/min.

4.2.4 Result and analysis of TWR using ring magnets with PMEDM

Results for TWR

TWR results for L27 OA for powder mixed EDM with ring magnet with S/N ratio calculation is presented in Table 4.22.

Table 4.22: TWR Results (L27 OA-Ring magnet)

S. No.	Magnetic Field (T)	Current (A)	Powder Conc. (gm/l)	Work piece	Tool	Powder	Pulse On Time (µs)	TWR (mm^3/min)			
								Trial 1	Trial 2	Mean	S/N (dB)
1	0	3	3	D2	Cu	Gr	20	0.2245	0.2245	0.2245	12.97567
2	0	3	6	D3	W-Cu	W	50	0.2285	0.1143	0.1714	14.86272
3	0	3	9	H13	C18000	Ti	100	0.1136	0.1136	0.1136	18.89243
4	0	5	3	D2	Cu	W	50	0.1122	0.2245	0.16835	15.01765
5	0	5	6	D3	W-Cu	Ti	100	0.1143	0.1143	0.1143	18.83908
6	0	5	9	H13	C18000	Gr	20	0.4543	0.4543	0.4543	6.853145
7	0	7	3	D2	Cu	Ti	100	0.2245	0.1122	0.16835	15.01765
8	0	7	6	D3	W-Cu	Gr	20	0.4571	0.3428	0.39995	7.872103
9	0	7	9	H13	C18000	W	50	0.5679	0.6815	0.6247	4.050814
10	0.075	3	3	D3	C18000	W	100	0.2271	0.1136	0.17035	14.91609
11	0.075	3	6	H13	Cu	Ti	20	0.2245	0.2245	0.2245	12.97567
12	0.075	3	9	D2	W-Cu	Gr	50	0	0.1143	0.05715	21.84938
13	0.075	5	3	D3	C18000	Ti	20	0.4543	0.3407	0.3975	7.925474
14	0.075	5	6	H13	Cu	Gr	50	0.2245	0.3368	0.28065	10.86625
15	0.075	5	9	D2	W-Cu	W	100	0.2285	0.1143	0.1714	14.86272
16	0.075	7	3	D3	C18000	Gr	50	0.5679	0.5679	0.5679	4.914563
17	0.075	7	6	H13	Cu	W	100	0.449	0.3368	0.3929	8.026709
18	0.075	7	9	D2	W-Cu	Ti	20	0.1143	0.2285	0.1714	14.86272
19	0.17	3	3	H13	W-Cu	Ti	50	0.1143	0.2285	0.1714	14.86272
20	0.17	3	6	D2	C18000	Gr	100	0.1136	0.1136	0.1136	18.89243
21	0.17	3	9	D3	Cu	W	20	0.2245	0.3368	0.28065	10.86625
22	0.17	5	3	H13	W-Cu	Gr	100	0.1143	0.1143	0.1143	18.83908
23	0.17	5	6	D2	C18000	W	20	0.3407	0.5679	0.4543	6.589743
24	0.17	5	9	D3	Cu	Ti	50	0.2245	0.3368	0.28065	10.86625
25	0.17	7	3	H13	W-Cu	W	20	0.3428	0.2285	0.28565	10.71287
26	0.17	7	6	D2	C18000	Ti	50	0.4543	0.4543	0.4543	6.853145
27	0.17	7	9	D3	Cu	Gr	100	0.2245	0.2245	0.2245	12.97567

Analysis of Variance of TWR

ANOVA table for TWR is given in Table 4.23 and response table is given in Table 4.24. As shown from ANOVA table and TWR plots (Figure 4.11), it is concluded that TWR is significantly affected by current, tool and pulse on time. With increase in current, TWR increases and reaches maximum at maximum current value. TWR is inversely proportional to the hardness of the tool material. Harder the tool, lesser is the tool wear. Hence TWR is

highest for C18000 tool, which decreases for copper and is significantly very low for tungsten-copper. With increase in pulse on time TWR decreases. With magnetic field, TWR is reduced by almost negligible amount. TWR increases with powder concentration from low value of concentration, but decreases afterwards. TWR is found highest for tungsten metal powder, which is of highest hardness amongst all the used powders and is found lowest for titanium powder. From interaction plots it is observed that TWR decreases with magnetic field at maximum current value while increases at moderate and low current values. Further best level for TWR is lower current and lower powder concentration. Response plot shows that current is the most significant input parameter while magnetic field is least.

Table 4.23: ANOVA Table for TWR (L27 OA-Ring magnet)

Parameter	DOF	SS	MS	*F* (calculated)
Magnetic Field (T)	2	0.000245	0.000122	0.01
Current (A)	2	0.172634	0.086317	8.71
Powder Conc. (gm/l)	2	0.006588	0.003294	0.33
Workpiece	2	0.031584	0.015792	1.59
Tool	2	0.164306	0.082153	8.29
Powder	2	0.021674	0.010837	1.09
Pulse On Time (µs)	2	0.116737	0.058369	5.89
Magnetic Field × Current	4	0.014060	0.003515	0.35
Current × Powder Conc.	4	0.016176	0.004044	0.41
Error	4	0.039641	0.009910	
Total	26	0.583643		
e (pooled)	20	0.132753	0.006637	

Table 4.24: Response Table for TWR (L27 OA-Ring magnet)

Level	Magnetic Field (T)	Current (A)	Powder Conc. (gm/l)	Workpiece	Tool	Powder	Pulse On Time (µs)
1	0.2711	0.1697	0.2520	0.2204	0.2495	0.2708	0.3214
2	0.2704	0.2706	0.2895	0.2897	0.1841	0.3022	0.3085
3	0.2644	0.3655	0.2643	0.2958	0.3723	0.2329	0.1759
Delta	0.0067	0.1958	0.0375	0.0754	0.1882	0.0693	0.1455
Rank	7	1	6	4	2	5	3

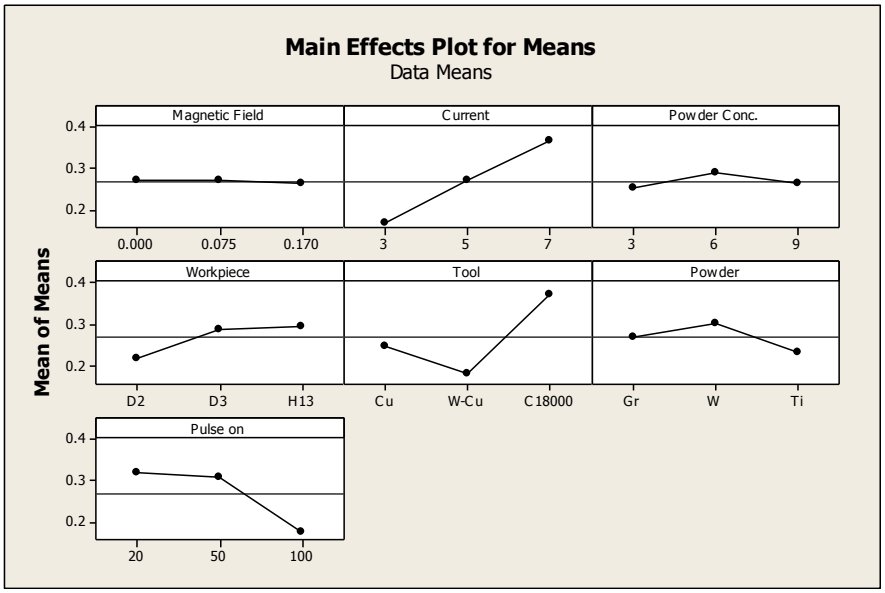

(a)

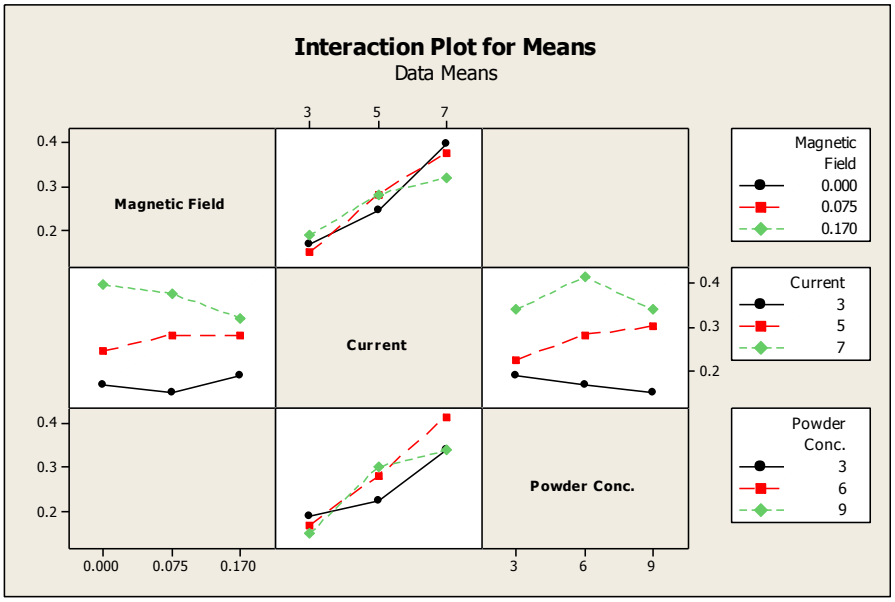

(b)

Figure 4.11: TWR plots (a) Mean effect plots; (b) Interaction plots (L27 OA-Ring magnet)

Analysis of variance of S/N ratio

ANOVA application for S/N ratio values (calculated using Equation 3.2) are provided in Table 4.25 and response table is provided in Table 4.26. From S/N ratio analysis and ANOVA plots for TWR (Figure 4.12), it is observed that current is the most significant parameter while magnetic field is least.

Table 4.25: ANOVA Table for S/N ratio for TWR (L27 OA-Ring magnet)

Parameter	DOF	SS	MS	*F* (calculated)
Magnetic Field (T)	2	0.694	0.3469	0.07
Current (A)	2	173.498	86.7492	16.32
Powder Conc. (gm/l)	2	7.236	3.6178	0.68
Workpiece	2	35.636	17.8178	3.35
Tool	2	127.544	63.7718	12.00
Powder	2	27.216	13.6081	2.56
Pulse On Time (µs)	2	148.046	74.0228	13.92
Magnetic Field × Current	4	14.548	3.6369	0.68
Current × Powder Conc.	4	36.527	9.1316	1.72
Error	4	21.265	5.3613	
Total	26			

Table 4.26: Response Table for S/N ratio for TWR (L27 OA-Ring magnet)

Level	Magnetic Field (T)	Current (A)	Powder Conc. (gm/l)	Workpiece	Tool	Powder	Pulse On Time (µs)
1	12.709	15.677	12.798	14.102	12.176	12.893	10.182
2	12.356	12.295	11.753	11.560	15.285	11.101	11.571
3	12.384	9.476	12.898	11.787	9.988	13.455	15.696
Delta	0.354	6.201	1.145	2.543	5.297	2.354	5.514
Rank	7	1	6	4	3	5	2

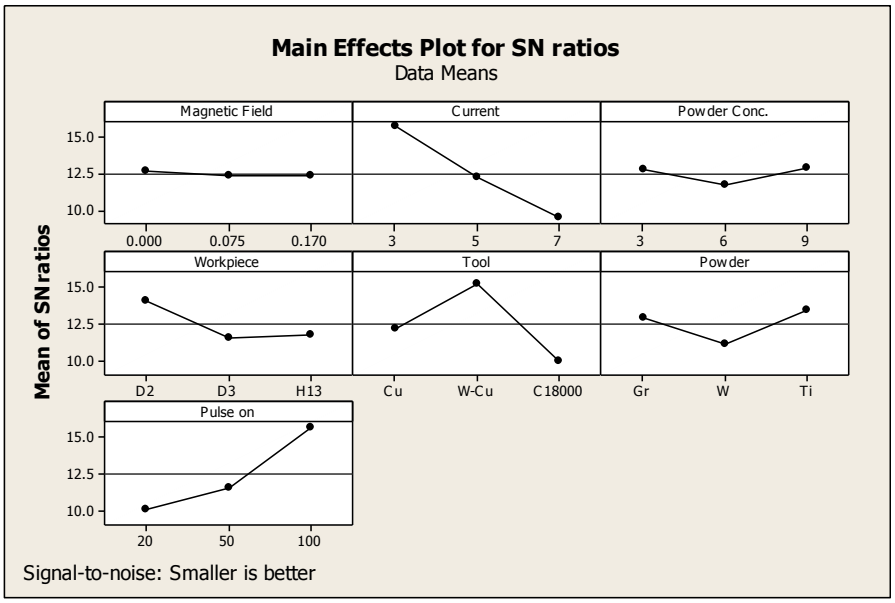

(a)

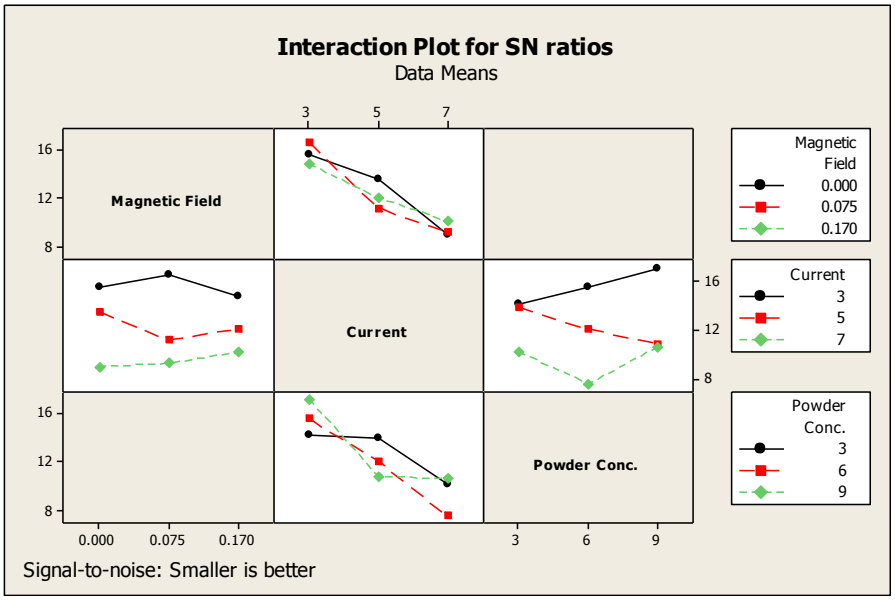

(b)

Figure 4.12: S/N ratio plots for TWR (a) Mean Effect plots; (b) Interaction plots (L27 OA-Ring magnet)

Optimal Design (Estimation of mean value)

In the experimental analysis, the mean effect plots corresponding to PMEDM (ring magnet assisted) (Figure 4.11) are used to estimate the mean TWR with optimal design conditions. Mean values of TWR are calculated to give an optimum TWR value. TWR is 'Lower the better' type response. Desired mean in this case is estimated as:

$\mu_{B_2,E_2,G_3} = \bar{B}_2 + \bar{E}_2 + \bar{G}_3 - 2\bar{T}$ = 0.2706 + 0.1841 + 0.1759 – 2 × 0.268 = 0.0946 mm^3/min

Confidence interval around the estimated TWR:

$$CI = \sqrt{\frac{F_{\alpha,v_1,v_2} V_e}{n_{eff}}}$$

$$n_{eff} = \frac{N}{1 + DOF_{B,E,G}} = \frac{27}{1+6} = 3.857$$

$$CI = \sqrt{\frac{4.35 \times 0.006637}{3.857}} = \pm 0.0865$$

Thus the optimum value of TWR is given by (0.0946 ± 0.0865) mm^3/min.

4.3 RESULT AND ANALYSIS OF OVERCUT

4.3.1 Introduction

OC is the amount by which cut made on the workpiece exceeds the used tool diameter. OC was measured comparing diameter of cut made in workpiece material with the tool to that of the tool electrode diameter that was measured on Nikon profile projector (Model V10-A) with voltage requirement of 220 V / 230 V / 240 V and current requirement of 0.6 A. OC being the dimension by which the hole in the workpiece exceeds the electrode diameter is calculated using Equation 4.3.

$$OC = \frac{(D-d)}{2} \text{ (mm)} \quad (4.3)$$

Where D =Diameter of cut made in workpiece material with the tool (in mm)

d =Diameter of the tool (in mm)

4.3.2 Result and analysis of OC using bar magnets with conventional EDM

Results for OC

OC results for trials conducted for L18 OA for EDM with bar magnet without powder being mixed in dielectric medium are listed in Table 4.27.

Table 4.27: OC Results (L18 OA)

S. No.	Current (A)	Magnetic Field (T)	Work piece	Tool	Pulse On Time (µs)	OVERCUT (mm)
1	3	0	D2	Cu	50	0.0665
2	3	0.09	D3	W-Cu	100	0.047
3	3	0.36	H13	C18000	200	0.049
4	4	0	D2	W-Cu	100	0.008
5	4	0.09	D3	C18000	200	0.0995
6	4	0.36	H13	Cu	50	0.1465
7	5	0	D3	Cu	200	0.14
8	5	0.09	H13	W-Cu	50	0.0575
9	5	0.36	D2	C18000	100	0.1365
10	6	0	H13	C18000	100	0.183
11	6	0.09	D2	Cu	200	0.1945
12	6	0.36	D3	W-Cu	50	0.159
13	7	0	D3	C18000	50	0.2005
14	7	0.09	H13	Cu	100	0.21
15	7	0.36	D2	W-Cu	200	0.1565
16	8	0	H13	W-Cu	200	0.17
17	8	0.09	D2	C18000	50	0.2685
18	8	0.36	D3	Cu	100	0.225

Analysis of Variance of OC

ANOVA and response results for OC are listed in Table 4.28 and 4.29 respectively. Figure 4.13 and 4.14 shows the main effect plots for OC and OC plots based on the current segregated values. From ANOVA results for OC, it is observed that current and tool materials are the most significant parameters for OC. With increase in current value, OC increases and reaches the maximum value at maximum current as at maximum current more particles will pass through the touching surface of tool and workpiece material. While OC follows the same pattern as that of the TWR corresponding to the tool materials. Harder the tool material, lower is the OC. D2 and H13 as workpiece material and more pulse on time has shown low OC values. While considering magnetic effect although it is an insignificant parameter but still an increase in overcut is observed as compared to no magnetic field condition to magnetic assisted condition. Segregated current plots show that higher OC values are observed with magnetic field assistance.

Table 4.28: ANOVA Table for OC (L18 OA)

Parameter	DOF	SS	MS	*F* (calculated)
Current (A)	5	0.065244	0.013049	11.52
Magnetic Field (T)	2	0.001268	0.000634	0.56
Workpiece	2	0.000271	0.000135	0.12
Tool	2	0.014713	0.007356	6.49
Pulse On Time (µs)	2	0.000880	0.000440	0.39
Error	4	0.004532	0.001133	
Total	17	0.086900		
e (pooled)	10	0.006943	0.000694	

Table 4.29: Response Table for OC (L18 OA)

Level	Current (A)	Magnetic Field (T)	Workpiece	Tool	Pulse On Time (µs)
1	0.05417	0.12800	0.13842	0.16375	0.14975
2	0.08467	0.14617	0.14517	0.09967	0.13492
3	0.11133	0.14542	0.13600	0.15617	0.13492
4	0.17883				
5	0.18900				
6	0.22117				
Delta	0.16700	0.01817	0.00917	0.06408	0.01483
Rank	1	3	5	2	4

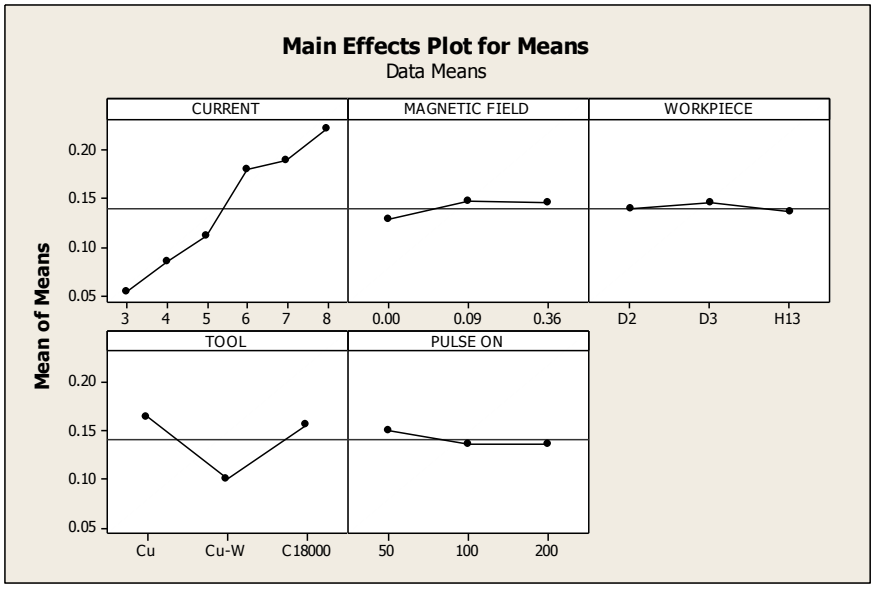

Figure 4.13: Mean Effect plots for OC (L18 OA)

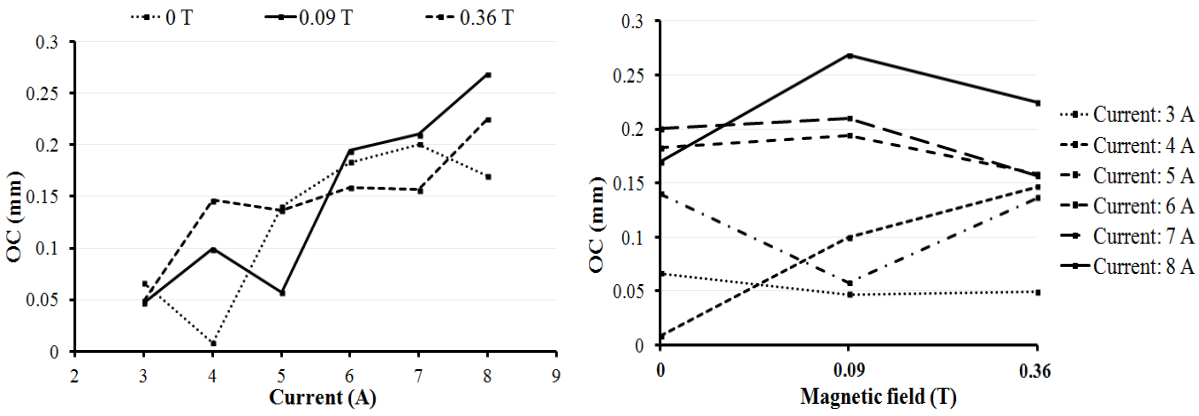

(a) (b)

Figure 4.14: OC plots for segregated current values (a) OC v/s Current; (b) OC v/s magnetic field (L18 OA)

Optimal design (Estimation of mean value)

In the experimental analysis, the mean effect plots (Figure 4.13) are used to estimate the mean OC values with optimal design conditions. Mean values of OC are calculated to give an optimum OC value. OC is 'Lower the better' type response. Desired mean in this case is estimated as:

$\mu_{A_1,D_2} = \bar{A}_1 + \bar{D}_2 - \bar{T}$ = 0.05417 + 0.09967 – 0.13986 = 0.01404 mm

Confidence interval around the estimated OC:

$$n_{eff} = \frac{N}{1 + DOF_{A,D}} = \frac{18}{1+7} = 2.25$$

$$CI = \sqrt{\frac{F_{\alpha,v_1,v_2} V_e}{n_{eff}}} = \sqrt{\frac{4.96 \times 0.000694}{2.25}} = \pm 0.039$$

Thus the optimum value of OC is given by (0.01404 ± 0.039) mm.

4.3.3 Result and analysis of OC using bar magnets with PMEDM

Results for OC

OC results for experimental trials for L27 OA for PMEDM with bar magnets are given in Table 4.30.

Table 4.30: OC Results (L27 OA-Bar magnet)

S. No.	Magnetic Field (T)	Current (A)	Powder Conc. (gm/l)	Work piece	Tool	Powder	Pulse On Time (μs)	OVECUT (mm)			
								Trial 1	Trial 2	Mean	S/N (dB)
1	0	3	3	D2	Cu	Gr	20	0.19215	0.198	0.195075	14.19499
2	0	3	6	D3	W-Cu	W	50	0.1118	0.1078	0.1098	19.18651
3	0	3	9	H13	C18000	Ti	100	0.13365	0.1378	0.135725	17.34579
4	0	5	3	D2	Cu	W	50	0.1795	0.1695	0.1745	15.16053
5	0	5	6	D3	W-Cu	Ti	100	0.1753	0.1823	0.1788	14.95099
6	0	5	9	H13	C18000	Gr	20	0.2873	0.27865	0.282975	10.96402
7	0	7	3	D2	Cu	Ti	100	0.2085	0.1938	0.20115	13.9238
8	0	7	6	D3	W-Cu	Gr	20	0.2208	0.195	0.2079	13.62622
9	0	7	9	H13	C18000	W	50	0.24015	0.23215	0.23615	12.535
10	0.09	3	3	D3	C18000	W	100	0.1788	0.1945	0.18665	14.57177
11	0.09	3	6	H13	Cu	Ti	20	0.17815	0.1858	0.181975	14.79785
12	0.09	3	9	D2	W-Cu	Gr	50	0.0118	0.01615	0.013975	36.98902
13	0.09	5	3	D3	C18000	Ti	20	0.26015	0.24865	0.2544	11.88744
14	0.09	5	6	H13	Cu	Gr	50	0.22365	0.2273	0.225475	12.93775
15	0.09	5	9	D2	W-Cu	W	100	0.16615	0.16565	0.1659	15.60306
16	0.09	7	3	D3	C18000	Gr	50	0.31	0.30565	0.307825	10.23371
17	0.09	7	6	H13	Cu	W	100	0.2033	0.20165	0.202475	13.8725
18	0.09	7	9	D2	W-Cu	Ti	20	0.17915	0.1833	0.181225	14.83507
19	0.36	3	3	H13	W-Cu	Ti	50	0.09715	0.09165	0.0944	20.49688
20	0.36	3	6	D2	C18000	Gr	100	0.1983	0.1923	0.1953	14.18493
21	0.36	3	9	D3	Cu	W	20	0.151	0.1388	0.1449	16.77094
22	0.36	5	3	H13	W-Cu	Gr	100	0.2043	0.19865	0.201475	13.91472
23	0.36	5	6	D2	C18000	W	20	0.2145	0.2285	0.2215	13.08819
24	0.36	5	9	D3	Cu	Ti	50	0.222	0.20115	0.211575	13.48018
25	0.36	7	3	H13	W-Cu	W	20	0.1948	0.2075	0.20115	13.92527
26	0.36	7	6	D2	C18000	Ti	50	0.25665	0.248	0.252325	11.95952
27	0.36	7	9	D3	Cu	Gr	100	0.25215	0.2673	0.259725	11.70603

Analysis of Variance of OC

From ANOVA table (Table 4.31), response table (Table 4.32) and OC plots (Figure 4.15) for main effect and interaction, it is concluded that current is the most significant parameter, then the tool material and then the workpiece material. OC increases with increase in current value and reaches maximum at maximum current value. Tungsten-copper results in minimum OC value and D2 die steel gives minimum OC response. Taking effect of other parameters in account, OC reduces with increase in powder concentration and with titanium and tungsten powder, lower OC value is reported. Moderate pulse on time is preferred for low OC value. Magnetic field although an insignificant parameter has shown some varying results with segregated result plots. Interaction plots have shown that for higher values of current, OC increases with increase in applied magnetic field strength. Interaction plots for current and powder concentration have shown that for all the values of current, higher powder concentration has reported lower OC values.

Table 4.31: ANOVA Table for OC (L27 OA-Bar magnet)

Parameter	DOF	SS	MS	*F* (calculated)
Magnetic Field (T)	2	0.000279	0.000140	0.16
Current (A)	2	0.039972	0.019986	23.49
Powder Conc. (gm/l)	2	0.002085	0.001042	1.23
Workpiece	2	0.003843	0.001921	2.26
Tool	2	0.029170	0.014585	17.15
Powder	2	0.003796	0.001898	2.23
Pulse On Time (µs)	2	0.003371	0.001685	1.98
Magnetic Field × Current	4	0.001228	0.000307	0.36
Current × Powder Conc.	4	0.006337	0.001584	1.86
Error	4	0.003403	0.000851	
Total	26	0.093482		
e (pooled)	18	0.016701	0.0009278	

Table 4.32: Response Table for OC (L27 OA-Bar magnet)

Level	Magnetic Field (T)	Current (A)	Powder Conc. (gm/l)	Workpiece	Tool	Powder	Pulse On Time (µs)
1	0.1913	0.1398	0.2018	0.1779	0.1996	0.2100	0.2079
2	0.1911	0.2130	0.1973	0.2068	0.1505	0.1826	0.1807
3	0.1980	0.2278	0.1814	0.1958	0.2303	0.1880	0.1919
Delta	0.0069	0.0880	0.0205	0.0290	0.0798	0.0274	0.0272
Rank	7	1	6	3	2	4	5

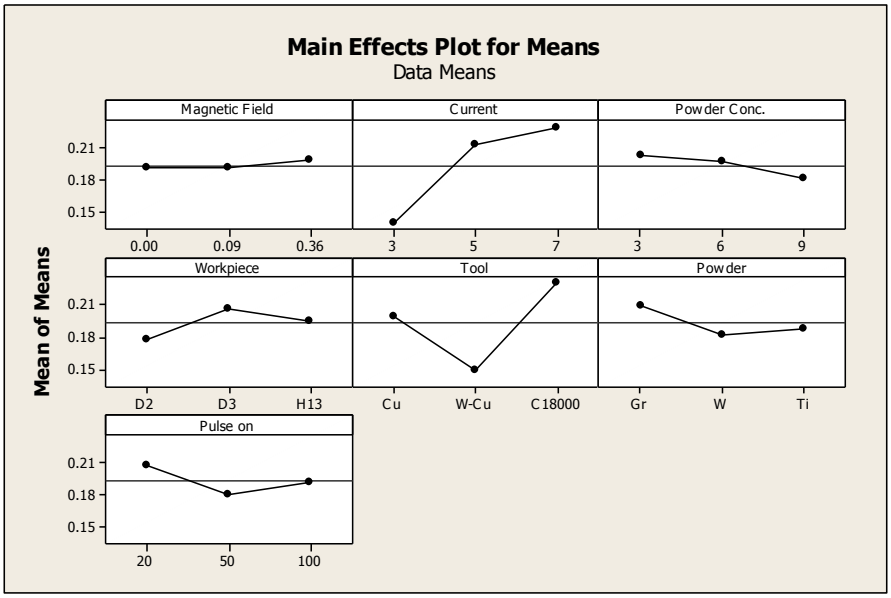

(a)

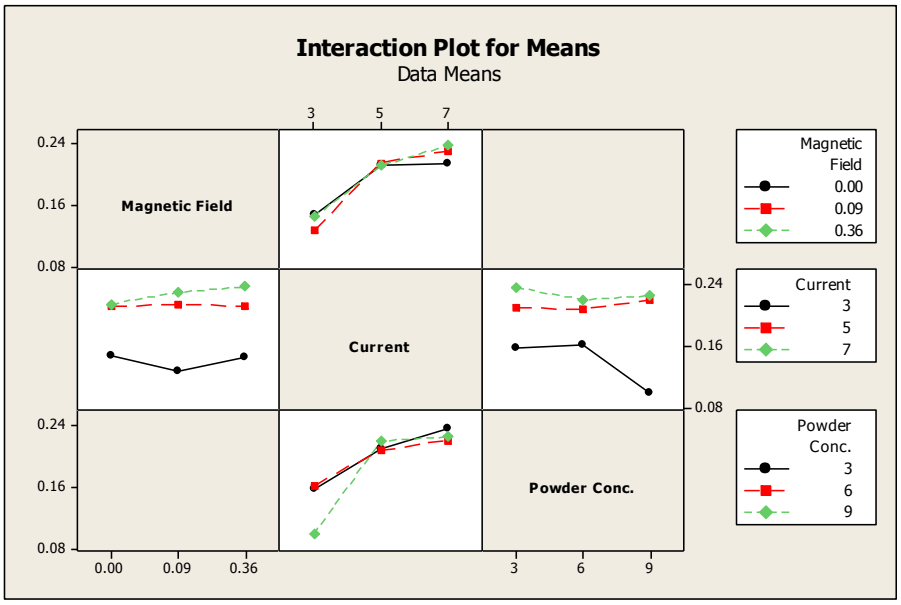

(b)

Figure 4.15: OC plots (a) Mean effect plots; (b) Interaction Plots (L27 OA-Bar magnet)

Analysis of variance of S/N ratio

Taking OC in account, as a consideration term, lower OC value is preferred as lower will be the overcut, higher will be the accuracy. Hence lower the better constraint is followed for calculating S/N ratio (using Equation 3.2) corresponding to OC values. ANOVA table (Table 4.33) and response table (Table 4.34) has shown that current is the most significant parameter while powder type is the least impacting parameter. Figure 4.16 has shown the mean effect and interaction plots for S/N ratio.

Table 4.33: ANOVA Table for S/N ratio for OC (L27 OA-Bar magnet)

Parameter	DOF	SS	MS	*F* (calculated)
Magnetic Field (T)	2	17.023	8.5114	0.53
Current (A)	2	181.176	90.5880	5.62
Powder Conc. (gm/l)	2	35.119	17.5593	1.09
Workpiece	2	34.788	17.3942	1.08
Tool	2	134.570	67.2852	4.17
Powder	2	1.597	0.7985	0.05
Pulse On Time (µs)	2	51.668	25.8342	1.60
Magnetic Field × Current	4	35.997	8.9992	0.56
Current × Powder Conc.	4	77.002	19.2505	1.19
Error	4	64.477	16.1193	
Total	26	633.417		

Table 4.34: Response Table for S/N ratio for OC (L27 OA-Bar magnet)

Level	Magnetic Field (T)	Current (A)	Powder Conc. (gm/l)	Workpiece	Tool	Powder	Pulse On Time (µs)
1	14.65	18.73	14.26	16.66	14.09	15.42	13.79
2	16.19	13.55	14.29	14.05	18.17	14.97	17.00
3	14.39	12.96	16.69	14.53	12.97	14.85	14.45
Delta	1.80	5.77	2.44	2.61	5.20	0.56	3.21
Rank	6	1	5	4	2	7	3

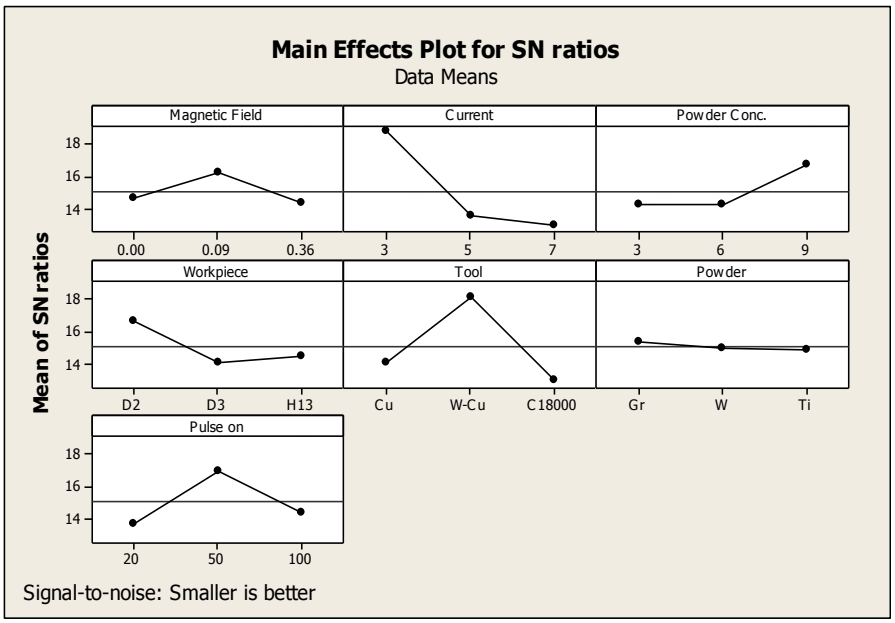

(a)

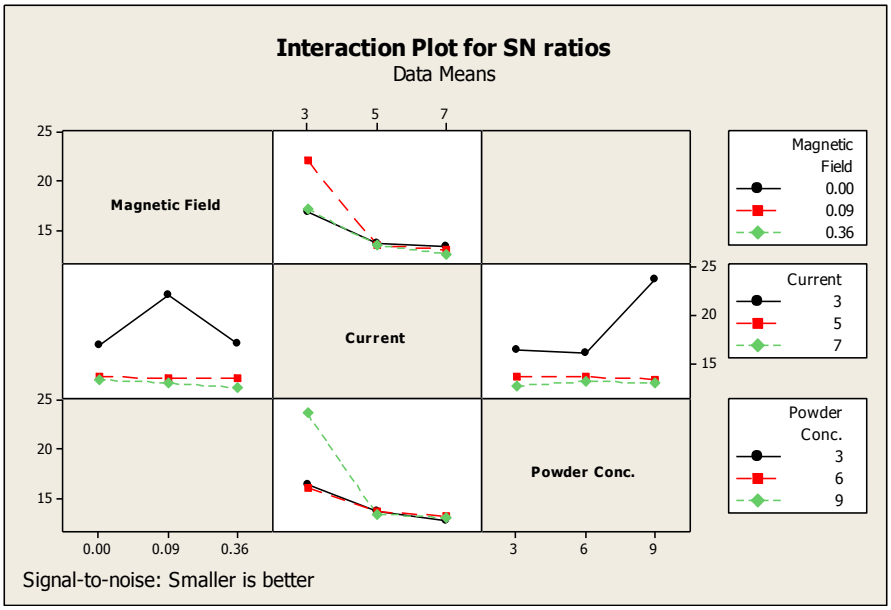

(b)

Figure 4.16: S/N ratio Plots for OC (a) Mean effect plots; (b) Interaction plots (L27 OA-Bar magnet)

Optimal Design (Estimation of mean value)

In the experimental analysis, the mean effect plots corresponding to PMEDM (bar magnets assisted) (Figure 4.15) are used to estimate the mean OC with optimal design conditions. Mean values of OC are calculated to give an optimum OC value. OC is 'Lower the better' type response. Desired mean in this case is estimated as:

$\mu_{B_1,D_1,E_2,F_2} = \bar{B}_1 + \bar{D}_1 + \bar{E}_2 + \bar{F}_2 - 3\bar{T}$ = 0.1398 + 0.1779 + 0.1505 + 0.1826 – 3 × 0.19349 = 0.07033 mm

Confidence interval around the estimated OC:

$$CI = \sqrt{\frac{F_{\alpha,v_1,v_2} V_e}{n_{eff}}}$$

$$n_{eff} = \frac{N}{1 + DOF_{B,D,E,F}} = \frac{27}{1+8} = 3$$

$$CI = \sqrt{\frac{4.41 \times 0.0009278}{3}} = \pm 0.0369$$

Thus the optimum value of OC is given by (0.07033 ± 0.0369) mm.

4.3.4 Result and analysis of OC using ring magnets with PMEDM

Results for OC

Table 4.35 has shown the OC results for PMEDM with ring magnet field assistance.

Table 4.35: OC Results (L27 OA-Ring magnet)

S. No.	Magnetic Field (T)	Current (A)	Powder Conc. (gm/l)	Work piece	Tool	Powder	Pulse On Time (µs)	OVERCUT (mm)			
								Trial 1	Trial 2	Mean	S/N (dB)
1	0	3	3	D2	Cu	Gr	20	0.20315	0.1968	0.199975	13.97939
2	0	3	6	D3	W-Cu	W	50	0.0965	0.09265	0.094575	20.48267
3	0	3	9	H13	C18000	Ti	100	0.1255	0.1213	0.1234	18.17244
4	0	5	3	D2	Cu	W	50	0.16165	0.16965	0.16565	15.61364
5	0	5	6	D3	W-Cu	Ti	100	0.184	0.17615	0.180075	14.88887
6	0	5	9	H13	C18000	Gr	20	0.2675	0.24015	0.253825	11.89672
7	0	7	3	D2	Cu	Ti	100	0.198	0.1925	0.19525	14.18732
8	0	7	6	D3	W-Cu	Gr	20	0.21715	0.2203	0.218725	13.20181
9	0	7	9	H13	C18000	W	50	0.24415	0.2515	0.247825	12.11614
10	0.075	3	3	D3	C18000	W	100	0.19665	0.1938	0.195225	14.18906
11	0.075	3	6	H13	Cu	Ti	20	0.172	0.1628	0.1674	15.52161
12	0.075	3	9	D2	W-Cu	Gr	50	0.07615	0.09115	0.08365	21.51591
13	0.075	5	3	D3	C18000	Ti	20	0.2155	0.23215	0.223825	12.99582
14	0.075	5	6	H13	Cu	Gr	50	0.27765	0.27765	0.27765	11.13005
15	0.075	5	9	D2	W-Cu	W	100	0.1503	0.16715	0.158725	15.97487
16	0.075	7	3	D3	C18000	Gr	50	0.2715	0.2675	0.2695	11.38859
17	0.075	7	6	H13	Cu	W	100	0.2395	0.23815	0.238825	12.43837
18	0.075	7	9	D2	W-Cu	Ti	20	0.187	0.1835	0.18525	14.64445
19	0.17	3	3	H13	W-Cu	Ti	50	0.10015	0.1155	0.107825	19.32366
20	0.17	3	6	D2	C18000	Gr	100	0.20565	0.2013	0.203475	13.82928
21	0.17	3	9	D3	Cu	W	20	0.1595	0.151	0.15525	16.17611
22	0.17	5	3	H13	W-Cu	Gr	100	0.19215	0.1983	0.195225	14.18821
23	0.17	5	6	D2	C18000	W	20	0.225	0.2208	0.2229	13.03741
24	0.17	5	9	D3	Cu	Ti	50	0.2123	0.1985	0.2054	13.74309
25	0.17	7	3	H13	W-Cu	W	20	0.25015	0.2468	0.248475	12.09415
26	0.17	7	6	D2	C18000	Ti	50	0.246	0.25465	0.250325	12.02862
27	0.17	7	9	D3	Cu	Gr	100	0.24015	0.2525	0.246325	12.1671

Analysis of Variance of OC

As a result of analysis of ANOVA (Table 4.36) and response table (Table 4.37) analysis, it is observed that overcut is significantly affected by current and tool while other factors are insignificant. From Figure 4.17, it is summarized that OC increases with increase in current, higher the current more is the OC as the material removal increases increasing the number of particles travelling in between workpiece and tool interface. OC is observed to decrease with the hardness of the tool. MRR is highest with C18000 tool, hence maximum OC is observed

with C18000 tool as more particles pass through the gap of tool and workpiece. While taking other parameters in account overcut gradually increases with increase in magnetic field strength and is found maximum with highest magnetic field strength. Overall 11% increase is observed in overcut with increase in magnetic strength as with the increase in magnetic strength particle size extracted increases. Overcut increases with powder concentration up to a limit and then decreases. From interaction plots, OC is observed to increase gradually with strength for all the current levels except for moderate current value and in terms of current and powder concentration, minimum current and maximum concentration provide lowest overcut.

Table 4.36: ANOVA Table for OC (L27 OA-Ring magnet)

Parameter	DOF	SS	MS	*F* (calculated)
Magnetic Field (T)	2	0.001486	0.002816	0.91
Current (A)	2	0.034997	0.069286	21.54
Powder Conc. (gm/l)	2	0.002242	0.003970	1.38
Workpiece	2	0.002168	0.003780	1.33
Tool	2	0.015966	0.038922	9.83
Powder	2	0.005649	0.010158	3.48
Pulse On Time (µs)	2	0.001871	0.004234	1.15
Magnetic Field × Current	4	0.000712	0.000517	0.22
Current × Powder Conc.	4	0.003100	0.002880	0.95
Error	4	0.003249	0.003008	
Total	26	0.07144		
e (pooled)	20	0.01483	.0007414	

Table 4.37: Response Table for OC (L27 OA-Ring magnet)

Level	Magnetic Field (T)	Current (A)	Powder Conc. (gm/l)	Workpiece	Tool	Powder	Pulse On Time (µs)
1	0.1866	0.1479	0.2001	0.1850	0.2057	0.2165	0.2084
2	0.2000	0.20933	0.2060	0.1988	0.1636	0.1919	0.1892
3	0.2039	0.2334	0.1844	0.2067	0.2211	0.1821	0.1929
Delta	0.0173	0.0855	0.0216	0.0217	0.0575	0.0344	0.0192
Rank	7	1	5	4	2	3	6

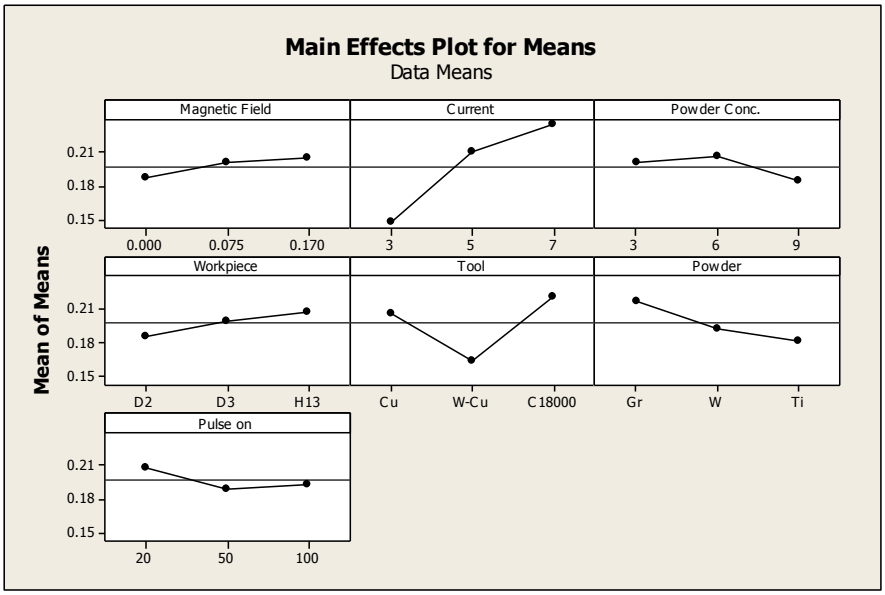

(a)

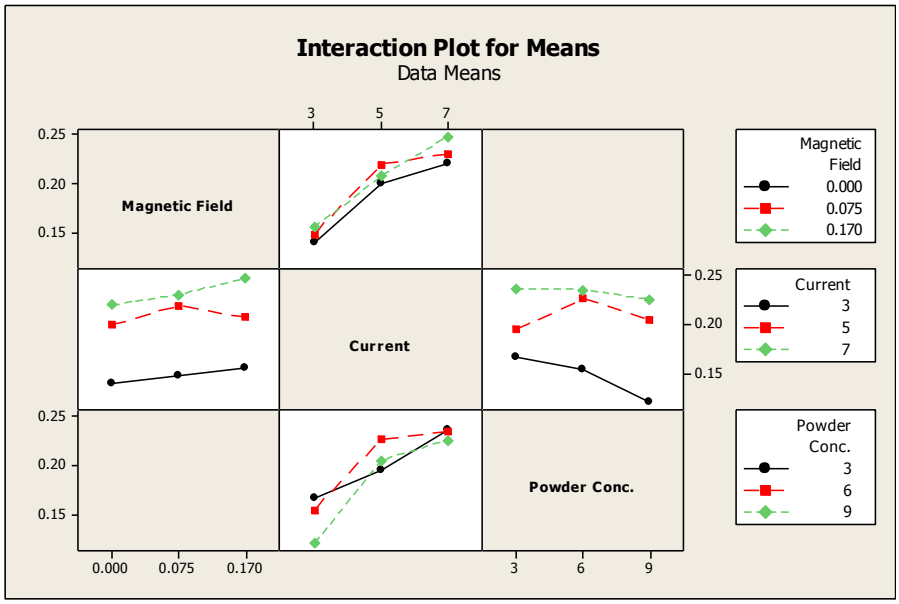

(b)

Figure 4.17: OC plots (a) Mean effect plots; (b) Interaction Plots (L27 OA-Ring magnet)

Analysis of Variance of S/N ratio

S/N ratio criterion for OC is taken as lower the better. ANOVA table (Table 4.38) and response table (Table 4.39) have shown that current is the most significant parameter while workpiece is the least affecting parameter. Figure 4.18 shows the main effect plots and interaction plots for S/N ratio.

Table 4.38: ANOVA Table for S/N ratio for OC (L27 OA-Ring magnet)

Parameter	DOF	SS	MS	*F* (calculated)
Magnetic Field (T)	2	6.481	3.240	0.23
Current (A)	2	324.809	162.404	11.38
Powder Conc. (gm/l)	2	131.150	65.575	4.60
Workpiece	2	7.606	3.803	0.27
Tool	2	16.800	8.400	0.59
Powder	2	135.810	67.905	4.76
Pulse On Time (µs)	2	117.307	58.654	4.11
Magnetic Field × Current	4	270.227	67.557	4.73
Current × Powder Conc.	4	15.000	3.750	0.26
Error	4	57.081	14.270	
Total	26			

Table 4.39: Response Table for S/N ratio for OC (L27 OA-Ring magnet)

Level	Magnetic Field (T)	Current (A)	Powder Conc. (gm/l)	Workpiece	Tool	Powder	Pulse On Time (µs)
1	14.95	17.02	14.22	14.98	13.88	13.70	13.73
2	14.42	13.72	14.06	14.36	16.26	14.68	15.26
3	14.07	12.70	15.16	14.10	13.29	15.06	14.45
Delta	0.88	4.32	1.09	0.88	2.96	1.36	1.53
Rank	6	1	5	7	2	4	3

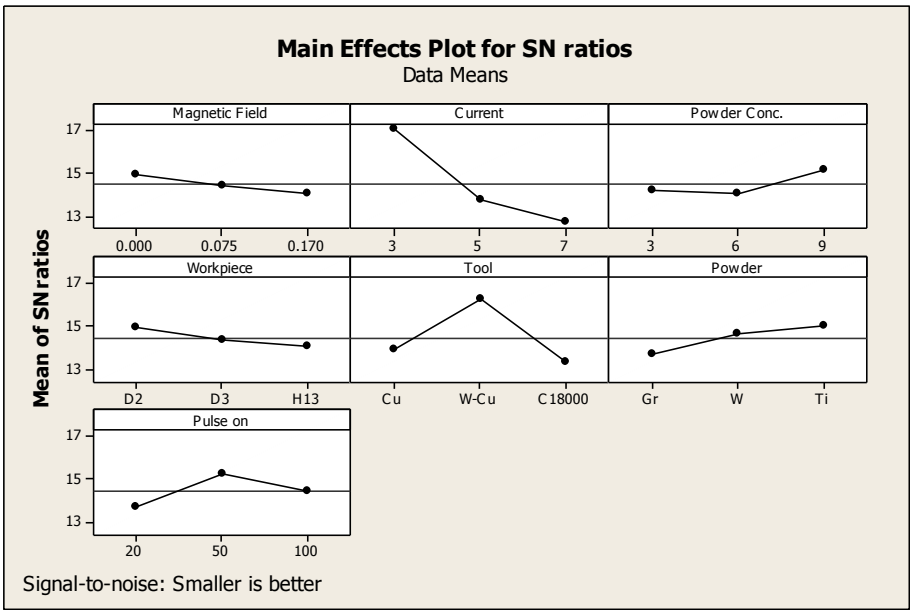

(a)

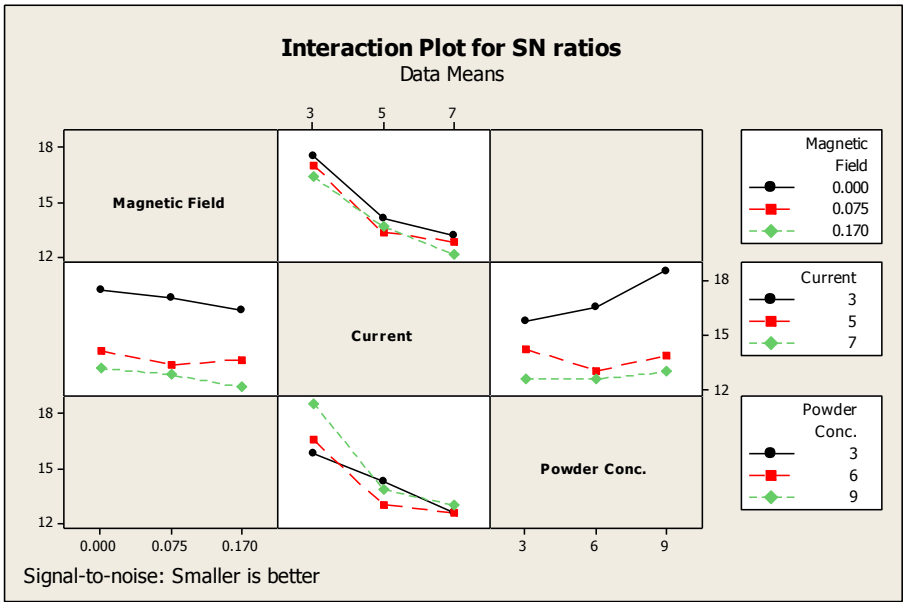

(b)

Figure 4.18: S/N ratio plots for OC (a) Mean effect plots; (b) Interaction plots (L27 OA-Ring magnet)

Optimal Design (Estimation of mean value)

In the experimental analysis, the mean effect plots corresponding to PMEDM (ring magnet assisted) (Figure 4.17) are used to estimate the mean OC with optimal design conditions. Mean values of OC are calculated to give an optimum OC value. OC is 'Lower the better' type response. Desired mean in this case is estimated as:

$\mu_{B_1,E_2,F_3} = \bar{B}_1 + \bar{E}_2 + \bar{F}_3 - 2\bar{T}$ = 0.1479 + 0.1636 + 0.1821 – 2 × 0.1968 = 0.1 mm

Confidence interval around the estimated OC:

$$CI = \sqrt{\frac{F_{\alpha,v_1,v_2} V_e}{n_{eff}}}$$

$$n_{eff} = \frac{N}{1 + DOF_{B,E,F}} = \frac{27}{1+6} = 3.85$$

$$CI = \sqrt{\frac{4.35 \times 0.0007414}{3.85}} = \pm 0.029$$

Thus the optimum value of OC is given by (0.1 ± 0.029) mm.

4.4 RESULT AND ANALYSIS OF SURFACE ROUGHNESS

4.4.1 Introduction

Surface roughness is a measure of the texture of a surface. It is a measure of waviness of the surface. Waviness provides peaks and valleys; hence surface roughness is quantified by the vertical distance between peak and valley. If these deviations are large, the surface is rough; if they are small the surface is smooth. It is measured in terms of R_a value (µm).

4.4.2 Result and analysis of SR using bar magnets with conventional EDM

Results for SR

Results for SR for magnetic field assisted EDM are listed in Table 4.40.

Table 4.40: SR Results (L18 OA)

S. No.	Current (A)	Magnetic Field (T)	Work piece	Tool	Pulse On Time (µs)	SR (µm)
1	3	0	D2	Cu	50	5.89
2	3	0.09	D3	W-Cu	100	6.97
3	3	0.36	H13	C18000	200	7.345
4	4	0	D2	W-Cu	100	6.68
5	4	0.09	D3	C18000	200	7.425
6	4	0.36	H13	Cu	50	7.485
7	5	0	D3	Cu	200	8.53
8	5	0.09	H13	W-Cu	50	7.47
9	5	0.36	D2	C18000	100	7.615
10	6	0	H13	C18000	100	6.89
11	6	0.09	D2	Cu	200	8.85
12	6	0.36	D3	W-Cu	50	8.82
13	7	0	D3	C18000	50	7.83
14	7	0.09	H13	Cu	100	9.5
15	7	0.36	D2	W-Cu	200	7.59
16	8	0	H13	W-Cu	200	8.37
17	8	0.09	D2	C18000	50	10.18
18	8	0.36	D3	Cu	100	9.71

Analysis of Variance of SR

ANOVA analysis of results obtained for SR for magnetic field assisted EDM (Table 4.41) and corresponding response table (Table 4.42) show that the most significant parameters that contribute towards SR is current and then the magnetic field. With increase in current value, energy available for machining increases which increases the crater size increasing the SR value. With the increase in strength of the magnetic field, the size of the particle that is

extracted out of the melted material increases hence increasing the SR value. From mean effect plots (Figure 4.19), it is observed that tungsten-copper as tool has reported lowest SR value, while D3 as workpiece is observed to show high roughness value as compared to other two workpieces.

Table 4.41: ANOVA table for SR (L18 OA)

Parameter	DOF	SS	MS	*F* (calculated)
Current (A)	5	13.1818	2.63637	3.32
Magnetic Field (T)	2	3.3884	1.69421	2.13
Workpiece	2	0.6203	0.31017	0.39
Tool	2	1.4236	0.71180	0.90
Pulse On Time (µs)	2	0.0467	0.02334	0.03
Error	4	3.1767	0.79417	
Total	17	21.8376		
e (pooled)	10	5.2674	0.52674	

Table 4.42: Response table for SR (L18 OA)

Level	Current (A)	Magnetic Field (T)	Workpiece	Tool	Pulse On Time (µs)
1	6.735	7.365	7.801	8.328	7.946
2	7.197	8.399	8.214	7.650	7.894
3	7.872	8.094	7.843	7.881	8.018
4	8.187				
5	8.307				
6	9.420				
Delta	2.685	1.034	0.413	0.678	0.124
Rank	1	2	4	3	5

Response table has shown that pulse on time is the most insignificant process parameter for roughness measurement. Plots based on the segregated current values (Figure 4.20) have clearly depicted that the SR is observed to increase with field strength.

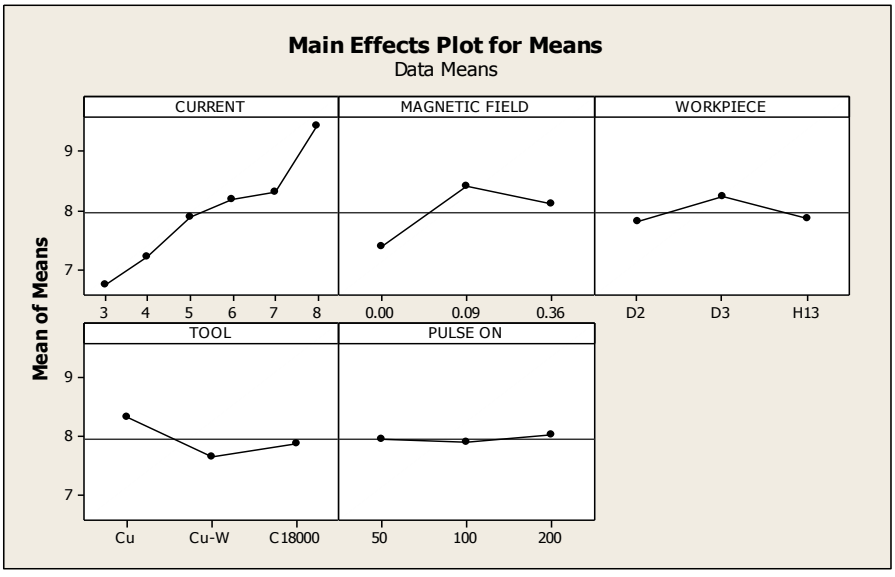

Figure 4.19: Mean effect plot for SR (L18 OA)

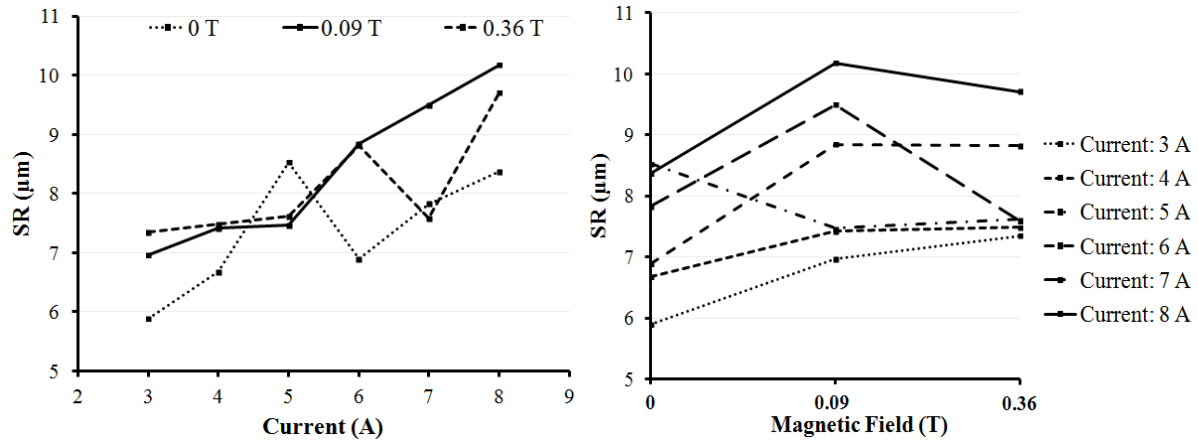

(a) (b)

Figure 4.20: SR plots for segregated current values (a) SR v/s Current; (b) SR v/s Magnetic Field (L18 OA)

Optimal design (Estimation of mean value)

In the experimental analysis, the mean effect plots (Figure 4.19) are used to estimate the mean SR values with optimal design conditions. Mean values of SR are calculated to give an optimum SR value. SR is 'Lower the better' type response. Desired mean in this case is estimated as:

$\mu_{A_1,B_1} = \bar{A}_1 + \bar{B}_1 - \bar{T}$ = 6.735 + 7.365 – 7.95228 = 6.1477 µm

Confidence interval around the estimated SR:

$$n_{eff} = \frac{N}{1 + DOF_{A,B}} = \frac{18}{1+7} = 2.25$$

$$CI = \sqrt{\frac{F_{\alpha,v_1,v_2} V_e}{n_{eff}}} = \sqrt{\frac{4.96 \times 0.52}{2.25}} = \pm 1.0775$$

Thus the optimum value of SR is given by (6.1477 ± 1.0775) µm.

4.4.3 Result and analysis of SR using bar magnets with PMEDM

Results for SR

SR results for powder mixed EDM with bar magnets is listed in Table 4.43.

Table 4.43: SR Results (L27 OA-Bar magnet)

S. No.	Magnetic Field (T)	Current (A)	Powder Conc. (gm/l)	Work piece	Tool	Powder	Pulse On Time (µs)	SURFACE ROUGHNESS (µm)			
								Trial 1	Trial 2	Mean	S/N (dB)
1	0	3	3	D2	Cu	Gr	20	7.805	6.58	7.1925	-17.169
2	0	3	6	D3	W-Cu	W	50	5.105	5.94	5.5225	- 14.867
3	0	3	9	H13	C18000	Ti	100	7.73	6.6	7.165	-17.131
4	0	5	3	D2	Cu	W	50	6.315	6.285	6.3	-15.986
5	0	5	6	D3	W-Cu	Ti	100	7.7	8.59	8.145	-18.230
6	0	5	9	H13	C18000	Gr	20	6.84	8.255	7.5475	-17.594
7	0	7	3	D2	Cu	Ti	100	6.33	7.335	6.8325	-16.71
8	0	7	6	D3	W-Cu	Gr	20	8.43	9.58	9.005	-19.107
9	0	7	9	H13	C18000	W	50	8.92	6.93	7.925	-18.047
10	0.09	3	3	D3	C18000	W	100	6.13	7.06	6.595	-16.405
11	0.09	3	6	H13	Cu	Ti	20	6.905	6.28	6.5925	-16.390
12	0.09	3	9	D2	W-Cu	Gr	50	5.795	5.83	5.8125	-15.287
13	0.09	5	3	D3	C18000	Ti	20	7.41	8.25	7.83	-17.887
14	0.09	5	6	H13	Cu	Gr	50	8.21	7.94	8.075	-18.144
15	0.09	5	9	D2	W-Cu	W	100	5.725	8.055	6.89	-16.886
16	0.09	7	3	D3	C18000	Gr	50	6.59	8.33	7.46	-17.513
17	0.09	7	6	H13	Cu	W	100	9.15	8.28	8.715	-18.816
18	0.09	7	9	D2	W-Cu	Ti	20	6.1	5.345	5.7225	-15.170
19	0.36	3	3	H13	W-Cu	Ti	50	7.485	6.155	6.82	-16.716
20	0.36	3	6	D2	C18000	Gr	100	5.39	5.835	5.6125	-14.989
21	0.36	3	9	D3	Cu	W	20	7.5	6.4	6.95	-16.866
22	0.36	5	3	H13	W-Cu	Gr	100	6.8	6.94	6.87	-16.739
23	0.36	5	6	D2	C18000	W	20	6.91	7.61	7.26	-17.228
24	0.36	5	9	D3	Cu	Ti	50	7.88	8.37	8.125	-18.200
25	0.36	7	3	H13	W-Cu	W	20	9.95	7.255	8.6025	-18.797
26	0.36	7	6	D2	C18000	Ti	50	6.76	6.41	6.585	-16.374
27	0.36	7	9	D3	Cu	Gr	100	6.06	10.9	8.48	-18.907

Analysis of Variance of SR

From analysis of ANOVA table (Table 4.44) and response table (Table 4.45), it is observed that, current and workpiece are the most significant parameters. As current increases, the crater size increases increasing the surface roughness. Figure 4.21 shows the ANOVA plots for SR for mean value results and interactions. Hence higher the current, more will be the surface roughness of the surface. D3 and H13 as workpiece has shown the higher SR as compared to D2 die steel as workpiece which is significantly very low. Further interaction of current and powder concentration shows that moderate concentration of powder has shown increase in SR with current for higher values of current which it is opposite for low value of current. Further moderate field strength, low powder concentration, moderate pulse on time and titanium as powder have shown low SR value, while copper tool as compared to

tungsten-copper and C18000 tool has shown more roughness value.

Table 4.44: ANOVA Table for SR (L27 OA-Bar magnet)

Parameter	DOF	SS	MS	*F* (calculated)
Magnetic Field (T)	2	0.24009	0.12004	0.15
Current (A)	2	7.58311	3.79155	4.82
Powder Conc. (gm/l)	2	0.06794	0.03397	0.04
Workpiece	2	7.41704	3.70852	4.71
Tool	2	0.96738	0.48369	0.61
Powder	2	0.28043	0.14022	0.18
Pulse On Time (µs)	2	0.95413	0.47706	0.61
Magnetic Field × Current	4	0.73690	0.18422	0.23
Current × Powder Conc.	4	3.30418	0.82605	1.05
Errors	4	3.14809	0.78702	
Total	26	24.6993		
e (pooled)	22	9.69915	0.44087	

Table 4.45: Response Table for SR (L27 OA-Bar magnet)

Level	Magnetic Field (T)	Current (A)	Powder Conc. (gm/l)	Workpiece	Tool	Powder	Pulse On Time (µs)
1	7.293	6.474	7.167	6.467	7.474	7.339	7.411
2	7.077	7.449	7.279	7.568	7.043	7.196	6.958
3	7.256	7.703	7.180	7.590	7.109	7.091	7.256
Delta	0.216	1.229	0.112	1.123	0.430	0.249	0.453
Rank	6	1	7	2	4	5	3

Interaction of magnetic field and current has shown that the varying results are shown while different combinations. Response table has shown that current is the most significant input parameter while powder concentration is least.

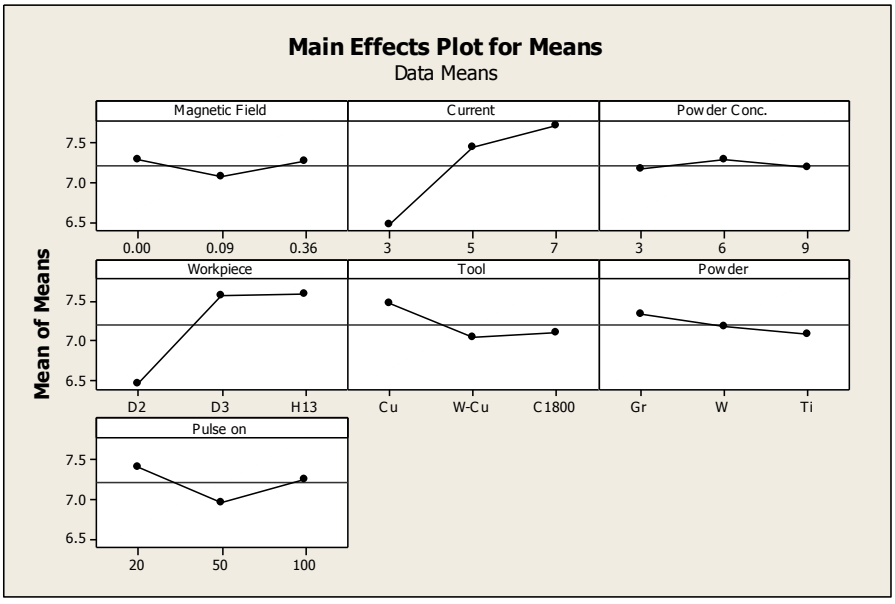

(a)

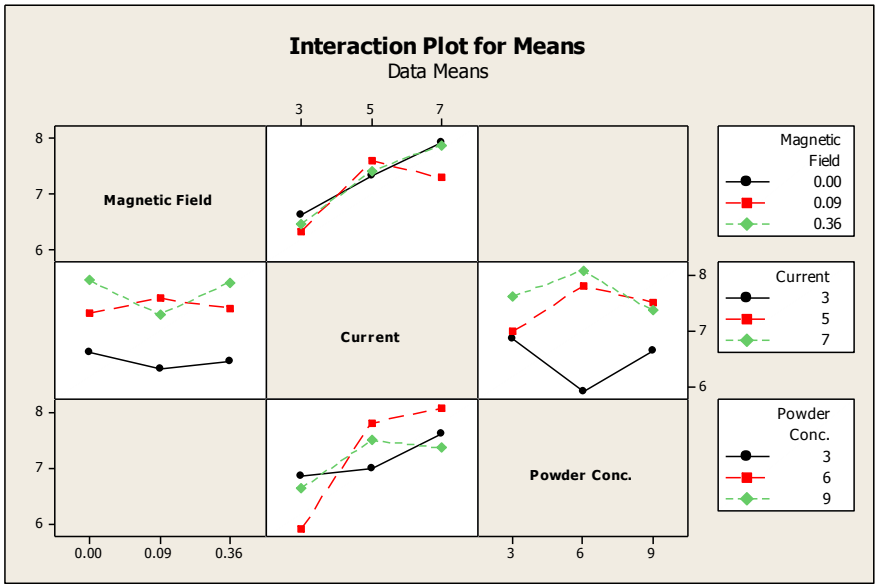

(b)

Figure 4.21: SR plots (a) Mean effect plots; (b) Interaction plots (L27 OA-Bar magnet)

Analysis of variance of S/N ratio

Lower the better criterion is used for calculating S/N ratio (using Equation 3.2) for SR results. From response table (Table 4.46) and ANOVA table for S/N ratio (Table 4.47), it is observed that current is the most significant parameter while powder concentration is the least affecting parameter. ANOVA plots for S/N ratio are shown in Figure 4.22.

Table 4.46: ANOVA Table for S/N ratio for SR (L27 OA-Bar magnet)

Parameter	DOF	SS	MS	*F* (calculated)
Magnetic Field (T)	2	0.4033	0.20166	0.17
Current (A)	2	11.6588	5.82941	5.06
Powder Conc. (gm/l)	2	0.0028	0.00142	0.00
Workpiece	2	11.3514	5.67572	4.92
Tool	2	1.7461	0.87305	0.76
Powder	2	0.3897	0.19487	0.17
Pulse On Time (µs)	2	1.5281	0.76405	0.66
Magnetic Field × Current	4	1.3743	0.34358	0.30
Current × Powder Conc.	4	5.3069	1.32674	1.15
Error	4	4.6125	1.15312	
Total	26	38.3741	S	

Table 4.47: Response Table for S/N ratio for SR (L27 OA-Bar magnet)

Level	Magnetic Field (T)	Current (A)	Powder Conc. (gm/l)	Workpiece	Tool	Powder	Pulse On Time (µs)
1	-17.12	-16.20	-17.510	-16.20	-17.47	-17.27	-17.36
2	-16.94	-17.43	-17.13	-17.55	-16.87	-17.10	-16.79
3	-17.20	-17.72	-17.13	-17.60	-17.02	-16.98	-17.20
Delta	0.26	1.51	0.02	1.40	0.60	0.29	0.56
Rank	6	1	7	2	3	5	4

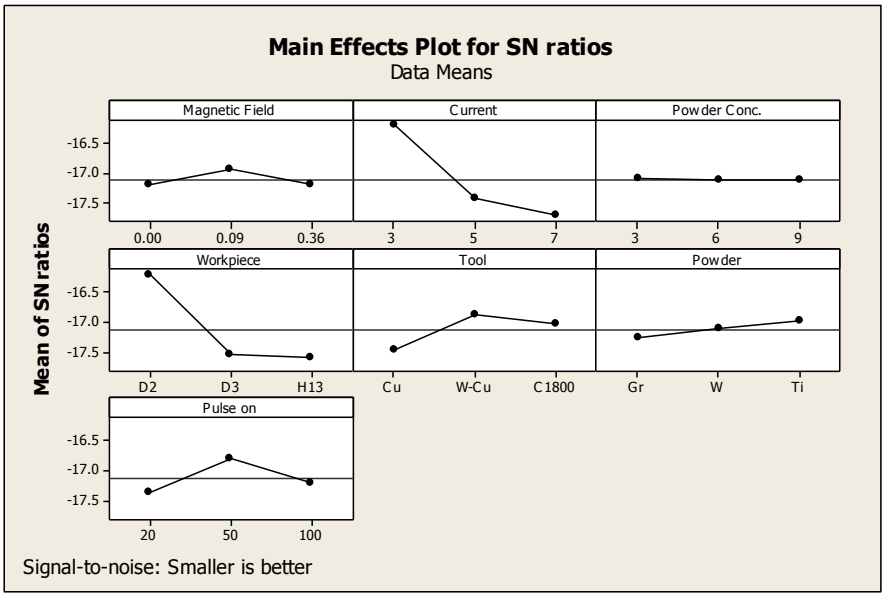

(a)

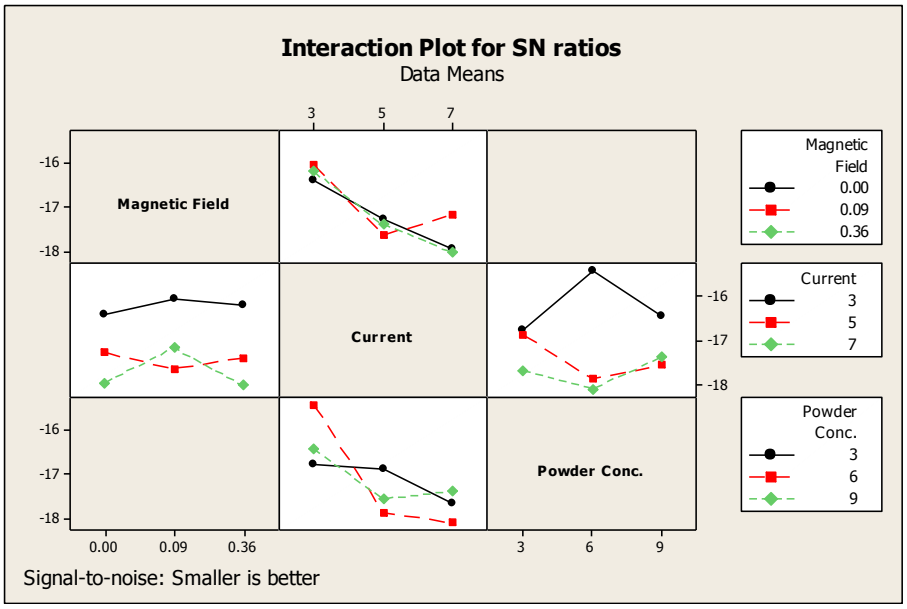

(b)

Figure 4.22: S/N ratio plots for SR (a) Mean effect plots; (b) Interaction plots (L27 OA-Bar magnet)

Optimal Design (Estimation of mean value)

In the experimental analysis, the mean effect plots corresponding to PMEDM (bar magnets assisted) (Figure 4.21) are used to estimate the mean SR with optimal design conditions. Mean values of SR are calculated to give an optimum SR value. SR is 'Lower the better' type response. Desired mean in this case is estimated as:

$\mu_{B_1,D_1} = \bar{B}_1 + \bar{D}_1 - \bar{T}$ = 6.474 + 6.467 - 7.2086 = 5.7324 µm

Confidence interval around the estimated SR:

$$CI = \sqrt{\frac{F_{\alpha,v_1,v_2} V_e}{n_{eff}}}$$

$$n_{eff} = \frac{N}{1 + DOF_{B,D}} = \frac{27}{1+4} = 5.4$$

$$CI = \sqrt{\frac{4.3 \times 0.44087}{5.4}} = \pm 0.5925$$

Thus the optimum value of SR is given by (5.7324 ± 0.5925) µm.

4.4.4 Result and analysis of SR using ring magnets with PMEDM

Results for SR

SR results for powder mixed EDM with ring magnet as magnetic assistance are listed in Table 4.48.

Table 4.48: SR Results (L27 OA-Ring magnet)

S. No.	Magnetic Field (T)	Current (A)	Powder Conc. (gm/l)	Work piece	Tool	Powder	Pulse On Time (µs)	SURFACE ROUGHNESS (µm)			
								Trial 1	Trial 2	Mean	S/N (dB)
1	0	3	3	D2	Cu	Gr	20	6.505	7	6.7525	-16.5951
2	0	3	6	D3	W-Cu	W	50	6.05	6.395	6.2225	-15.8826
3	0	3	9	H13	C18000	Ti	100	7.25	7.47	7.36	-17.3385
4	0	5	3	D2	Cu	W	50	7.09	8.075	7.5825	-17.6145
5	0	5	6	D3	W-Cu	Ti	100	8.68	6.53	7.605	-17.7079
6	0	5	9	H13	C18000	Gr	20	7.645	6.92	7.2825	-17.2564
7	0	7	3	D2	Cu	Ti	100	8.155	6.675	7.415	-17.4453
8	0	7	6	D3	W-Cu	Gr	20	6.09	5.68	5.885	-15.4002
9	0	7	9	H13	C18000	W	50	8.3	7.04	7.67	-17.7251
10	0.075	3	3	D3	C18000	W	100	6.69	7.47	7.08	-17.0138
11	0.075	3	6	H13	Cu	Ti	20	7.5	6.975	7.2375	-17.1975
12	0.075	3	9	D2	W-Cu	Gr	50	6.425	5.535	5.98	-15.558
13	0.075	5	3	D3	C18000	Ti	20	6.02	6.94	6.48	-16.2533
14	0.075	5	6	H13	Cu	Gr	50	8.155	8.575	8.365	-18.4521
15	0.075	5	9	D2	W-Cu	W	100	6.835	6.715	6.775	-16.6185
16	0.075	7	3	D3	C18000	Gr	50	6.89	9.07	7.98	-18.1203
17	0.075	7	6	H13	Cu	W	100	8.64	8.785	8.7125	-18.8032
18	0.075	7	9	D2	W-Cu	Ti	20	7.65	6.63	7.14	-17.0961
19	0.17	3	3	H13	W-Cu	Ti	50	7.435	6.365	6.9	-16.803
20	0.17	3	6	D2	C18000	Gr	100	4.84	6.46	5.65	-15.1293
21	0.17	3	9	D3	Cu	W	20	6.705	7.13	6.9175	-16.8031
22	0.17	5	3	H13	W-Cu	Gr	100	6.545	8.295	7.42	-17.4681
23	0.17	5	6	D2	C18000	W	20	7.44	6.23	6.835	-16.7287
24	0.17	5	9	D3	Cu	Ti	50	7.15	6.36	6.755	-16.6073
25	0.17	7	3	H13	W-Cu	W	20	7.47	7.885	7.6775	-17.7076
26	0.17	7	6	D2	C18000	Ti	50	8.77	7.08	7.925	-18.0291
27	0.17	7	9	D3	Cu	Gr	100	9.275	10.745	10.01	-20.032

Analysis of Variance of SR

From ANOVA results (Table 4.49), it is observed that current and tool materials are the most significant factors. With increase in current MRR is observed to increase, while maximum SR is observed for H13 workpiece. From response table (Table 4.50), it is observed that current is the most significant input parameter while powder and powder concentration are the least. From ANOVA plots (Figure 4.23), main effect plots it is observed that SR increases with strength of magnetic field and pulse on time. With increase in magnetic field strength,

the size of particles that is pulled out from the crater increases hence increasing the surface roughness. Surface roughness is observed lowest with the tungsten-copper tool and highest with the copper tool. From interaction plots, it is observed that while taking interaction of magnetic field and current in account, SR is found to decrease with increase in field strength for lower values of current while it increases for highest value of current. For highest and lowest current value, moderate concentration gives low SR while for moderate value of current, high concentration is supposed to work well.

Table 4.49: ANOVA Table for SR (L27 OA-Ring magnet)

Parameter	DOF	SS	MS	*F* (calculated)
Magnetic Field (T)	2	0.34724	0.17362	0.60
Current (A)	2	5.91291	2.95645	10.29
Powder Conc. (gm/l)	2	0.11834	0.05917	0.21
Workpiece	2	2.41020	1.20510	4.19
Tool	2	3.83140	1.91570	6.67
Powder	2	0.02623	0.01312	0.05
Pulse On Time (µs)	2	1.88690	0.94345	3.28
Magnetic Field × Current	4	3.82878	0.95720	3.33
Current × Powder Conc.	4	1.99028	0.49757	1.73
Error	4	1.14969	0.28742	
Total	26	21.5020		
e (pooled)	20	9.34757	0.46780	

Table 4.50: Response Table for SR (L27 OA-Ring magnet)

Level	Magnetic Field (T)	Current (A)	Powder Conc. (gm/l)	Workpiece	Tool	Powder	Pulse On Time (µs)
1	7.086	6.678	7.254	6.895	7.750	7.258	6.912
2	7.306	7.233	7.160	7.215	6.845	7.275	7.264
3	7.343	7.824	7.321	7.625	7.140	7.202	7.559
Delta	0.257	1.146	0.161	0.730	0.905	0.073	0.647
Rank	5	1	6	3	2	7	4

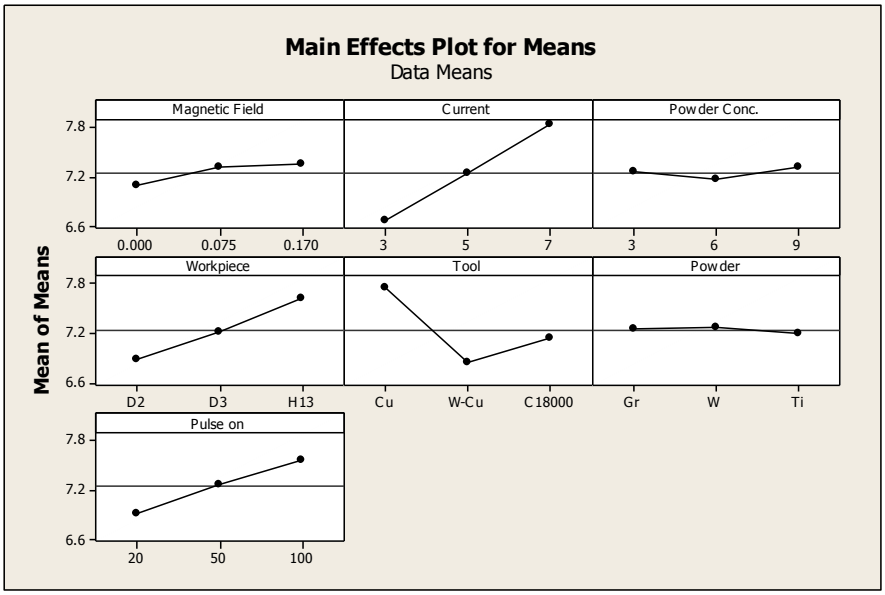

(a)

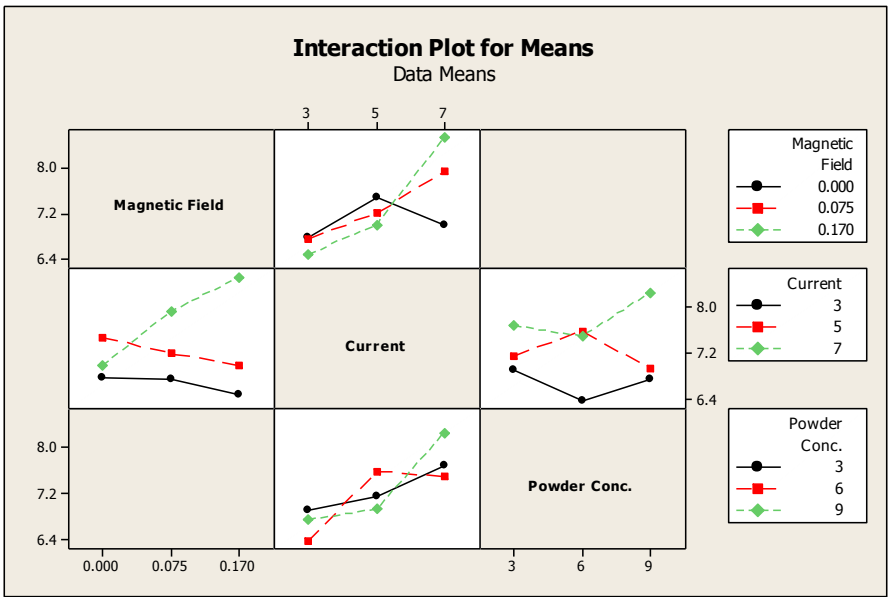

(b)

Figure 4.23: SR Plots (a) Mean effect plots; (b) Interaction plots (L27 OA-Ring magnet)

Analysis of variance of S/N ratio

Lower the better criterion is followed for calculating S/N ratio for roughness results. From ANOVA table (Table 4.51) and response table (Table 4.52), it is observed that current is the most contributing factor for S/N ratio while powders are the least. Figure 4.24 shows the ANOVA plots for S/N ratio.

Table 4.51: ANOVA Table for S/N ratio for SR (L27 OA-Ring magnet)

Parameter	DOF	SS	MS	*F* (calculated)
Magnetic Field (T)	2	0.37540	0.18770	0.41
Current (A)	2	8.06045	4.03022	8.90
Powder Conc. (gm/l)	2	0.21347	0.10673	0.24
Workpiece	2	3.56813	1.78407	3.94
Tool	2	4.93882	2.46941	5.45
Powder	2	0.04361	0.02181	0.05
Pulse On Time (µs)	2	2.37892	1.18946	2.63
Magnetic Field × Current	4	5.09232	1.27308	2.81
Current × Powder Conc.	4	2.78184	0.69546	1.54
Error	4	1.81189	0.45297	
Total	26	29.2649		

Table 4.52: Response Table for S/N ratio for SR (L27 OA-Ring magnet)

Level	Magnetic Field (T)	Current (A)	Powder Conc. (gm/l)	Workpiece	Tool	Powder	Pulse On Time (µs)
1	-17.00	-16.48	-17.22	-16.76	-17.73	-17.11	-16.78
2	-17.23	-17.19	-17.04	-17.09	-16.69	-17.21	-17.20
3	-17.26	-17.82	-17.23	-17.64	-17.07	-17.16	-17.51
Delta	0.26	1.34	0.19	0.88	1.03	0.10	0.72
Rank	5	1	6	3	2	7	4

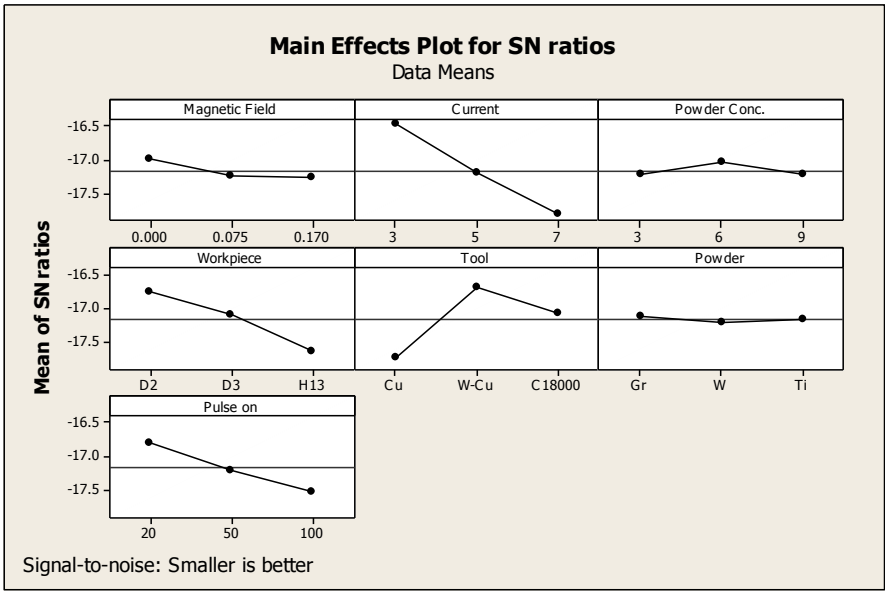

(a)

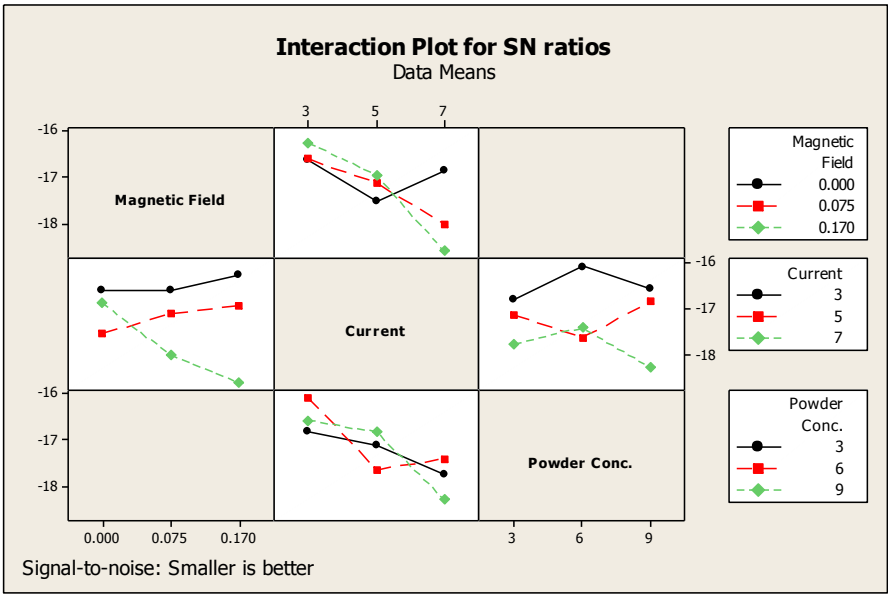

(b)

Figure 4.24: S/N ratio plots for SR (a) Mean effect plots; (b) Interaction plots (L27 OA-Ring magnet)

Optimal Design (Estimation of mean value)

In the experimental analysis, the mean effect plots corresponding to PMEDM (ring magnet assisted) (Figure 4.23) are used to estimate the mean SR with optimal design conditions. Mean values of SR are calculated to give an optimum SR value. SR is 'Lower the better' type response. Desired mean in this case is estimated as:

$\mu_{B_1,D_1,E_2} = \bar{B}_1 + \bar{D}_1 + \bar{E}_2 - 2\bar{T}$ = 6.678 + 6.895 + 6.845 – 2 × 7.245 = 5.568 µm

Confidence interval around the estimated SR:

$$CI = \sqrt{\frac{F_{\alpha,v_1,v_2} V_e}{n_{eff}}}$$

$$n_{eff} = \frac{N}{1 + DOF_{B,D,E}} = \frac{27}{1+6} = 3.85$$

$$CI = \sqrt{\frac{4.35 \times 0.4678}{3.85}} = \pm 0.727$$

Thus the optimum value of SR is given by (5.568 ± 0.727) µm.

4.5 RESULT AND ANALYSIS OF MICRO HARDNESS

4.5.1 Introduction

Microhardness being the surface characteristics, gives the value of hardness at micro level. It is calculated by applying some amount of force on the surface with the help of indenter. Then the size of the indent that is formed on the surface with respect to the force applied gives the MH value at that particular point. MH value is calculated in terms of Vickers's Hardness Number (VHN).

4.5.2 Result and analysis of MH using bar magnets with conventional EDM

Results for MH

MH results for conventional EDM with magnetic assistance are given in Table 4.53.

Table 4.53: MH Results (L18 OA)

S. No.	Current (A)	Magnetic Field (T)	Work piece	Tool	Pulse On Time (μs)	MH (VHN)
1	3	0	D2	Cu	50	191.3456
2	3	0.09	D3	W-Cu	100	261.057
3	3	0.36	H13	C18000	200	155.7333
4	4	0	D2	W-Cu	100	226.748
5	4	0.09	D3	C18000	200	213.23
6	4	0.36	H13	Cu	50	174.6093
7	5	0	D3	Cu	200	198.436
8	5	0.09	H13	W-Cu	50	233.1847
9	5	0.36	D2	C18000	100	187.28
10	6	0	H13	C18000	100	127.6564
11	6	0.09	D2	Cu	200	222.1353
12	6	0.36	D3	W-Cu	50	301.1573
13	7	0	D3	C18000	50	207.9245
14	7	0.09	H13	Cu	100	221.8952
15	7	0.36	D2	W-Cu	200	292.4432
16	8	0	H13	W-Cu	200	213.6374
17	8	0.09	D2	C18000	50	219.6353
18	8	0.36	D3	Cu	100	272.3296

Analysis of Variance of MH

From ANOVA table (Table 4.54) and response table (Table 4.55), it is summarized that for conventional EDM process tool material is the most significant factor that affects MH as material addition is only through the tool electrode. As tungsten-copper being the hardest tool material, maximum MH is observed for tungsten-copper tool. Then the workpiece material

and then magnetic field are next significant input parameters. D3 die steel as workpiece has shown maximum hardness followed by D2 and then H13. Increase in magnetic field strength has shown positive effect on MH increasing the MH. The presence of magnetic field facilitates the particles to stay on the machined surface for more time enhancing the compound formation and hence the MH. With increase in current also, MH is found to increase as material addition increases, as with the increase in current, more energy will be available which leads to more melting and hence more material addition. Figure 4.25 shows the ANOVA plots for MH. Form MH plots based on segregated current values (Figure 4.26), it is observed that MH shows varying results for interaction of current and magnetic field. For lower values of current, up to 5 A, it is observed that MH decreases with increase in magnetic field strength, while for higher values of current, it is observed that MH increases drastically with increase in magnetic field strength.

Table 4.54: ANOVA Table for MH (L18 OA)

Parameter	DOF	SS	MS	*F* (calculated)
Current (A)	5	4072.9	814.58	4.74
Magnetic Field (T)	2	4987.7	2493.83	14.50
Workpiece	2	9202.1	4601.05	26.75
Tool	2	14644.4	7322.22	42.57
Pulse On Time (µs)	2	110.9	55.43	0.32
Error	4	688.0	172.01	
Total	17	33706.0		
e (pooled)	6	798.9	133.15	

Table 4.55: Response Table for MH (L18 OA)

Level	Current (A)	Magnetic Field (T)	Workpiece	Tool	Pulse On Time (µs)
1	202.7	194.3	223.2	213.5	221.3
2	204.9	228.5	242.4	254.7	216.2
3	206.3	230.6	187.8	185.2	215.9
4	217.0				
5	240.8				
6	235.2				
Delta	38.0	36.3	54.6	69.5	5.4
Rank	3	4	2	1	5

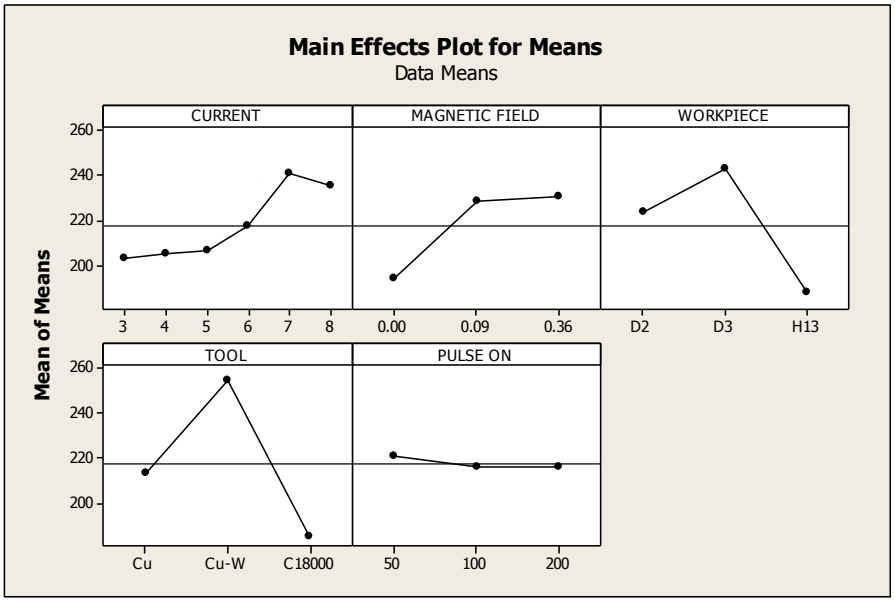

Figure 4.25: Mean effect plots for MH (L18 OA)

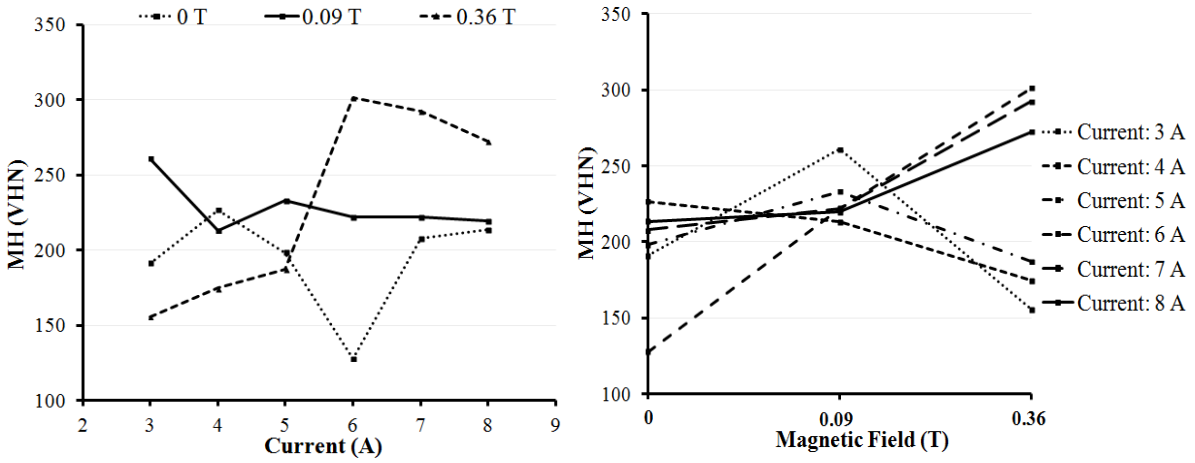

(a) (b)

Figure 4.26: MH plots for segregated current values (a) MH v/s Current; (b) MH v/s Magnetic Field (L18 OA)

Optimal design (Estimation of mean value)

In the experimental analysis, the mean effect plots (Figure 4.25) are used to estimate the mean MH values with optimal design conditions. Mean values of MH are calculated to give an optimum MH value. MH is 'Higher the better' type response. Desired mean in this case is estimated as:

$\mu_{A_6,B_3,C_2,D_2} = \bar{A}_6 + \bar{B}_3 + \overline{C_2} + \overline{D_2} - 3\bar{T}$ = 235.2 + 230.6 + 242.4 + 254.7 -3×217.8029 = 309.4937 VHN

Confidence interval around the estimated MH:

$$n_{eff} = \frac{N}{1 + DOF_{A,B,C,D}} = \frac{18}{1+11} = 1.5$$

$$CI = \sqrt{\frac{F_{\alpha,v_1,v_2} V_e}{n_{eff}}} = \sqrt{\frac{5.99 \times 133.15}{1.5}} = \pm 23.058$$

Thus the optimum value of SR is given by (309.4937 ± 23.058) VHN.

4.5.3 Result and analysis of MH using bar magnets with PMEDM

Results for MH

MH results for powder mixed EDM with bar magnets is listed in Table 4.56.

Table 4.56: MH Results (L27 OA-Bar magnet)

S. No.	Magnetic Field (T)	Current (A)	Powder Conc. (gm/l)	Work piece	Tool	Powder	Pulse On Time (μs)	MH (VHN)			
								Trial 1	Trial 2	Mean	S/N (dB)
1	0	3	3	D2	Cu	Gr	20	146.5065	149.8377	148.172	43.41368
2	0	3	6	D3	W-Cu	W	50	199.5407	170.699	185.119	45.26991
3	0	3	9	H13	C18000	Ti	100	200.016	200.88	200.448	46.03997
4	0	5	3	D2	Cu	W	50	201.4377	205.376	203.406	46.16609
5	0	5	6	D3	W-Cu	Ti	100	218.4418	223.0096	220.725	46.87566
6	0	5	9	H13	C18000	Gr	20	114.9062	110.6511	112.778	41.0399
7	0	7	3	D2	Cu	Ti	100	246.3681	258.0374	252.202	48.02802
8	0	7	6	D3	W-Cu	Gr	20	235.989	234.34	235.164	47.42728
9	0	7	9	H13	C18000	W	50	330.1585	336.915	333.536	50.46154
10	0.09	3	3	D3	C18000	W	100	292.2865	298.9581	295.622	49.41308
11	0.09	3	6	H13	Cu	Ti	20	169.4777	164.5243	167.001	44.45152
12	0.09	3	9	D2	W-Cu	Gr	50	209.4089	212.976	211.192	46.49264
13	0.09	5	3	D3	C18000	Ti	20	222.51	221.65	222.08	46.93014
14	0.09	5	6	H13	Cu	Gr	50	157.094	155.823	156.458	43.88777
15	0.09	5	9	D2	W-Cu	W	100	230.8149	228.3243	229.569	47.2179
16	0.09	7	3	D3	C18000	Gr	50	214.5998	213.6674	214.133	46.61363
17	0.09	7	6	H13	Cu	W	100	261.9815	256.0249	259.003	48.26438
18	0.09	7	9	D2	W-Cu	Ti	20	254.8351	238.6188	246.727	47.83026
19	0.36	3	3	H13	W-Cu	Ti	50	162.805	159.2916	161.048	44.13757
20	0.36	3	6	D2	C18000	Gr	100	207.5296	205.3063	206.418	46.29457
21	0.36	3	9	D3	Cu	W	20	273.406	270.6978	272.051	48.69271
22	0.36	5	3	H13	W-Cu	Gr	100	152.452	148.9559	150.704	43.56074
23	0.36	5	6	D2	C18000	W	20	250.387	249.7797	250.083	47.96168
24	0.36	5	9	D3	Cu	Ti	50	254.781	251.4772	253.129	48.06629
25	0.36	7	3	H13	W-Cu	W	20	283.877	287.818	285.847	49.12207
26	0.36	7	6	D2	C18000	Ti	50	294.7878	320.163	307.475	49.73402
27	0.36	7	9	D3	Cu	Gr	100	153.184	138.877	146.030	43.25759

Analysis of Variance of MH

ANOVA of MH (Table 4.57) has shown that highest *F*-value is observed for powder proving it the most significant factor. ANOVA plots (Figure 4.27) have shown that amongst the used powders, tungsten powder is the hardest and hence maximum hardness is observed with the

tungsten powder followed by titanium and then graphite powder. Then current is the next significant input parameter, which tends to increase MH with increase in current. For powder mixed EDM, tool electrode has shown not significant effect, in this case, MH is high for C18000 tool followed by tungsten-copper and then copper. MH is found to increase with increase in magnetic field. Interaction plots have shown that for lower values of current, MH increases with increase in field strength while it decreases for higher values of current. For higher current values, moderate powder concentration has given good results while for low value of current, higher concentration gives better MH values. Interaction plots have shown that except for higher current, MH is found to increase with the increase in magnetic field strength.

Table 4.57: ANOVA Table for MH (L27 OA-Bar magnet)

Parameter	DOF	SS	MS	*F* (calculated)
Magnetic Field (T)	2	1224.4	612.2	0.21
Current (A)	2	15606.9	7803.5	2.74
Powder Conc. (gm/l)	2	314.3	157.1	0.06
Workpiece	2	3684.9	1842.4	0.65
Tool	2	4921.0	2460.5	0.86
Powder	2	30377.4	15188.7	5.32
Pulse On Time (µs)	2	442.8	221.4	0.08
Magnetic Field × Current	4	6562.7	1640.7	0.58
Current × Powder Conc.	4	3775.7	943.9	0.33
Error	4	11412.4	2853.1	
Total	26	78322.5		
e (pooled)	18	17169.6	1318.46	

Table 4.58: Response Table for MH (L27 OA-Bar magnet)

Level	Magnetic Field (T)	Current (A)	Powder Conc. (gm/l)	Workpiece	Tool	Powder	Pulse On Time (µs)
1	210.2	205.2	214.8	228.4	206.4	175.7	215.5
2	222.4	199.0	220.8	227.1	214.0	257.1	225.1
3	225.9	253.3	222.8	203.0	238.1	225.6	217.9
Delta	15.7	53.5	8.0	25.4	31.7	81.5	9.5
Rank	5	2	7	4	3	1	6

Response table (Table 4.58) has shown that powder is the most significant factor while powder concentration has the least effect on the MH results.

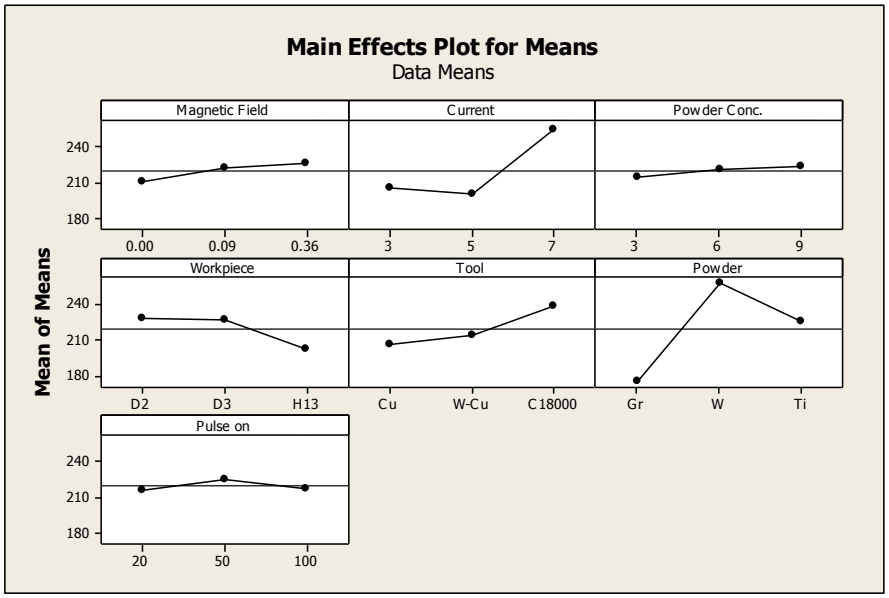

(a)

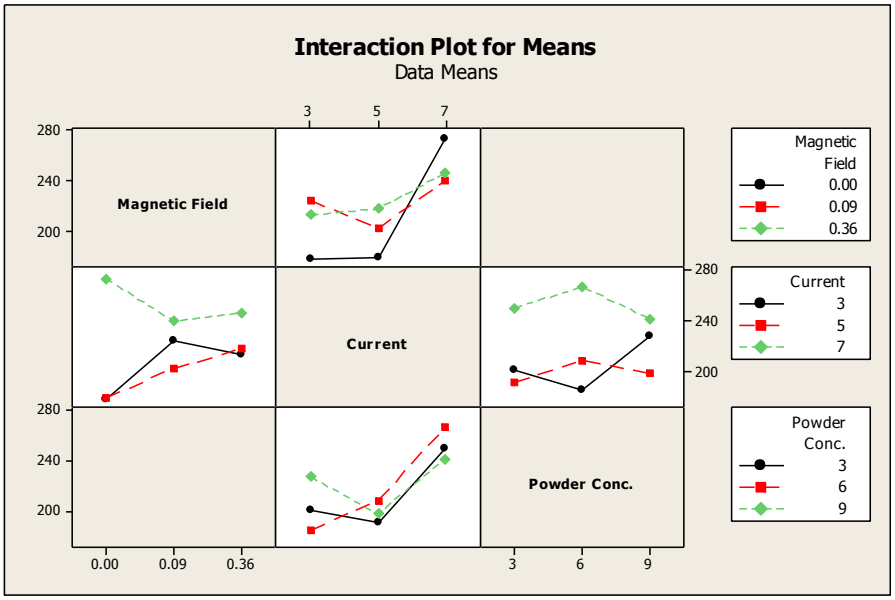

(b)

Figure 4.27: MH plots (a) Main effect plots; (b) Interaction plots (L27 OA-Bar magnet)

Analysis of variance of S/N ratio

As in case of MH, higher MH values are preferred as it offers better surface resistance. Hence higher the better criterion is followed to calculate S/N ratios (using Equation 3.1) for MH. ANOVA table for S/N ratios (Table 4.59) and response table (Table 4.60) have shown that powder is the most significant input parameter responding towards S/N ratio while powder concentration is the least affecting input parameter. Figure 4.28 shows the S/N ratio plots.

Table 4.59: ANOVA Table for S/N ratio for MH (L27 OA-Bar magnet)

Parameter	DOF	SS	MS	*F* (calculated)
Magnetic Field (T)	2	2.8905	1.4452	0.30
Current (A)	2	23.7716	11.8858	2.48
Powder Conc. (gm/l)	2	0.4376	0.2188	0.05
Workpiece	2	10.4688	5.2344	1.09
Tool	2	5.9990	2.9995	0.63
Powder	2	53.6746	26.8373	5.60
Pulse On Time (µs)	2	0.8721	0.4360	0.09
Magnetic Field × Current	4	11.121223	2.7860	0.58
Current × Powder Conc.	4	8.3442	2.0860	0.43
Error	4	19.1838	4.7960	
Total	26	136.764		

Table 4.60: Response Table for S/N ratio for MH (L27 OA-Bar magnet)

Level	Magnetic Field (T)	Current (A)	Powder Conc. (gm/l)	Workpiece	Tool	Powder	Pulse On Time (µs)
1	46.08	46.02	46.38	47.02	46.03	44.67	46.32
2	46.79	45.75	46.69	46.95	46.44	48.06	46.76
3	46.76	47.86	46.57	45.66	47.17	46.90	46.55
Delta	0.71	2.11	0.31	1.35	1.14	3.40	0.44
Rank	5	2	7	3	4	1	6

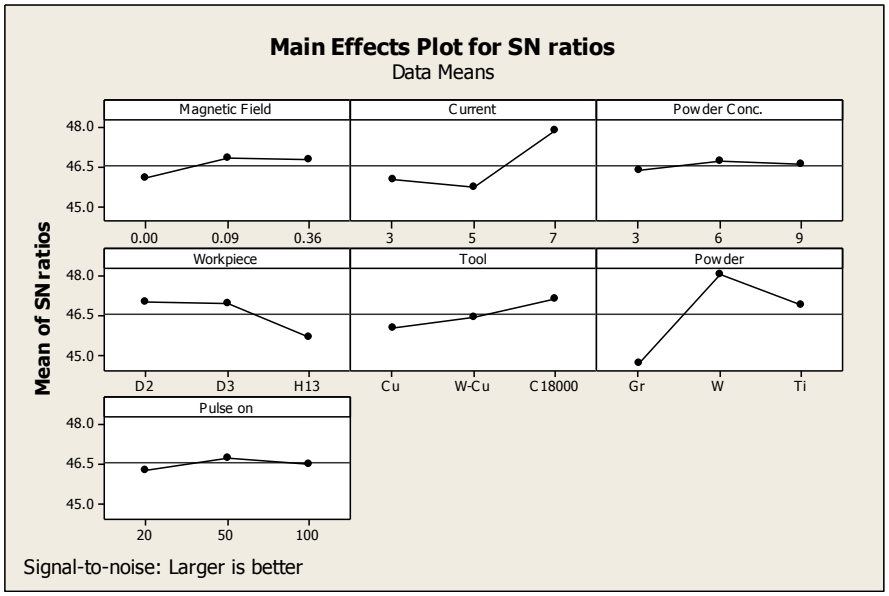

(a)

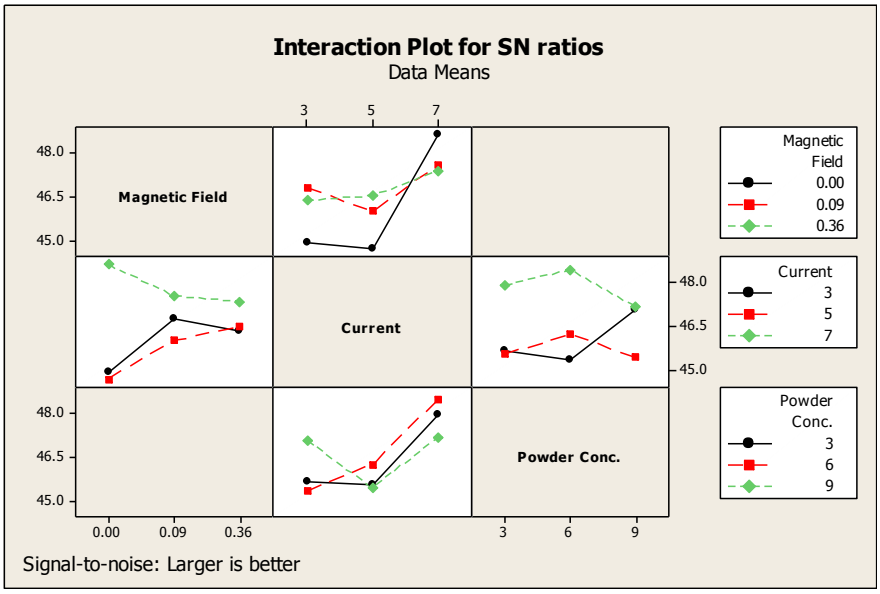

(b)

Figure 4.28: S/N ratio plots for MH (a) Main effect plots; (b) Interaction plots (L27 OA-Bar magnet)

Optimal Design (Estimation of mean value)

In the experimental analysis, the mean effect plots corresponding to PMEDM (bar magnets assisted) (Figure 4.27) are used to estimate the mean MH with optimal design conditions. Mean values of MH are calculated to give an optimum MH value. MH is 'Higher the better' type response. Desired mean in this case is estimated as:

$\mu_{B_3,D_1,E_3,F_2} = \bar{B}_3 + \bar{D}_1 + \bar{E}_3 + \bar{F}_2 - 3\bar{T}$ = 253.3 + 228.4 + 238.1 + 257.1 – 3 × 219.4863 = 318.46 VHN

Confidence interval around the estimated MH:

$$CI = \sqrt{\frac{F_{\alpha,v_1,v_2} V_e}{n_{eff}}}$$

$$n_{eff} = \frac{N}{1 + DOF_{B,D,E,F}} = \frac{27}{1+8} = 3$$

$$CI = \sqrt{\frac{4.41 \times 1318.46}{3}} = \pm 44.024$$

Thus the optimum value of MH is given by (318.46 ± 44.024) VHN.

4.5.4 Result and analysis of MH using ring magnet with PMEDM

Results for MH

MH results for PMEDM with ring magnet for field assistance are provided in Table.

Table 4.61: MH Results (L27 OA-Ring magnet)

S. No.	Magnetic Field (T)	Current (A)	Powder Conc. (gm/l)	Work piece	Tool	Powder	Pulse On Time (µs)	MH (VHN)			
								Trial 1	Trial 2	Mean	S/N (dB)
1	0	3	3	D2	Cu	Gr	20	157.17	156.0395	156.6078	43.8960
2	0	3	6	D3	W-Cu	W	50	180.78	184.049	182.419	45.2203
3	0	3	9	H13	C18000	Ti	100	206.86	201.2091	204.0358	46.1916
4	0	5	3	D2	Cu	W	50	230.46	228.2026	229.3313	47.2089
5	0	5	6	D3	W-Cu	Ti	100	221.29	223.0037	222.1513	46.9327
6	0	5	9	H13	C18000	Gr	20	114.01	113.5726	113.7956	41.1224
7	0	7	3	D2	Cu	Ti	100	254.57	255.0774	254.825	48.1248
8	0	7	6	D3	W-Cu	Gr	20	229.95	236.5947	233.2745	47.3547
9	0	7	9	H13	C18000	W	50	330.49	335.64	333.07	50.4499
10	0.075	3	3	D3	C18000	W	100	309.64	307.3973	308.5206	49.7855
11	0.075	3	6	H13	Cu	Ti	20	164.17	160.45	162.31	44.2051
12	0.075	3	9	D2	W-Cu	Gr	50	210.33	204.2754	207.3056	46.3294
13	0.075	5	3	D3	C18000	Ti	20	221.85	225.3495	223.6045	46.9888
14	0.075	5	6	H13	Cu	Gr	50	152.04	149.077	150.5589	43.5528
15	0.075	5	9	D2	W-Cu	W	100	225.82	228.1318	226.9764	47.1192
16	0.075	7	3	D3	C18000	Gr	50	216.98	215.549	216.269	46.6997
17	0.075	7	6	H13	Cu	W	100	257.31	246.015	251.6645	48.0098
18	0.075	7	9	D2	W-Cu	Ti	20	246.82	243.2612	245.0435	47.7841
19	0.17	3	3	H13	W-Cu	Ti	50	156.24	160.063	158.1561	43.9798
20	0.17	3	6	D2	C18000	Gr	100	203.48	205.8844	204.6858	46.2213
21	0.17	3	9	D3	Cu	W	20	274.40	272.7895	273.5968	48.7421
22	0.17	5	3	H13	W-Cu	Gr	100	150.38	149.1018	149.7434	43.5067
23	0.17	5	6	D2	C18000	W	20	253.85	251.943	252.8994	48.0587
24	0.17	5	9	D3	Cu	Ti	50	253.11	249.576	251.343	48.0046
25	0.17	7	3	H13	W-Cu	W	20	283.70	281.508	282.605	49.0234
26	0.17	7	6	D2	C18000	Ti	50	309.79	297.473	303.6321	49.6415
27	0.17	7	9	D3	Cu	Gr	100	142.17	138.731	140.4525	42.9486

Analysis of Variance of MH

ANOVA analysis of MH (Table 4.62) and response table (Table 4.63) has shown that powder is the most significant parameter while powder concentration has as such no effect on the MH results. Current is the next significant input parameter. From ANOVA plots (Figure 4.29), it is concluded that amongst the used powders, tungsten powder has shown the maximum MH results as it is the hardest powder and then for titanium and then graphite powder. Then current being the next significant input parameter, MH is observed to increase with the

increase in current. For powder mixed EDM, tool electrode has shown no significant effect, in this case, MH is high for C18000 tool followed by tungsten-copper and then copper. MH is found to increase with increase in magnetic field. Interaction plots have shown that for lower values of current, MH increases with increase in field strength while it decreases for higher values of current. For higher current values, moderate powder concentration has given good results while for low value of current, higher concentration gives better MH values. As on comparison it is observed that almost same results are obtained irrespective of the configuration of the magnet, whether bar magnet or the ring magnet.

Table 4.62: ANOVA Table for MH (L27 OA-Ring magnet)

Parameter	DOF	SS	MS	*F* (calculated)
Magnetic Field (T)	2	452.9	226.5	0.08
Current (A)	2	13256.9	6628.4	2.24
Powder Conc. (gm/l)	2	57.0	28.5	0.01
Workpiece	2	5076.8	2538.4	0.86
Tool	2	5529.3	2764.7	0.93
Powder	2	33146.0	16573.0	5.59
Pulse On Time (µs)	2	479.4	239.7	0.08
Magnetic Field × Current	4	6377.1	1594.3	0.54
Current × Powder Conc.	4	4024.7	1006.2	0.34
Error	4	11857.3	2964.3	
Total	26	80257.3		
e (pooled)	22	33854.4	1538.8	

Table 4.63: Response Table for MH (L27 OA-Ring magnet)

Level	Magnetic Field (T)	Current (A)	Powder Conc. (gm/l)	Workpiece	Tool	Powder	Pulse On Time (µs)
1	214.4	206.4	220.0	231.3	207.9	174.7	216.0
2	221.4	202.3	218.2	228.0	212.0	260.1	225.8
3	224.1	251.2	221.7	200.7	240.1	225.0	218.1
Delta	9.7	48.9	3.6	30.6	32.2	85.4	9.8
Rank	6	2	7	4	3	1	5

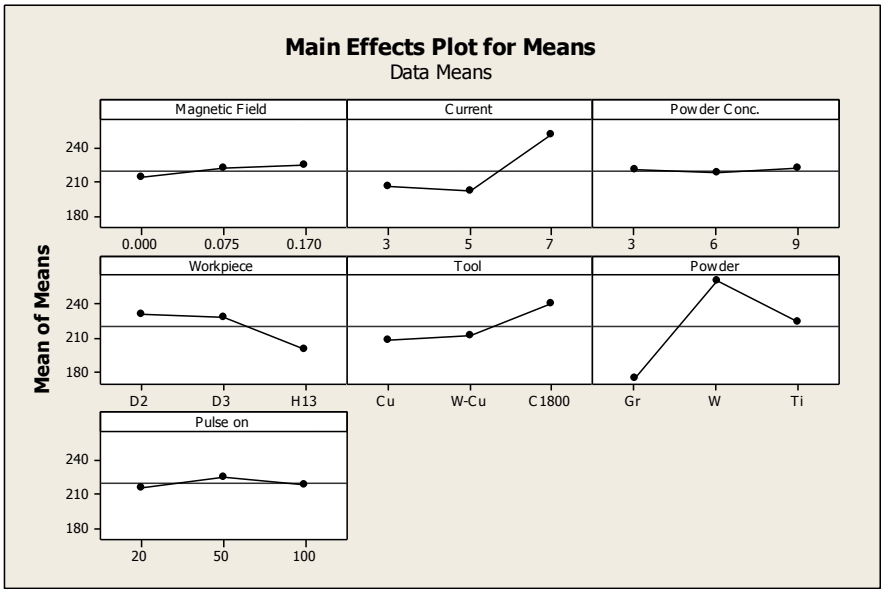

(a)

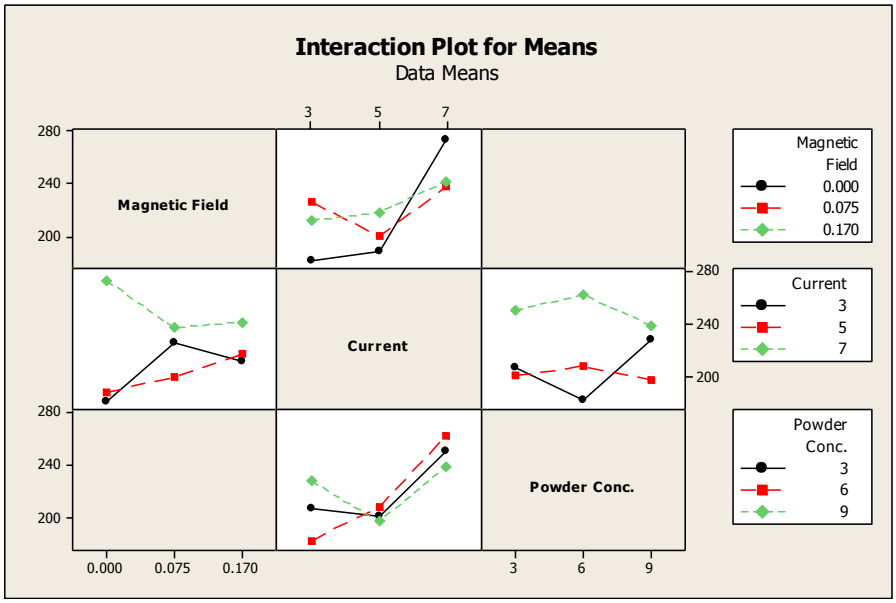

(b)

Figure 4.29: MH plots (a) Main effect plots; (b) Interaction plots (L27 OA-Ring magnet)

Analysis of variance of S/N ratio

Higher the better criterion is followed for S/N ratio calculation for MH. ANOVA table (Table 4.64), ANOVA plots (Figure 4.30) and response table (Table 4.65) has concluded that MH results are the most varied by the type of the powder signifying tungsten as powder while powder concentration is supposed to be the insignificant parameter for MH calculation.

Table 4.64: ANOVA Table for S/N ratio for MH (L27 OA-Ring magnet)

Parameter	DOF	SS	MS	*F* (calculated)
Magnetic Field (T)	2	1.0759	0.05380	0.10
Current (A)	2	20.4146	10.2073	1.97
Powder Conc. (gm/l)	2	0.0195	0.0098	0.00
Workpiece	2	13.6399	6.8199	1.32
Tool	2	6.6164	3.3082	0.64
Powder	2	58.1644	29.0822	5.61
Pulse On Time (µs)	2	0.8563	0.4282	0.08
Magnetic Field × Current	4	9.9649	2.4912	0.48
Current × Powder Conc.	4	8.8415	2.2104	0.43
Error	4	20.7301	5.1825	
Total	26	140.324		

Table 4.65: Response Table for S/N ratio for MH (L27 OA-Ring magnet)

Level	Magnetic Field (T)	Current (A)	Powder Conc. (gm/l)	Workpiece	Tool	Powder	Pulse On Time (µs)
1	46.28	46.06	46.58	47.15	46.08	44.63	46.35
2	46.72	45.83	46.58	46.96	46.36	48.18	46.79
3	46.68	47.78	46.52	45.56	47.24	46.87	46.54
Delta	0.44	1.95	0.06	1.59	1.16	3.55	0.43
Rank	5	2	7	3	4	1	6

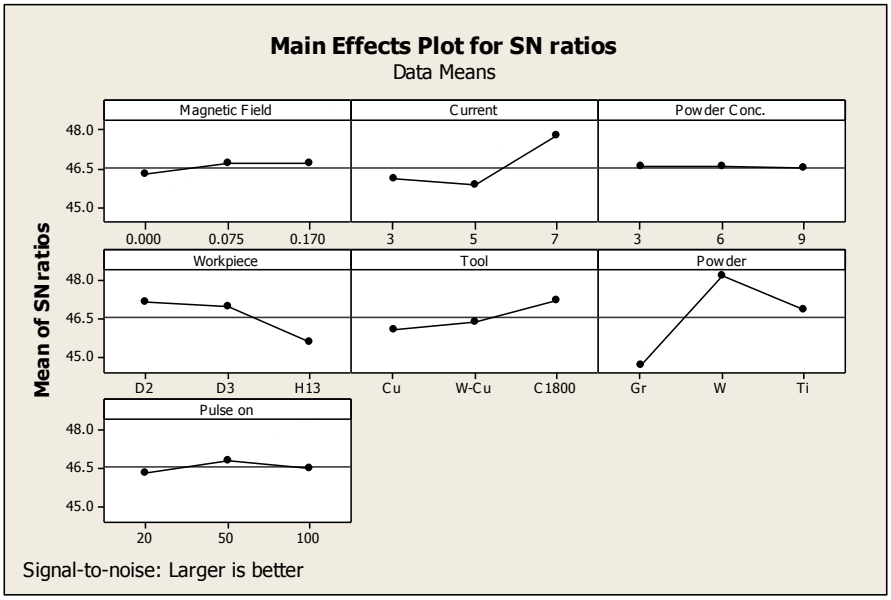

(a)

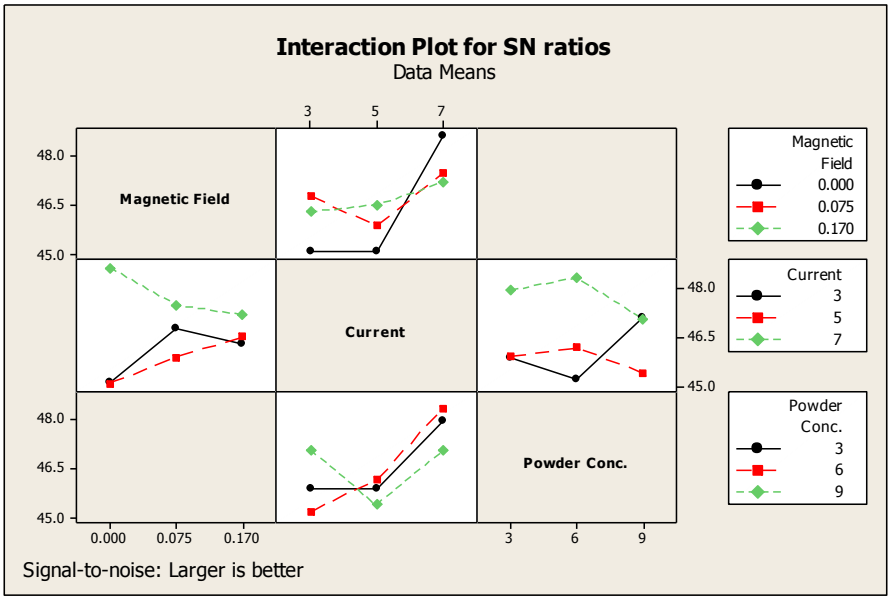

(b)

Figure 4.30: S/N ratio Plots for MH (a) Main effect plots; (b) Interaction plots (L27 OA-Ring magnet)

Optimal Design (Estimation of mean value)

In the experimental analysis, the mean effect plots corresponding to PMEDM (ring magnets assisted) (Figure 4.29) are used to estimate the mean MH with optimal design conditions. Mean values of MH are calculated to give an optimum MH value. MH is 'Higher the better' type response. Desired mean in this case is estimated as:

$\mu_{B_3,F_2} = \bar{B}_3 + \bar{F}_2 - \bar{T}$ = 251.2 + 260.1 – 219.958 = 291.342 VHN

Confidence interval around the estimated MH:

$$CI = \sqrt{\frac{F_{\alpha,v_1,v_2} V_e}{n_{eff}}}$$

$$n_{eff} = \frac{N}{1+ DOF_{B,F}} = \frac{27}{1+4} = 5.4$$

$$CI = \sqrt{\frac{4.3 \times 1538.836}{5.4}} = \pm 30$$

Thus the optimum value of MH is given by (291.342 ± 30) VHN.

CHAPTER 5
METALLURGICAL ANALYSIS

5.1 INTRODUCTION

Metallurgical analysis is basically based on the microstructure, phase and composition study of the parent and machined samples. In present study, various input parameters are used like current, pulse on time, work piece material, tool electrode material, powders, powder concentration and magnetic field are varied while machining with EDM and PMEDM. Input parameters mainly decide the total amount of energy available for machining, which further affects the response characteristics. Higher the current and pulse on time, more is the available energy for machining. During machining a very high temperature of the range 8000℃ is generated, this temperature causes material to melt and even evaporate. Re-solidification of melted metal takes place by rapid cooling by dielectric forming the craters and hence the subsequent change in microstructure. While other input parameters support better material removal and other response characteristics but also add on to the change in surface properties, mainly composition. Material may be deposited in free or compound form to the machined surface, from the used electrodes and powders, which further changes the microstructure and composition of the machined surface. Hence analysis of metallurgical aspects of machining is done on SEM (Scanning Electron Microscope) for microstructure analysis, XRD (X-Ray Diffraction) for phase and composition analysis. Further metallurgical microscope is also used for microstructure analysis to study of crater behaviour.

5.2 MICROSTUCTURE ANALYSIS

Microstructure analysis was carried out on some selected samples using SEM machine (Model-LEO 435 VP, SEMTech Solutions, USA) to study change in microstructure after machining on EDM. SEM is mainly used for imaging the surface and detecting small surface features. Sample preparation was done as per standard requirement. SEM micrographs are taken at 200×, 500× and 1000×. Sample preparation mainly involves cutting the machined samples group in smaller size, so that 2-4 samples can be accommodated on a slit in a manner to properly accommodate the samples on SEM machine, cleaning of samples by acetone and ECG gel to properly clean the machined surface. SEM micrographs are arranged as per workpiece material.

5.2.1 Microstructure analysis of AISI D2 work piece material

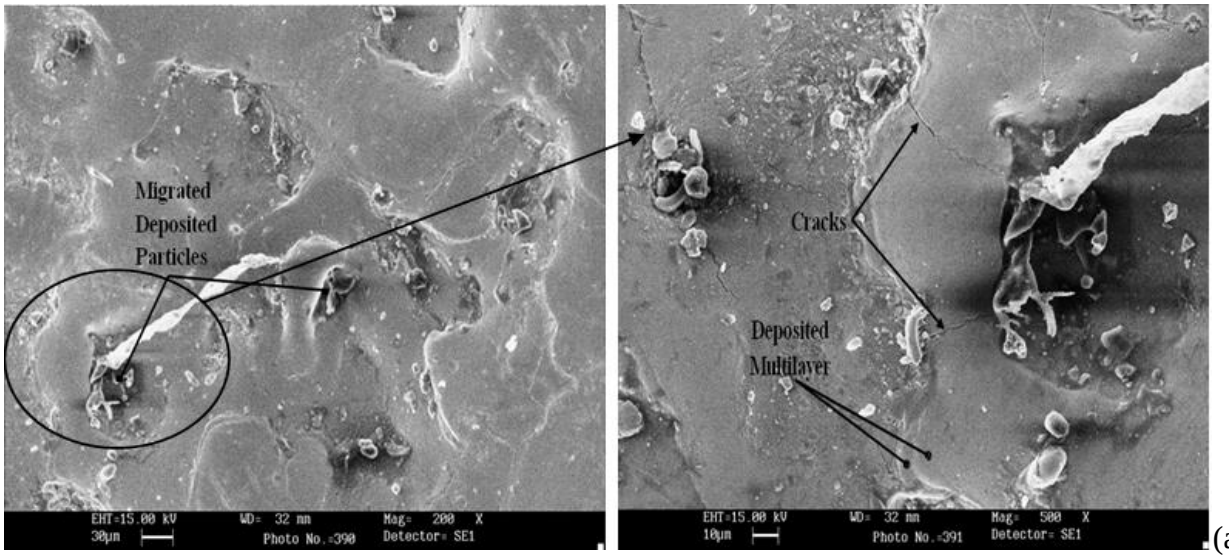

(a) (b)

Figure 5.1: SEM micrograph for AISI-D2 workpiece machined with tungsten powder (conc. 3 gm/l) with copper tool without magnetic field at 5 A current, 50 µs pulse on time (a) 200×; (b) 500×

Figure 5.1 shows SEM micrograph for AISI-D2 workpiece machined with tungsten powder with concentration 3 gm/l, using copper tool without any field assistance at different magnifications at 5 A current. As current is low, hence energy available is also low; because of this surface cracks are found low. Less multilayer deposition because of less frequency is observed as a result of low powder concentration making surface roughness value low (R_a=6.3 µm). Some migrated deposited particles are observed, migrated from tool or powder mixed.

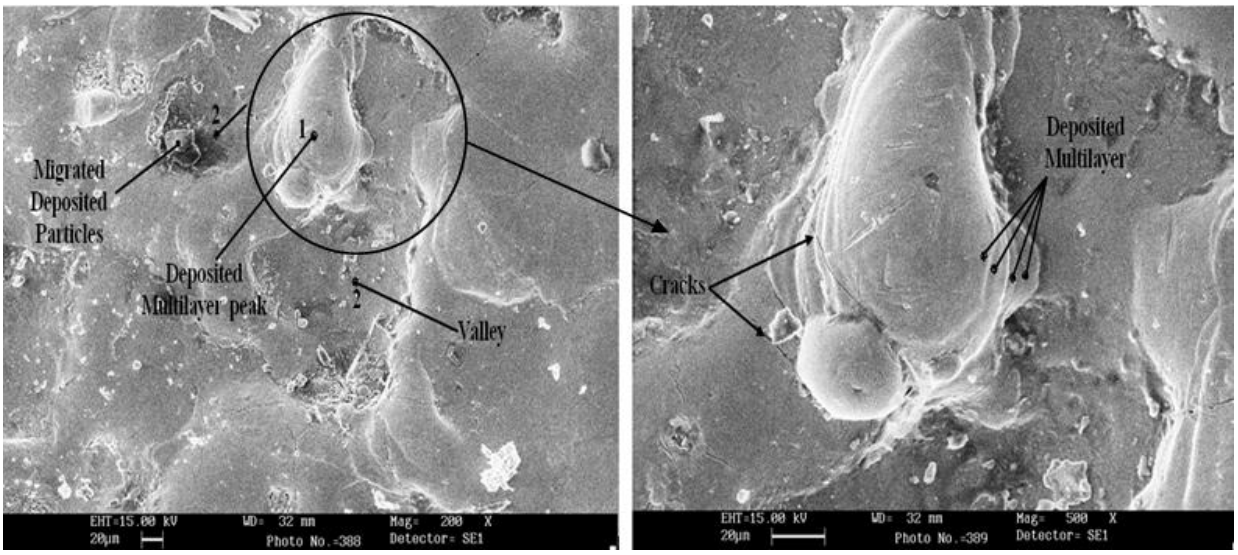

(a) (b)

Figure 5.2: SEM micrograph for AISI-D2 workpiece machined with tungsten powder (conc. 6 gm/l) with C18000 tool with 0.36 T bar magnets at 5 A current, 20 µs pulse on time (a)

200×; (b) 500×

SEM micrograph for AISI-D2 workpiece machined with tungsten powder (concentration 6 gm/l) and C18000 tool under magnetic field assistance of bar magnets with field strength 0.36 T at 5 A current is shown in Figure 5.2. Higher spark frequency is observed as powder concentration is more. Due to this more overlapped deposition is observed causing a large difference to be created between deposited peak and valley (deep groove), which have resulted in higher roughness (R_a=7.3 µm). Fewer cracks are there, which are visible at 500× magnification.

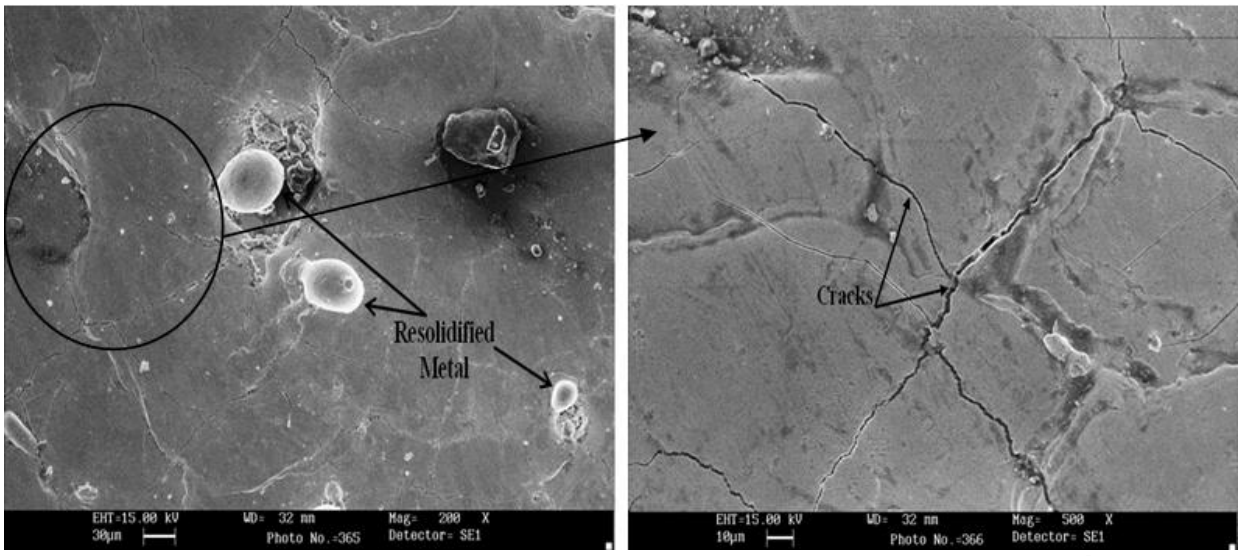

(a) (b)

Figure 5.3: SEM micrograph for AISI-D2 workpiece machined without powder with tungsten-copper tool with 0.36 T bar magnets at 7 A current, 200 µs pulse on time (a) 200×; (b) 500×

SEM micrograph for AISI-D2 workpiece machined with tungsten-copper tool and bar magnets of strength 0.36 T at 7 A current and 200 µs pulse on time at two different magnifications is shown in Figure 5.3. From the micrograph it is observed that as the current is very high, so more surface cracks are present. As powder is not used hence, low frequency of sparks is present avoiding multilayer deposition. Surface is quite smooth with peaks and valleys, giving a moderate SR value (R_a =7.59 µm). In this case, plasma impulse force is high leading to splash out metal droplets (resolidified metal).

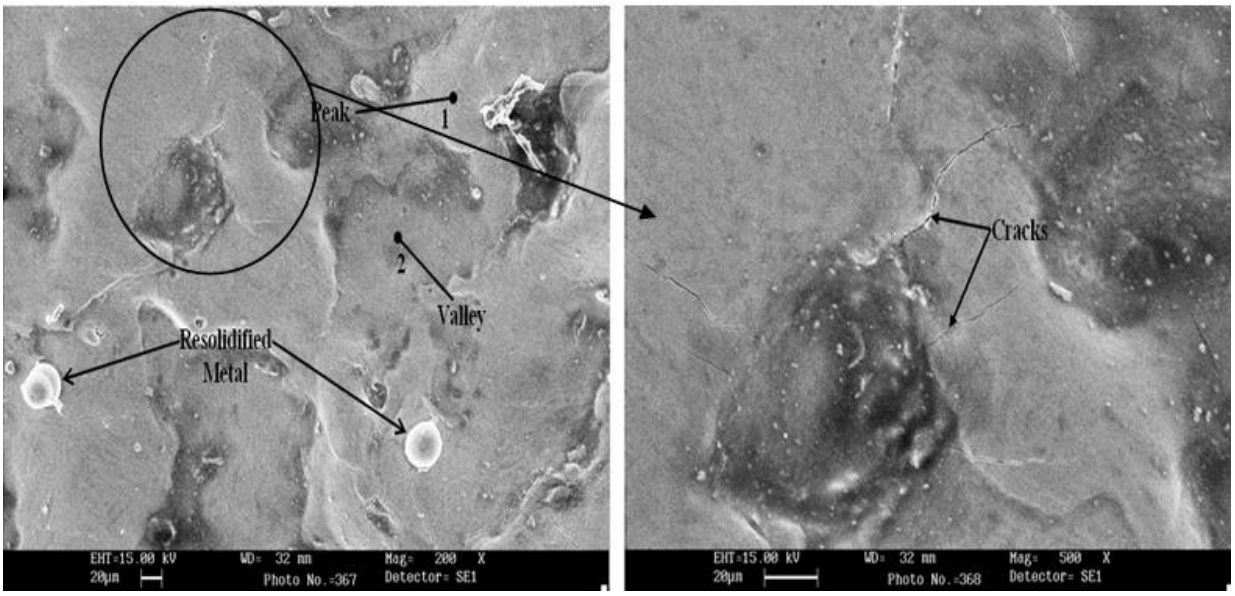

(a) (b)

Figure 5.4: SEM micrograph for AISI-D2 workpiece machined without powder with C18000 tool with 0.09 T bar magnets at 8 A current, 50 µs pulse on time (a) 200×; (b) 500×

Figure 5.4 shows SEM micrograph for AISI-D2 workpiece machined with C18000 tool and bar magnets with strength 0.09 T at 8 A current, 50 µs pulse on time. From micrograph, it is observed that surface appearance as quite rough including a large number of peaks and valleys leading to a very high SR value (R_a = 10.18 µm). Impulse force is observed high giving resolidified splash out metal. Moderate cracks are observed even at very high current value.

5.2.2 Microstructure analysis of AISI D3 work piece material

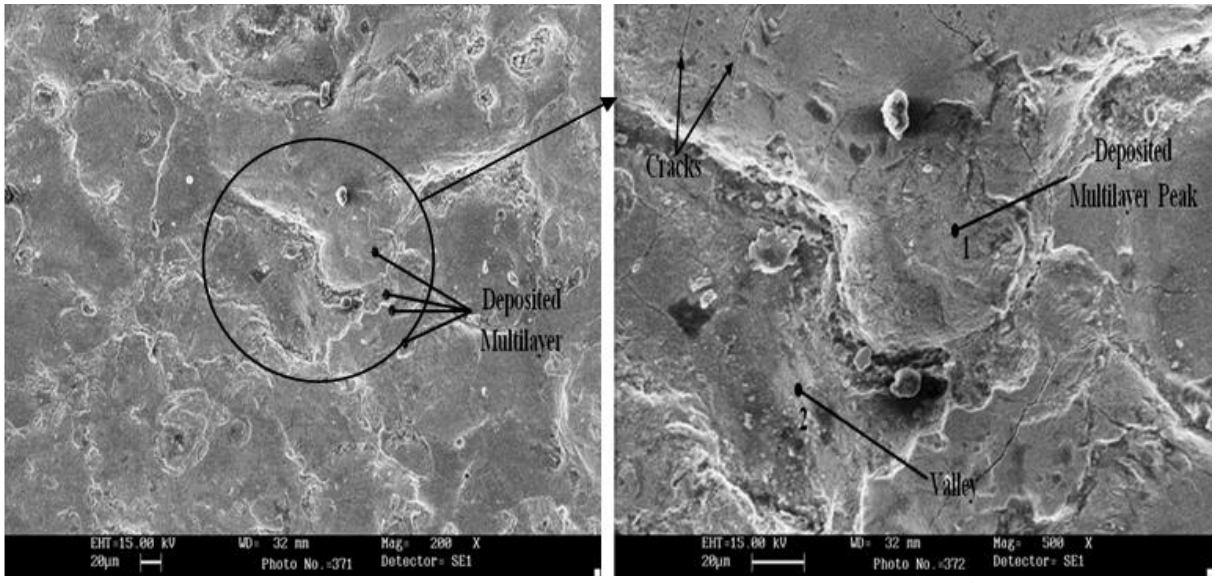

(a) (b)

Figure 5.5: SEM micrograph for AISI-D3 workpiece machined with titanium powder (conc. 3 gm/l) with C18000 tool with 0.075 T ring magnet at 5 A current, 20 µs pulse on time (a) 200×; (b) 500×

Figure 5.5 shows micrograph for AISI-D3 workpiece machined with titanium powder with concentration 3 gm/l using C18000 tool with 0.075 T ring magnet at 5 A current, 20 µs pulse on time. Micrograph shows that more uniform spark is there all over the surface leading to high MRR (MRR =14.4085 mm^3/min) value. High frequency of spark is observed leading to deposited multilayer as a result of mixed powder. As moderate current is used, cracks found are fewer on the surface, which are visible at 500×.

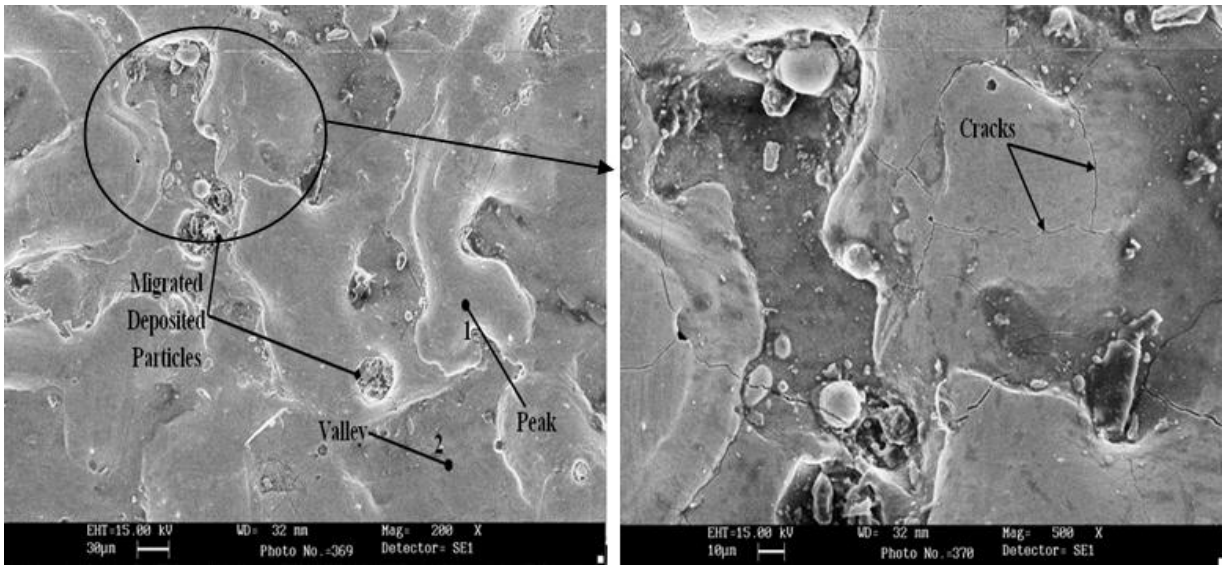

(a) (b)

Figure 5.6: SEM micrograph for AISI-D3 workpiece machined with titanium powder (conc. 9 gm/l) with copper tool with 0.17 T ring magnet at 5 A current, 50 µs pulse on time (a) 200×; (b) 500×

Figure 5.6 shows microstructure of AISI-D3 workpiece machined with titanium powder at concentration 9 gm/l with copper tool with 0.17 T ring magnet at 5 A current and 50 µs pulse on time. Migrated deposited particles are observed, migrated from tool or powder. Moderate surface cracks are observed as machining is done on a moderate current value. Uniform spark is observed with some overlapped metal layers leading to a moderate roughness value (R_a = 6.755 µm).

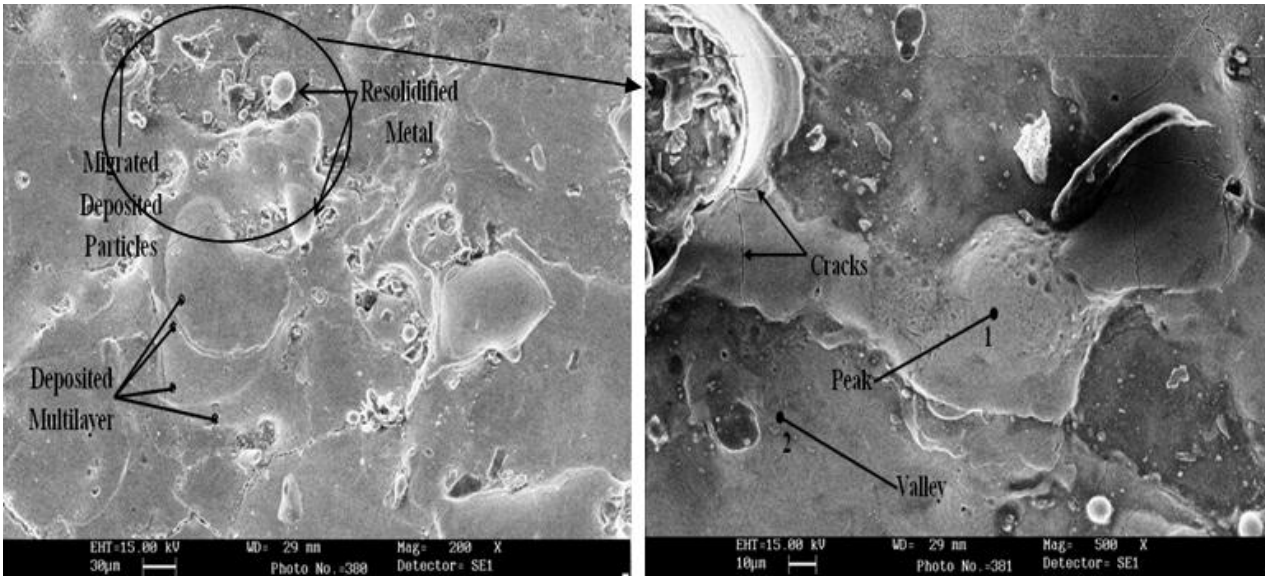

(a) (b)

Figure 5.7: SEM micrograph for AISI-D3 workpiece machined with graphite powder (conc. 3 gm/l) with C18000 tool with 0.075 T ring magnet at 7 A current, 50 µs pulse on time (a) 200×; (b) 500×

Microstructure of AISI D3 workpiece machined with graphite powder at concentration 3 gm/l with C18000 tool with 0.075 T ring magnet at 7 A current and 50 µs pulse on time is shown in Figure 5.7. Deposited multilayer are observed as a result of high spark frequency leading to high MRR value (MRR = 16.008 mm^3/min) and high SR value (R_a = 7.98 µm). Migrated deposited particles are noticed at some points, migrated from tool electrode or used powder. As graphite powder is used, cracks are low even at high current, because graphite absorbs heat reducing total heat available.

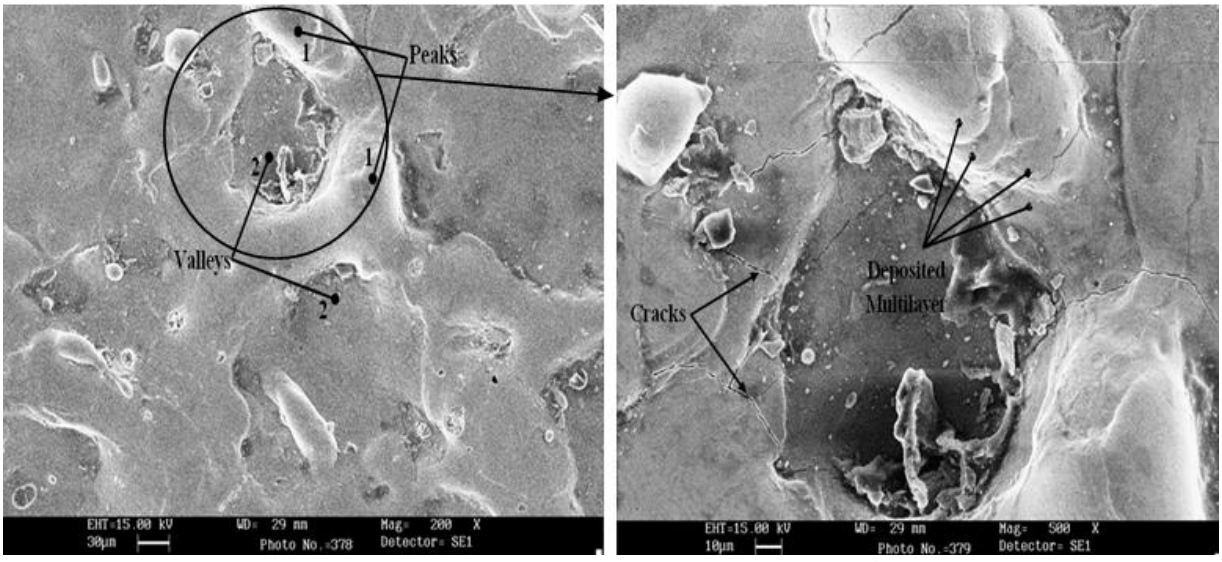

(a) (b)

Figure 5.8: SEM micrograph for AISI-D3 workpiece machined with graphite powder (conc. 6 gm/l) with tungsten- copper tool without magnet at 7 A current, 20 µs pulse on time (a) 200×; (b) 500×

Microstructure of AISI-D3 workpiece machined at 7 A current and 20 µs pulse on time with tungsten-copper tool and graphite powder at 6 gm/l concentration is shown in Figure 5.8. From the microstructure, it is observed that, even though the current value is quite high, surface cracks are too low, even at 500× because of graphite powder that is used for machining, which utilises heat produced, leaving lesser heat for surface to gain leading to lesser surface cracks. More peaks and valleys are observed reporting presence of more craters leading to a very high MRR value (MRR =19.8695 mm^3/min). Peaks and valleys that are formed are shallow in nature, with smooth multilayer seen at 500× leading to very low SR value (R_a =5.81 µm).

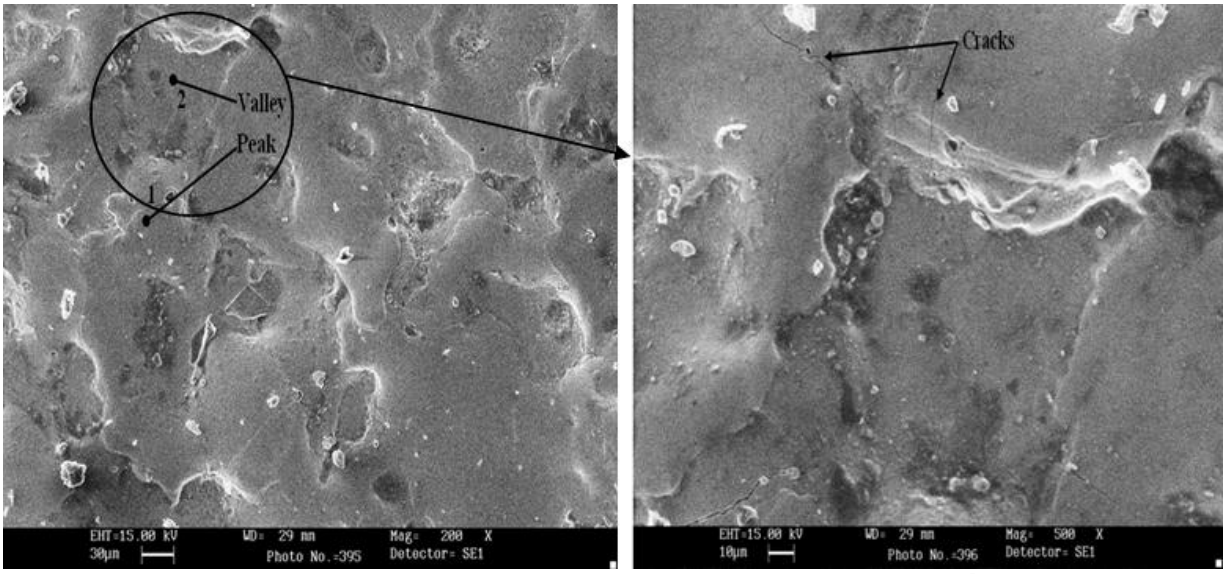

(a) (b)

Figure 5.9: SEM micrograph for AISI-D3 workpiece machined without powder with tungsten-copper tool with 0.09 T bar magnets at 3 A current, 100 µs pulse on time (a) 200×; (b) 500×

Figure 5.9 shows micrograph for AISI-D3 workpiece machined with tungsten-copper tool with 0.09 T bar magnets at 3 A current and 100 µs pulse on time. As current is very low, very low energy is available, hence surface cracks are very minute and MRR is very low (MRR = 2.926 mm^3/min). Randomly distributed shallow peaks and valleys are present on the machined surface.

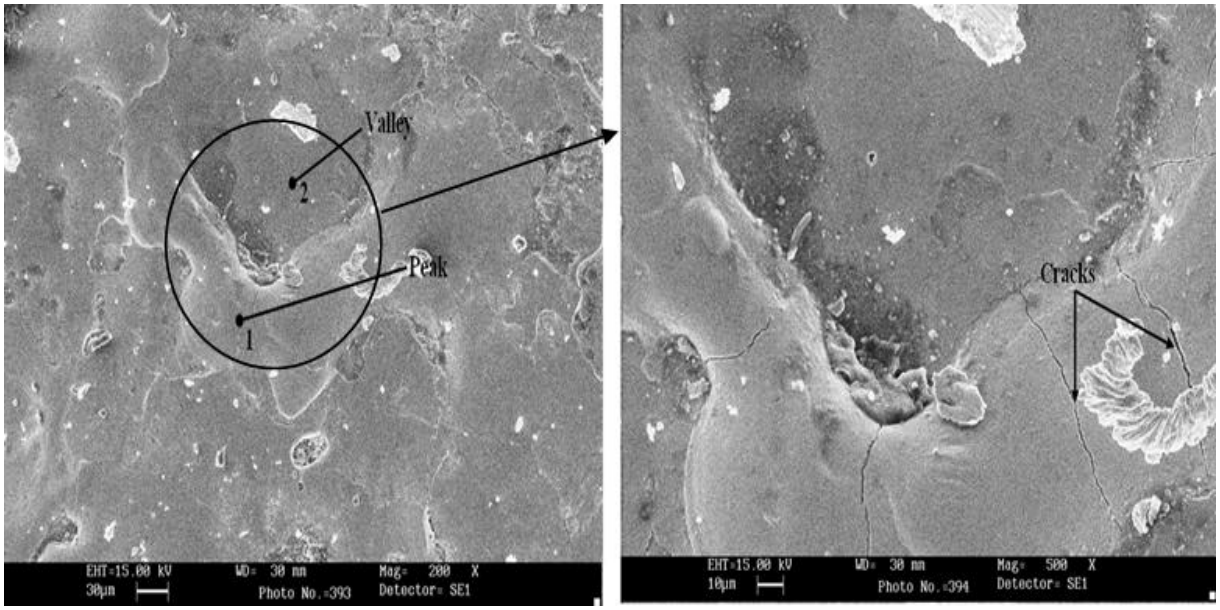

(a) (b)

Figure 5.10: SEM micrograph for AISI-D3 workpiece machined without powder with copper tool with 0.36 T bar magnets at 8 A current, 100 µs pulse on time (a) 200×; (b) 500×

SEM micrograph for AISI-D3 workpiece machined with copper tool with 0.36 T bar magnets at 8 A current and 100 µs pulse on time is shown in Figure 5.10. As deposited multilayer is absent, it implies that lesser spark frequency is there. But craters are observed to be deep and wider, leading to a good MRR value (MRR = 11.57 mm^3/min) and very high roughness value (R_a = 9.71 µm).

5.2.3 Microstructure analysis of AISI H13 work piece material

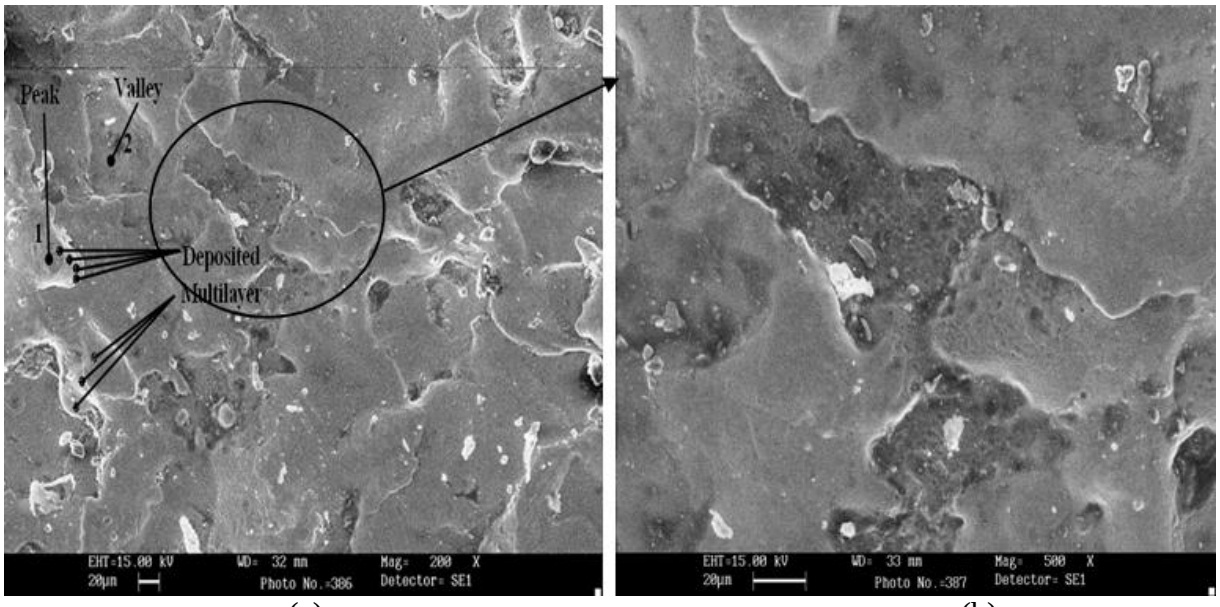

(a) (b)

Figure 5.11: SEM micrograph for AISI-H13 workpiece machined with titanium powder (conc. 6 gm/l) with copper tool with 0.09 T bar magnets at 3 A current, 20 µs pulse on time (a) 200×; (b) 500×

Figure 5.11 shows microstructure of AISI-H13 workpiece machined at 3 A current and 20 µs pulse on time with titanium powder at concentration 6 gm/l with copper tool under the effect of 0.09 T bar magnets. Uniformly deposited multilayer are present throughout the machined surface reporting the high spark frequency, which have maintained an optimum MRR (MRR =6.297 mm^3/min) even at very low current value. No cracks are observed on the surface even at 500× magnification.

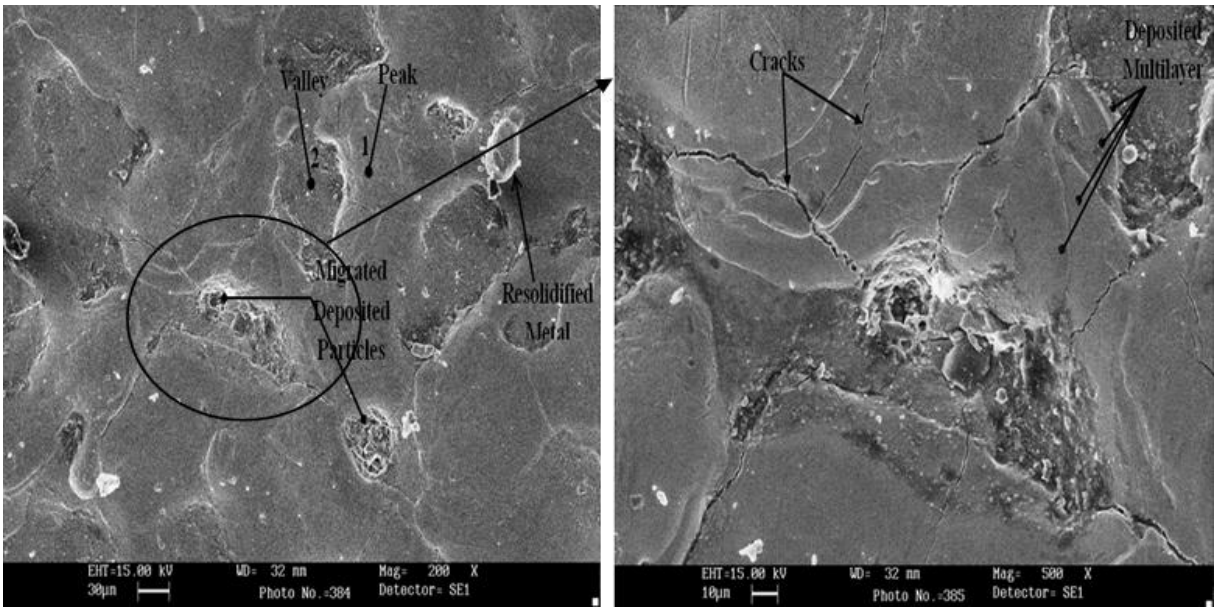

(a) (b)

Figure 5.12: SEM micrograph for AISI-H13 workpiece machined with titanium powder (conc. 3 gm/l) with tungsten- copper tool with 0.36 T bar magnets at 3 A current, 50 µs pulse on time (a) 200×; (b) 500×

Microstructure of AISI-H13 workpiece material machined with tungsten-copper tool under the effect of 0.36 T bar magnets at 3 A current and 50 µs pulse on time with titanium powder at concentration 3 gm/l is shown in Figure 5.12. Microstructure shows some resolidified metal particles showing higher impact force. Some migrated deposited particles are seen, from tool or used powder. Some multilayer is present, mainly seen at 500× magnification.

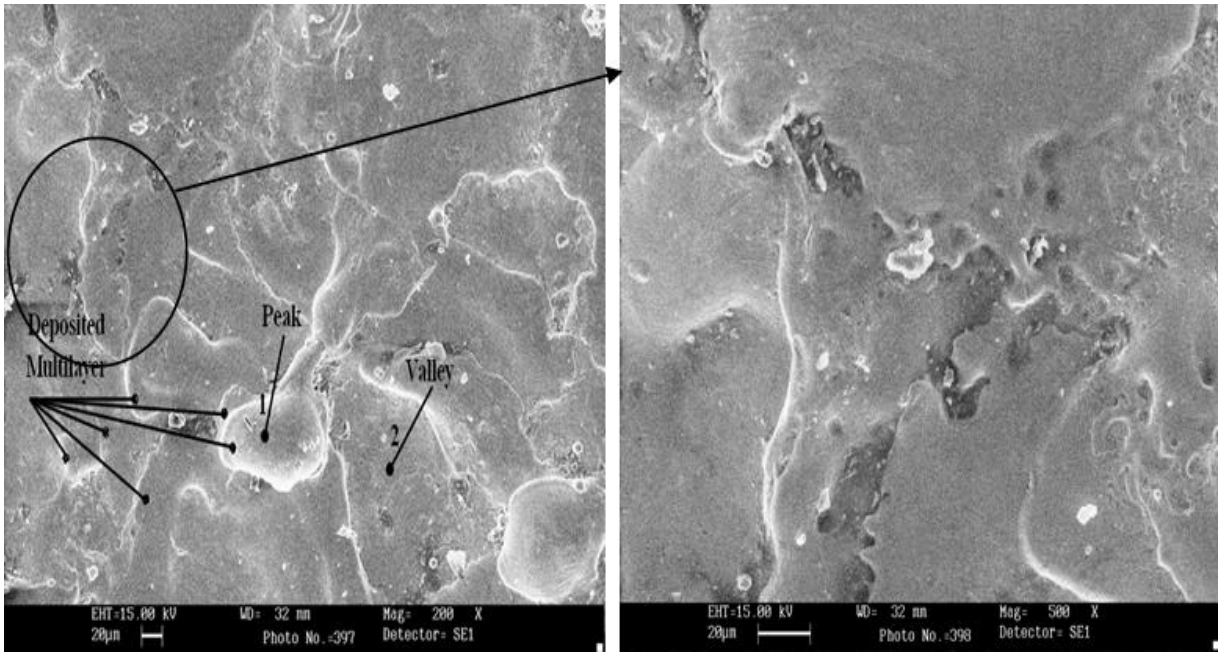

(a) (b)

Figure 5.13: SEM micrograph for AISI-H13 workpiece machined with titanium powder (conc. 6 gm/l) with copper tool with 0.075 T ring magnet at 3 A current, 20 µs pulse on time (a) 200×; (b) 500×

Figure 5.13 shows micrograph for AISI-H13 workpiece machined with titanium powder at concentration 6 gm/l using copper tool with 0.075 T ring magnet at 3 A current and 20 µs pulse on time. Multilayer deposition is observed throughout the entire surface. As current is very low, no surface cracks are observed on the surface.

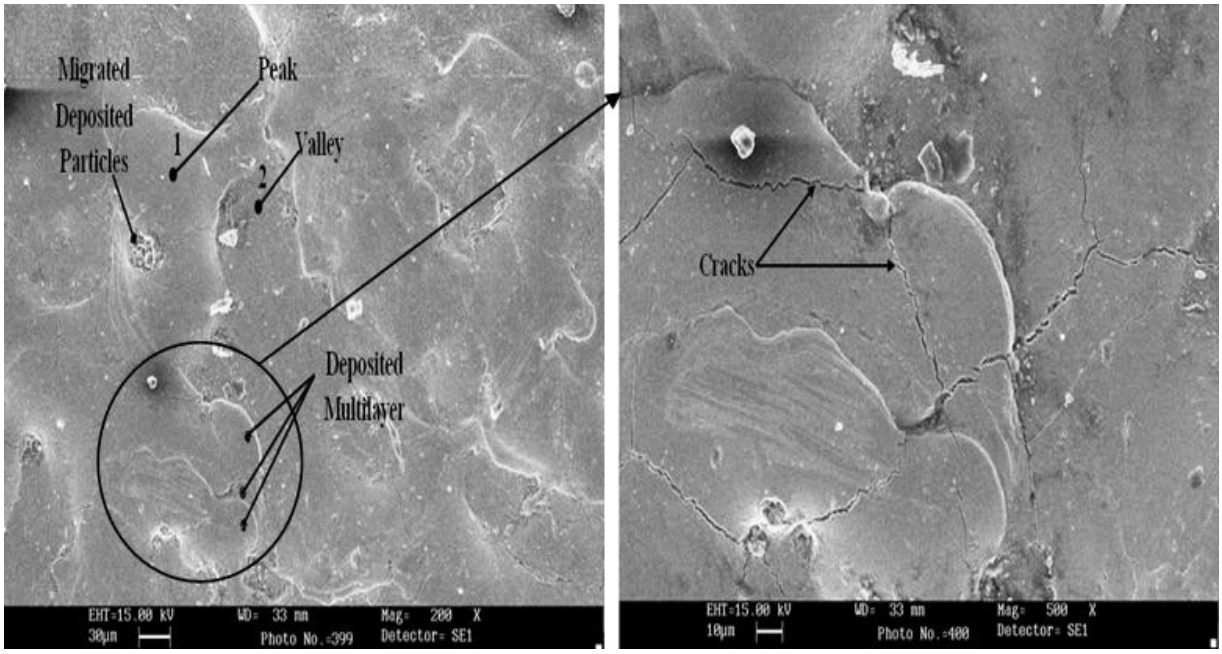

(a) (b)

Figure 5.14: SEM micrograph for AISI-H13 workpiece machined with tungsten powder (conc. 6 gm/l) with copper tool with 0.075 T ring magnet at 7 A current, 100 µs pulse on time (a) 200×; (b) 500×

SEM micrograph for AISI-H13 workpiece machined copper tool and tungsten powder at concentration 6 gm/l with 0.075 T ring magnet at 7 A current and 100 µs pulse on time is shown in Figure 5.14. Migrated deposited particles are observed, from tool or powder. Deposited multilayer (due to more spark frequency) is observed with thick deposited layers creating a wide gap between peak and valley increasing roughness of the surface (R_a =8.7125 µm). As current is very high, hence more cracks are observed on the surface (clearly visible on 500× magnification). Uniform spark is observed over the entire surface leading to high MRR (MRR = 13.055 mm^3/min).

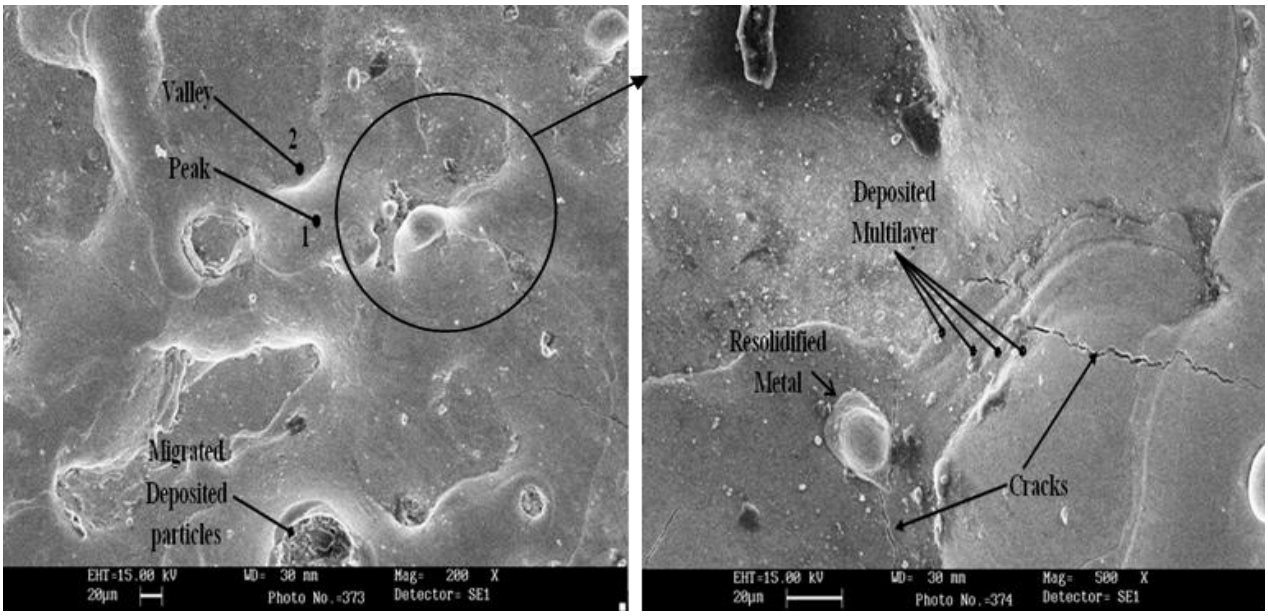

(a) (b)

Figure 5.15: SEM micrograph for AISI-H13 workpiece machined without powder with C18000 tool without magnet at 6 A current, 100 µs pulse on time (a) 200×; (b) 500×

SEM micrograph for AISI-H13 workpiece machined with C18000 tool at 6 A current and 100 µs pulse on time without any field assistance is shown in Figure 5.15. Some migrated particles are found deposited on the surface, from tool electrode. Smooth multilayer deposition is noticed at 500× magnification. Higher impact force is noticed as resolidified metal is also observed on the surface.

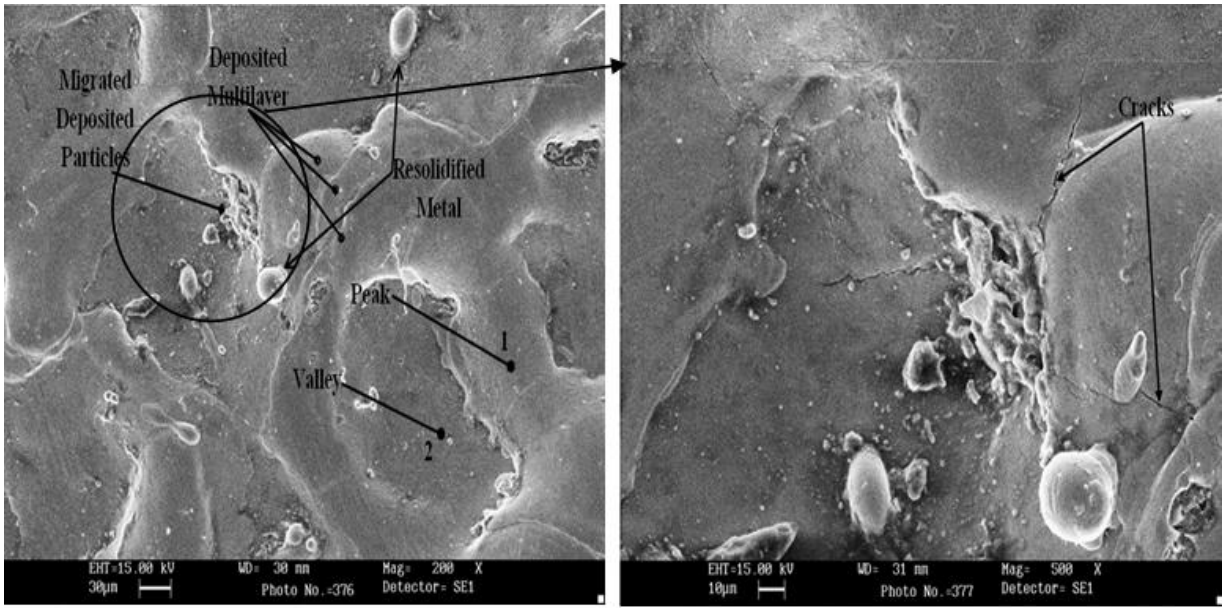

(a) (b)

Figure 5.16: SEM micrograph for AISI-H13 workpiece machined without powder with tungsten-copper tool without magnet at 8 A current, 200 µs pulse on time (a) 200×; (b) 500×

Microstructure of AISI-H13 workpiece machined at 8 A current, 200 µs pulse on time with tungsten-copper tool without any field assistance and powder is shown in Figure 5.16. Resolidified metal droplets as a result of high impact force are observed on the surface. Several peaks and valleys are observed on the surface, which leads to high roughness value (R_a =8.37 µm). Migrated deposited particles are observed which must be included from tungsten-copper tool as no powder is used in this case. More cracks are observed as machining is carried out at higher current value.

5.3 XRD ANALYSIS

XRD analysis was carried out on some selected samples using XRD machine (Model-D8 ADVANCE, Bruker Corporation, USA), to detect phases / composition change in workpiece after machining on EDM targeting copper (Cu-K-alpha1, with wavelength λ=1.5406Å) using the range of Bragg's angle 2θ from 5^o to 120^o at a scan speed of 5 ^{o}/min for every sample. Sample preparation was done as per standard requirement by cutting the machined sample each in diameter 10 mm (only the machined part) with thickness 5 mm, cleaning of samples by acetone and ECG gel to properly clean the machined surface. XRD patterns are arranged as per workpiece material.

5.3.1 XRD analysis of AISI D2 work piece material

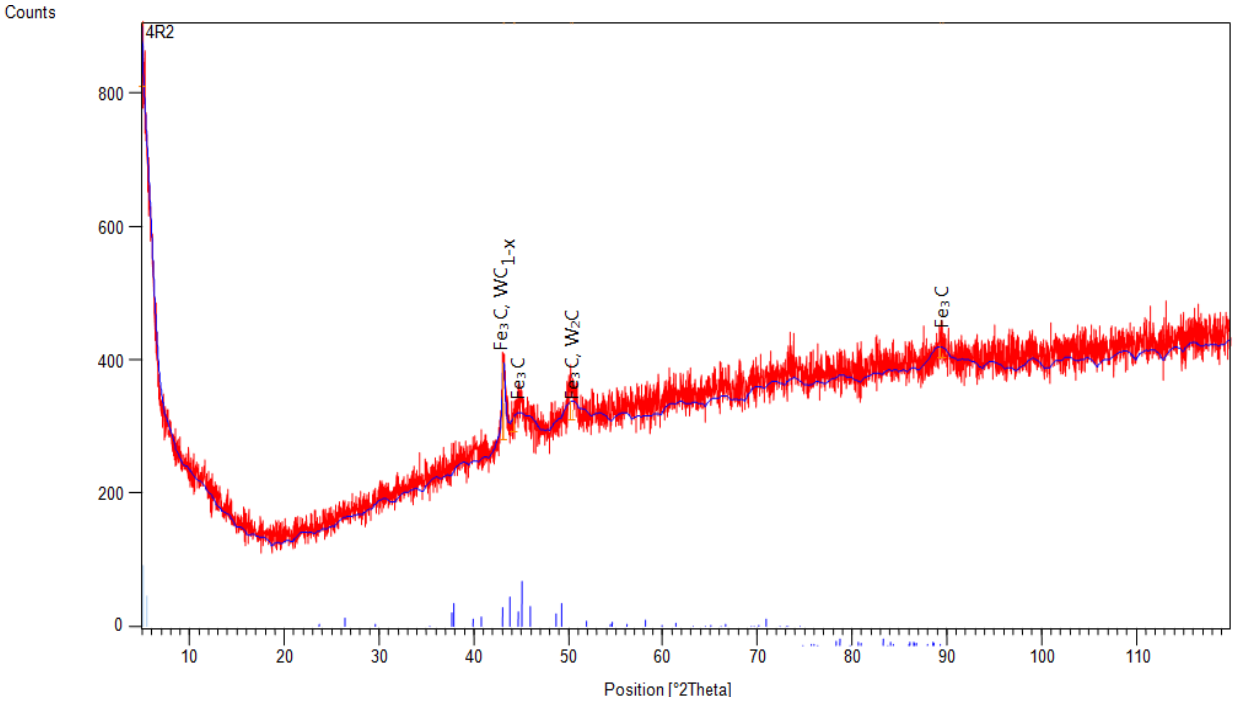

Figure 5.17: XRD pattern for AISI-D2 workpiece machined with tungsten powder (conc. 3 gm/l) with copper tool without magnet at 3 A current, 50 µs pulse on time

XRD pattern for AISI D2 workpiece machined with tungsten powder at concentration 3 gm/l and copper tool at 3 A current and 50 µs pulse on time is shown in Figure 5.17. Some traces of tungsten carbide (in two forms WC_{1-x} and W_2C) are observed on the surface. With increase in tungsten carbide formation hardness increases [Koutsomichalis et al., 2008]. Synthetic cohenite (Fe_3C) formation is also observed on the surface. Cohenite is a brittle and hard iron meteorite, which enhances hardness of the surface [Handbook, Mineral Data Publishing, version 1]. At low current lesser material addition takes place, hence an average MH value (193.407 VHN) is observed. From composition testing on Spectrometer, it is observed that carbon percentage increases from 1.51 % to 3.81 % and tungsten percentage increases from <0.02 % to 0.215 %. Pattern list is provided in Table 5.1, showing reference code and other details regarding existing material [Standard: JCPDS card].

Table 5.1: Pattern list (AISI-D2 workpiece machined with copper tool and tungsten powder (conc. 3 gm/l) at 3 A current, 50 µs pulse on time without magnetic field)

S. No.	Ref. Code	Score	Compound Name	Scale Factor	Chemical Formula
1	01-075-0910	10	Cohenite, synthetic	0.074	Fe_3C
2	03-065-3896	0	Tungsten Carbide	0.005	W_2C
3	00-020-1316	0	Tungsten Carbide	0.014	WC_{1-x}

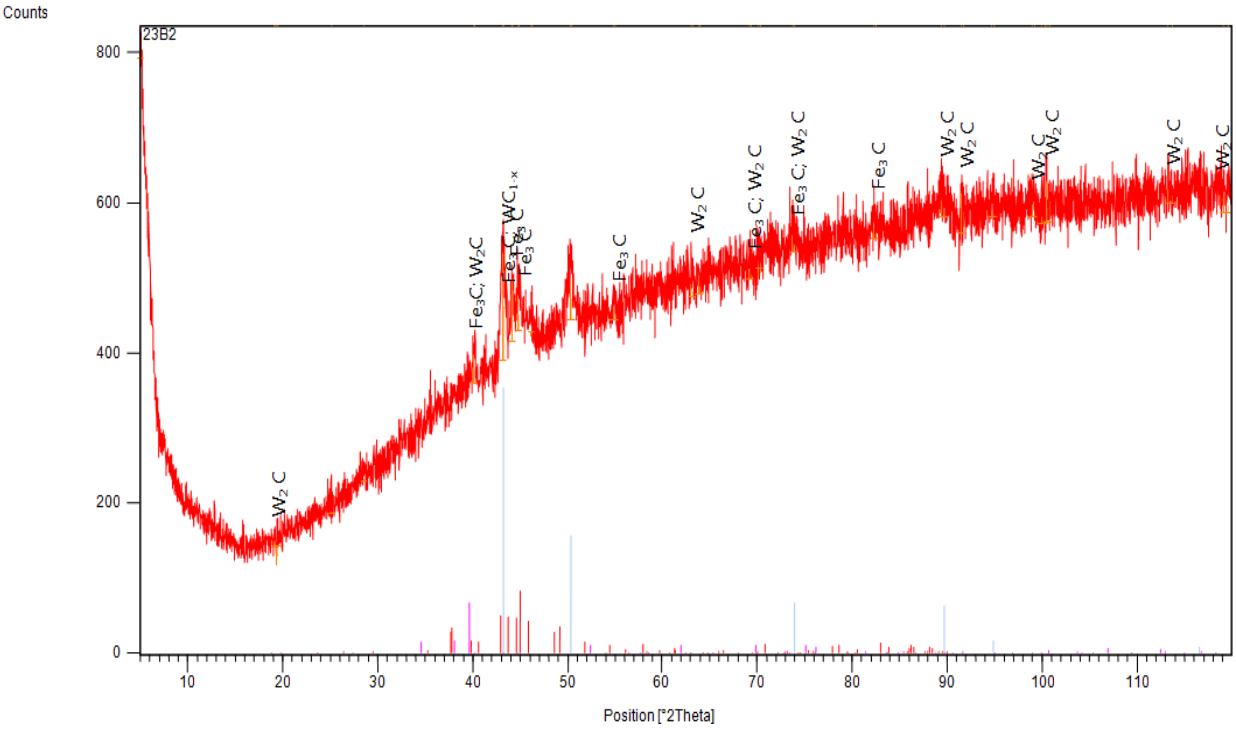

Figure 5.18: XRD pattern for AISI-D2 workpiece machined with tungsten powder (conc. 6 gm/l) with C18000 tool with 0.36 T bar magnets at 5 A current, 20 µs pulse on time

XRD pattern for AISI-D2 workpiece machined with tungsten powder at concentration 6 gm/l with C18000 tool at 5 A current, 20 µs pulse on time under the effect of 0.36 T bar magnets is shown in Figure 5.18. This sample is found very rich in tungsten traces in the form of tungsten carbides (W_2C and WC_{1-x}) and carbon in the form of synthetic cohenite (Fe_3C) increasing the MH (249.78 VHN). Pattern list is given in Table 8.2. As moderate current is used, hence more amounts of tungsten and carbon is added to the machined surface. Spectrometry analysis has reported that carbon increases from 1.51 % to 4.4 %, while tungsten increases from <0.02 % to 0.255 % in the machined surface.

Table 5.2: Pattern list (AISI-D2 workpiece machined with C18000 tool and tungsten powder (conc. 6 gm/l) at 5 A current, 20 µs pulse on time with 0.36 T bar magnets)

S. No.	Ref. Code	Score	Compound Name	Scale Factor	Chemical Formula
1	01-085-1317	7	Cohenite, synthetic	0.093	$Fe_3 C$
2	03-065-3896	0	Tungsten Carbide	0.075	$W_2 C$
3	00-020-1316	0	Tungsten Carbide	0.005	$W C_{1-x}$

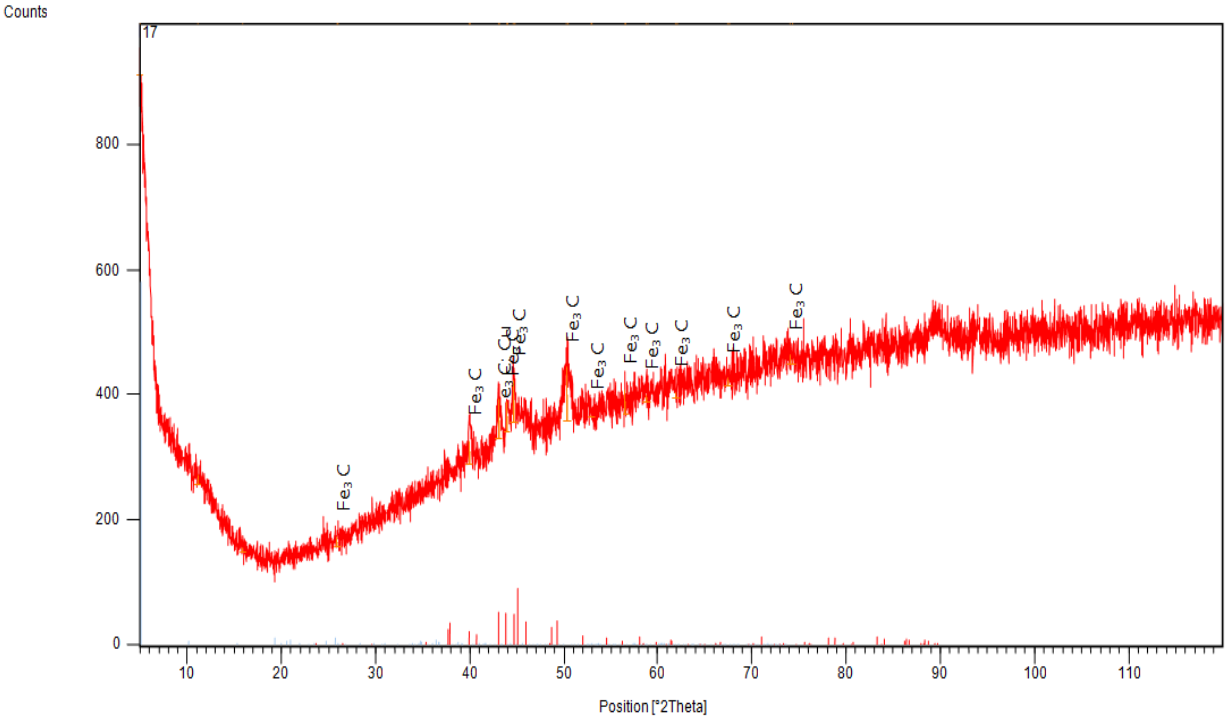

Figure 5.19: XRD pattern for AISI-D2 workpiece machined without powder with C18000 tool with 0.09 T bar magnets at 8 A current, 50 µs pulse on time

Figure 5.19 shows the XRD pattern for AISI-D2 machined with C18000 tool under the effect of 0.09 T bar magnets at 8 A current and 50 µs pulse on time. No powder is used. Cohenite synthetic is observed on the machined surface, i.e. iron-carbon compound. Synthetic copper (Cu) is observed on a single peak reporting presence of copper traces in the machined surface. Copper increases corrosion resistance property of the surface [ASTM B432 – 09a] and the strength. Pattern list is given in the Table 5.3. A good value of hardness (219.636 VHN) is observed, mainly because of increase in carbon content (migrated from dielectric) in the sample

Table 5.3: Pattern list (AISI-D2 workpiece machined with C18000 tool without powder at 8 A current, 50 µs pulse on time with 0.09 T bar magnets)

S. No.	Ref. Code	Score	Compound Name	Scale Factor	Chemical Formula
1	01-089-2867	15	Cohenite, synthetic	0.094	Fe3 C
2	00-004-0836	0	Copper, synthetic	0.005	Cu

5.3.2 XRD analysis of AISI D3 work piece material

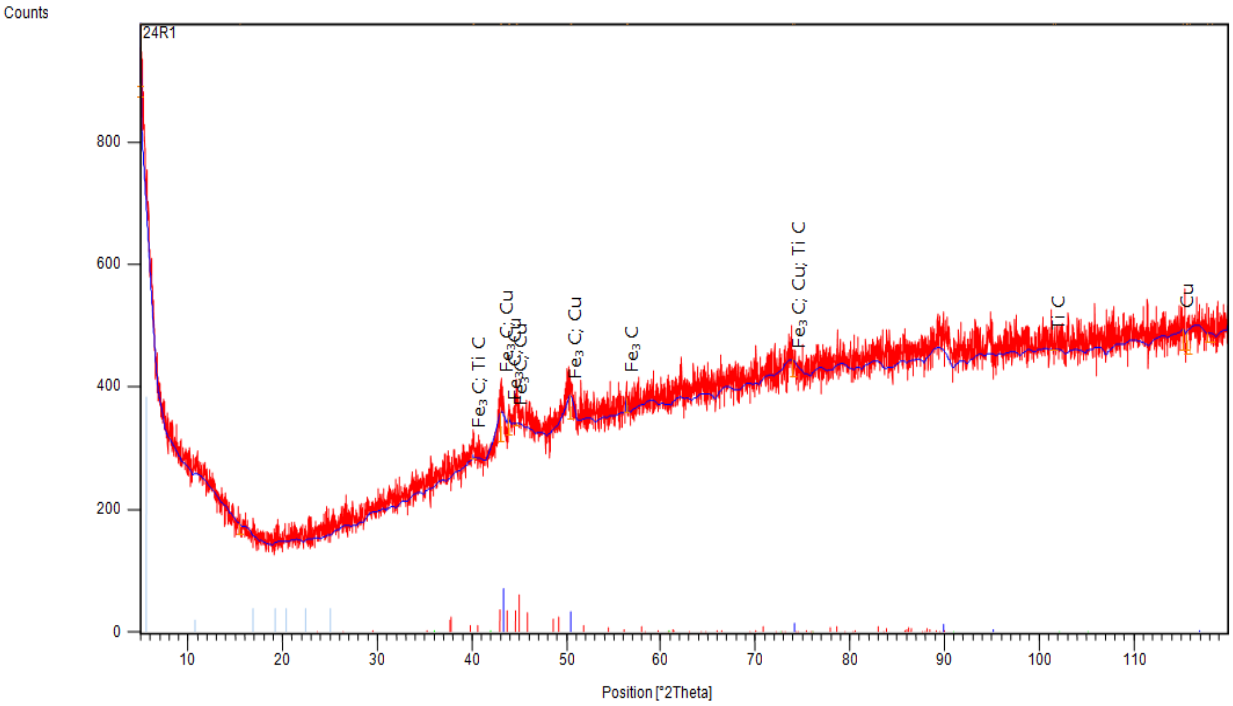

Figure 5.20: XRD pattern for AISI-D3 workpiece machined with titanium powder (conc. 9 gm/l) with copper tool with 0.17 T ring magnet at 5 A current, 50 µs pulse on time

XRD pattern for AISI D3 machined with titanium powder at concentration 9 gm/l with copper tool under the effect of 0.17 T ring magnet at 5 A current, 50 µs pulse on time is shown in Figure 5.20. Cohenite synthetic, copper synthetic and titanium carbide is observed on the machined surface. Titanium carbide formation enhances hardness and wear resistance [Hintermann et al., 1978]. Hence titanium carbide along with cohenite imparts very good hardness (248.843 VHN) with good strength because of copper to the machined surface. Pattern list is shown in Table 5.4. From spectrometry analysis, it is observed that carbon is increased from 1.54 % to 3.46 %, copper is increased from 0.0098 % to 0.139 % and titanium from 0.0172 % to 0.022 %.

Table 5.4: Pattern list (AISI-D3 workpiece machined with copper tool and titanium powder (conc. 9 gm/l) at 5 A current, 50 µs pulse on time with 0.17 T ring magnet)

S. No.	Ref. Code	Score	Compound Name	Scale Factor	Chemical Formula
1	01-085-1317	3	Cohenite, synthetic	0.063	Fe_3C
2	00-004-0836	22	Copper, synthetic	0.074	Cu
3	00-001-1222	0	Titanium Carbide	0.002	Ti C

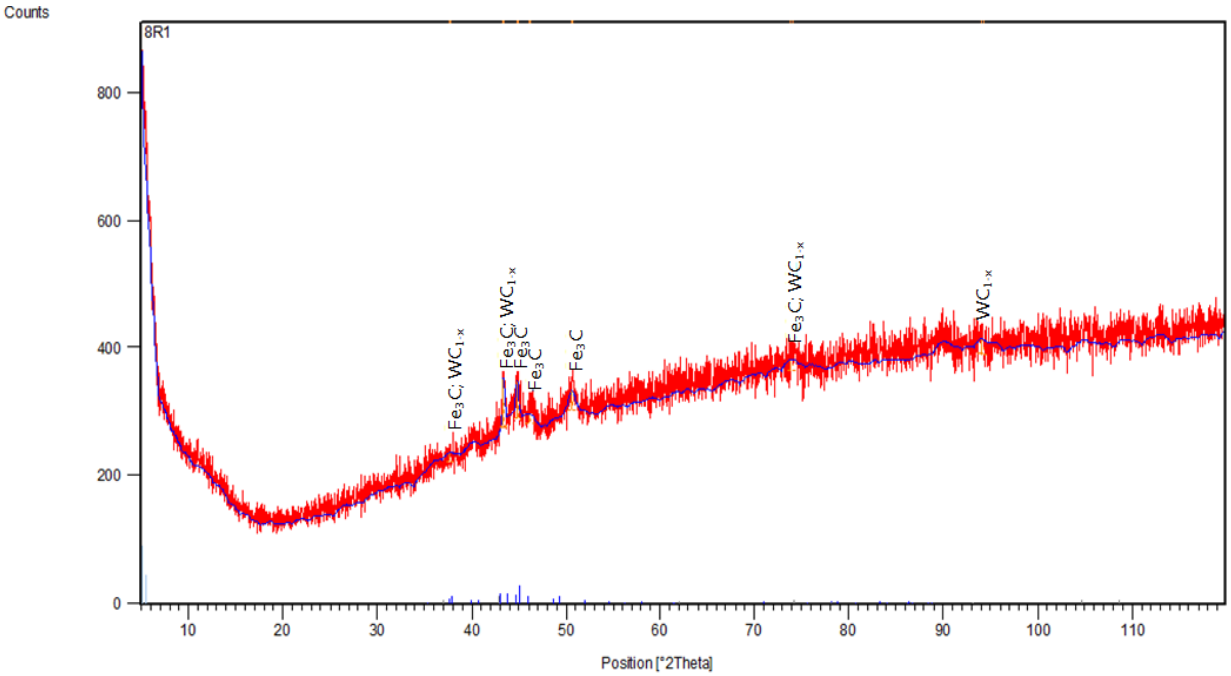

Figure 5.21: XRD pattern for AISI-D3 workpiece machined with graphite powder (conc. 6 gm/l) with tungsten-copper tool without magnet at 7 A current, 20 µs pulse on time

Figure 5.21 shows XRD pattern for AISI D3 workpiece machined with tungsten-copper tool with graphite mixed at concentration 6 gm/l at 7 A current and 20 µs pulse on time without any field assistance. Cohenite synthetic (Fe_3C) and tungsten carbide (WC_{1-x}) is observed on the surface. As high current is used for machining, more amount of carbon (from dielectric and powder used) and tungsten (from electrode) is added providing a good MH value (233.24 VHN). Pattern list for XRD pattern is given in Table 5.5. From spectrometry analysis, it is observed that carbon is increased from 1.54 % to 4.46 %, tungsten is increased from 0.0606 % to 1.78 %.

Table 5.5: Pattern list (AISI-D3 workpiece machined with tungsten-copper tool and graphite powder (conc. 6 gm/l) at 7 A current, 20 µs pulse on time without magnetic field)

S. No.	Ref. Code	Score	Compound Name	Scale Factor	Chemical Formula
1	01-089-2867	7	Cohenite, synthetic	0.031	Fe_3 C
2	00-020-1316	0	Tungsten Carbide	0.014	W C_{1-x}

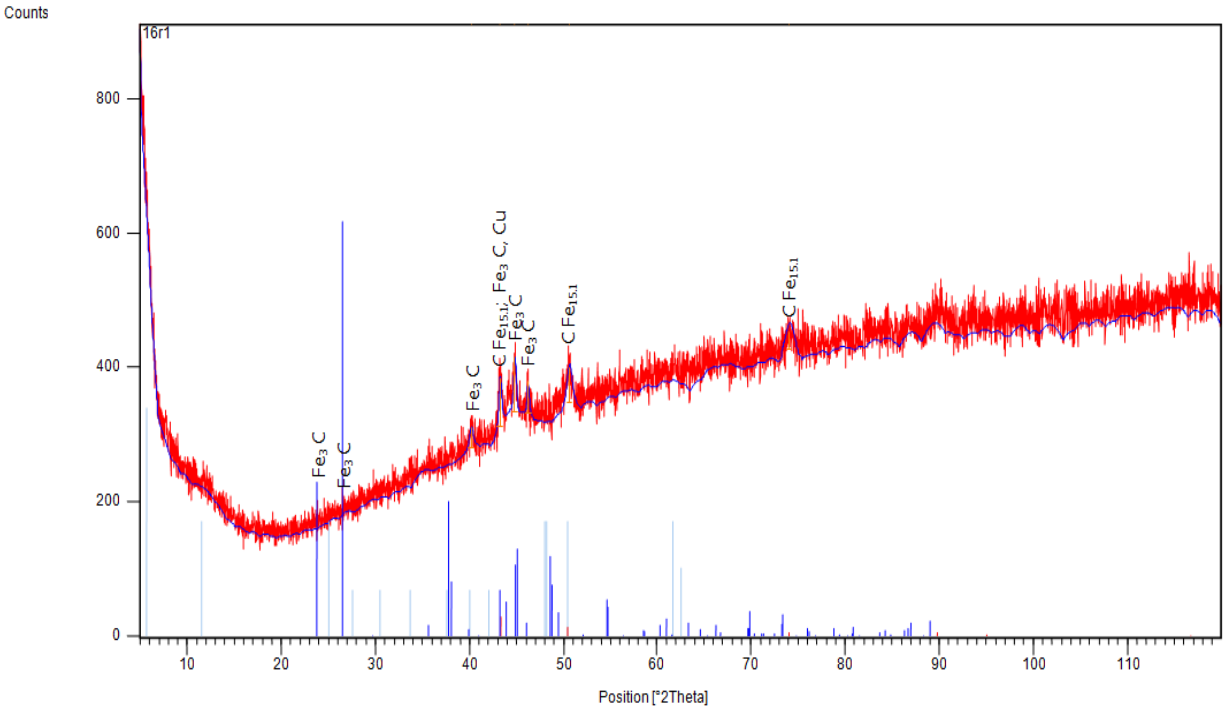

Figure 5.22: XRD pattern for AISI-D3 workpiece machined with graphite powder (conc. 3 gm/l) with C18000 tool with 0.075 T ring magnet at 7 A current, 50 µs pulse on time

XRD pattern for AISI D3 material machined with graphite powder at concentration 3 gm/l with C18000 tool with 0.075 T ring magnet at 7 A current and 50 µs pulse on time is shown in Figure 5.22. As graphite powder is used, carbon content in the machined surface is increased which has resulted in formation of austenite ($CFe_{15.1}$) and cementite (Fe_3C). Cementite is a very hard phase, even harder than martensite, hence hardness (216.269 VHN) in this sample is imparted by the presence of cementite in the sample. Copper is also observed on the surface (from tool electrode) supporting strength. Pattern list of the XRD pattern is given in the Table 5.6. From spectrometry analysis, it is observed that carbon increases from 1.54 % to 3.6 % while copper increases from 0.0098 % to 1.92 %.

Table 5.6: Pattern list (AISI-D3 workpiece machined with C18000 tool and graphite powder (conc. 3 gm/l) at 7 A current, 50 µs pulse on time with 0.075 T ring magnet)

S. No.	Ref. Code	Score	Compound Name	Scale Factor	Chemical Formula
1	00-052-0512	0	Austenite	0.031	C $Fe_{15.1}$
2	01-085-0871	2	Cementite	0.678	Fe_3 C
3	00-004-0836	0	Copper, Synthetic	0.005	Cu

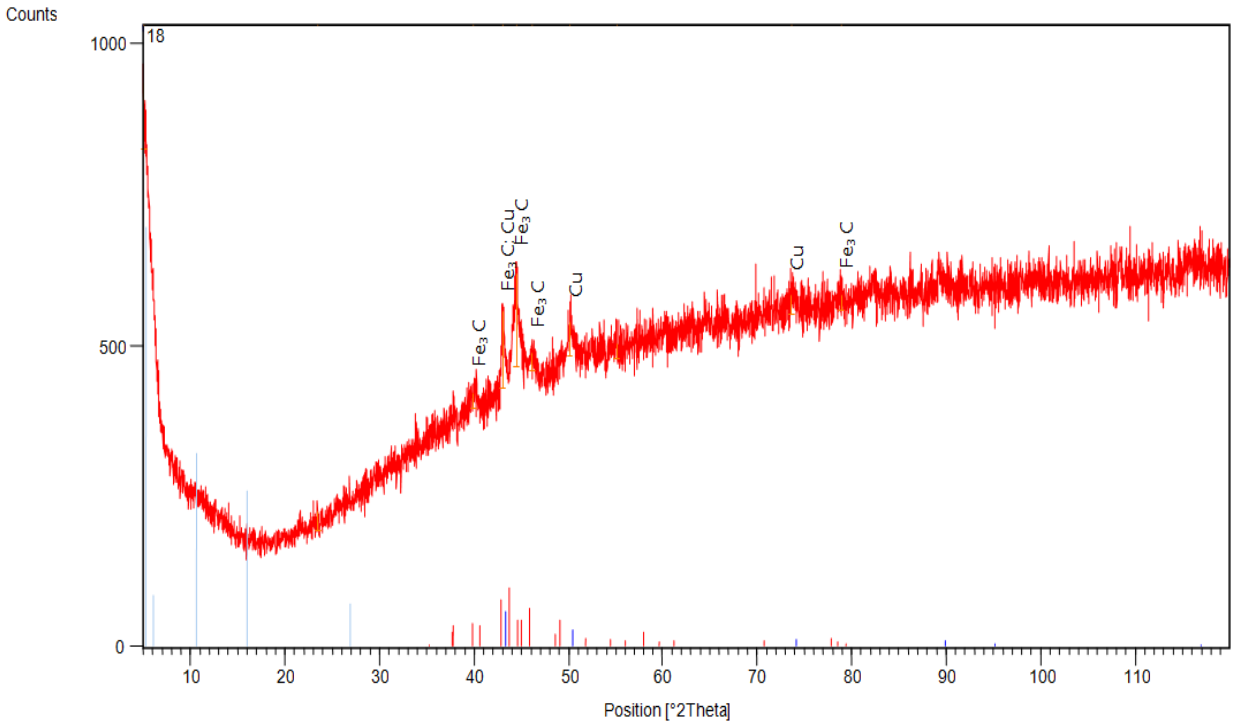

Figure 5.23: XRD pattern for AISI-D3 workpiece machined without powder with copper tool with 0.36 T bar magnets at 8 A current, 100 µs pulse on time

XRD pattern for AISI D3 workpiece machined with copper tool at 8 A current and 100 µs pulse on time with 0.36 T bar magnets is shown in Figure 5.23. From XRD pattern, it is observed that carbon in the form of cementite (Fe_3C) (Carbon from dielectric) and copper synthetic (from tool) is present on the machined surface. High current for machining is responsible for higher carbon liberation from dielectric. Cementite is the main source for very good hardness (272.33 VHN) in the sample, with copper acting as a supporting element for increasing strength. Pattern list for XRD pattern is given Table 5.7.

Table 5.7: Pattern list (AISI-D3 workpiece machined with copper tool without powder at 8 A current, 100 µs pulse on time with 0.36 T bar magnets)

S. No.	Ref. Code	Score	Compound Name	Scale Factor	Chemical Formula
1	00-034-0001	6	Cementite	0.093	Fe_3 C
2	00-004-0836	9	Copper, Synthetic	0.056	Cu

5.3.3 XRD analysis of AISI H13 work piece material

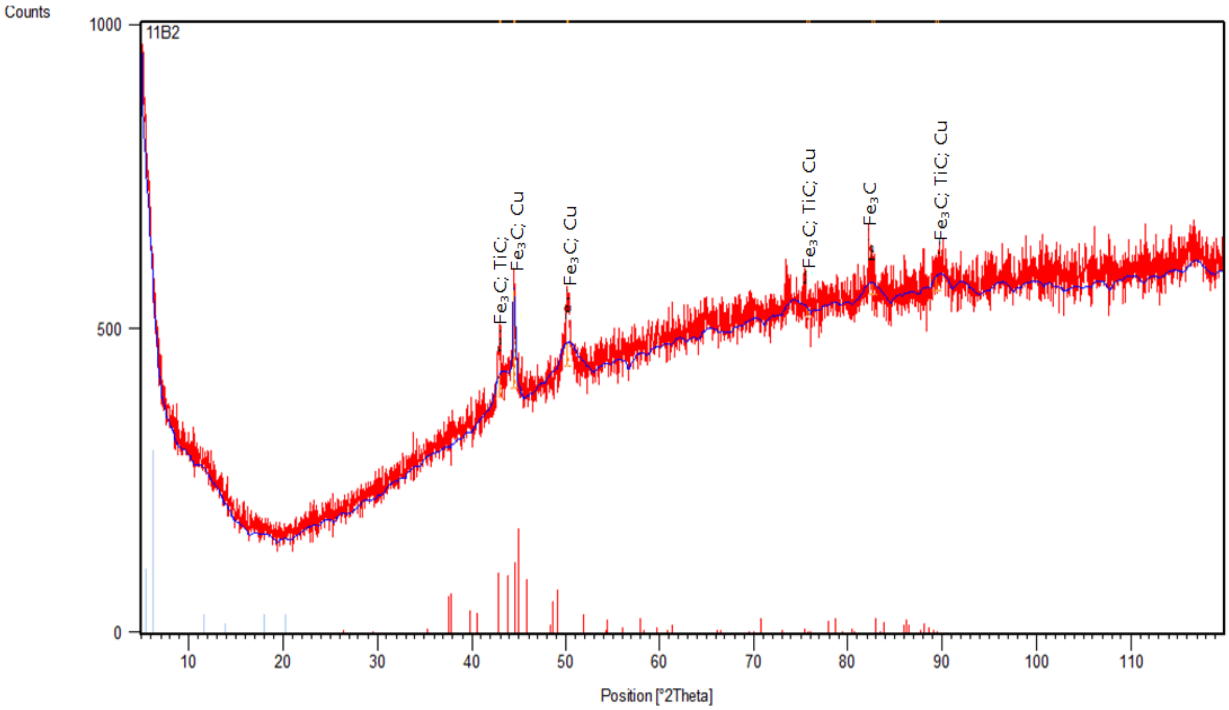

Figure 5.24: XRD pattern for AISI-H13 workpiece machined with titanium powder (conc. 6 gm/l) with copper tool with 0.09 T bar magnets at 3 A current, 20 µs pulse on time

Figure 5.24 shows XRD pattern for AISI H13 workpiece machined with copper tool with titanium powder mixed in dielectric at concentration 6 gm/l at 3 A current and 20 µs pulse on time with 0.09 T bar magnets. Titanium in the form of titanium carbide (TiC), copper synthetic and cohenite synthetic (Fe_3C) is observed on the machined surface. A moderate hardness value (164.529 VHN) is observed irrespective of the low hardness value of workpiece material (75.318 VHN), which is even possible with titanium carbide and copper. Spectrometry analysis has reported that carbon increases from 0.368 % to 2.04 %, copper from 0.0909 % to 0.493 % and titanium from 0.0055 % to 0.0125 %. Pattern list for XRD pattern is given in Table 5.8.

Table 5.8: Pattern list (AISI-H13 workpiece machined with copper tool and titanium powder (conc. 6 gm/l) at 3 A current, 20 µs pulse on time with 0.09 T bar magnets)

S. No.	Ref. Code	Score	Compound Name	Scale Factor	Chemical Formula
1	01-072-1110	10	Cohenite, synthetic	0.170	Fe_3 C
2	00-001-1222	3	Titanium Carbide	0.000	Ti C
3	00-004-0836	25	Copper, synthetic	0.141	Cu

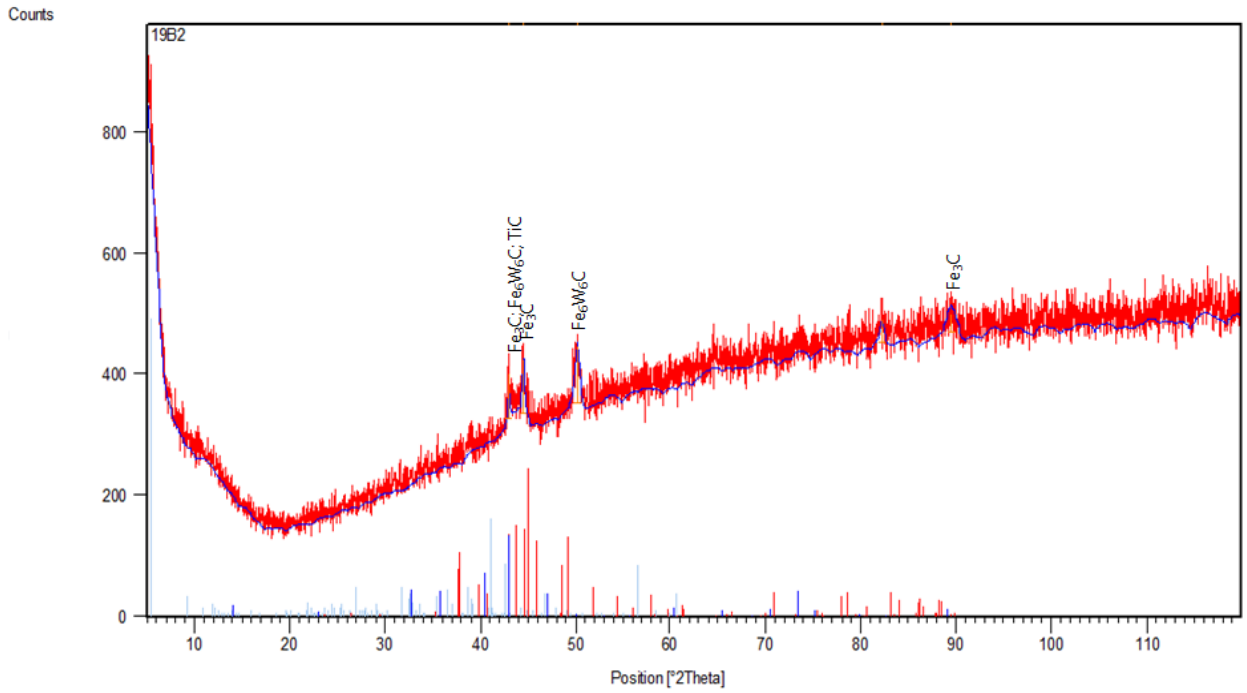

Figure 5.25: XRD pattern for AISI-H13 workpiece machined with titanium powder (conc. 3 gm/l) with tungsten-copper tool with 0.36 T bar magnets at 3 A current, 50 µs pulse on time

XRD pattern for AISI-H13 workpiece machined with titanium powder (conc. 3 gm/l) with tungsten-copper tool with 0.36 T bar magnets at 3 A current and 50 µs pulse on time is shown in Figure 5.25. A different compound formation is observed in this pattern. Iron tungsten carbide (Fe_6 W_6 C) is found with cohenite synthetic (Fe_3C) and some extract of titanium carbide (TiC) is seen showing MH value (159.292 VHN). Spectrometry analysis has shown that carbon content increases from 0.368 % to 1.98 % and titanium increases from 0.0055 % to 0.0079 %, while no significant change in tungsten amount is observed, means tungsten from the base material has participated in carbide formation. Pattern list for XRD analysis is shown in Table 5.9.

Table 5.9: Pattern list (AISI-H13 workpiece machined with tungsten-copper tool and titanium powder (conc. 3 gm/l) at 3 A current, 50 µs pulse on time with 0.36 T bar magnets)

S. No.	Ref. Code	Score	Compound Name	Scale Factor	Chemical Formula
1	01-089-2722	Unmatched Strong	Cohenite, synthetic	0.249	Fe_3 C
2	01-089-2616	8	Iron Tungsten Carbide	0.136	Fe_6 W_6 C
3	00-001-1222	0	Titanium Carbide	0.005	TiC

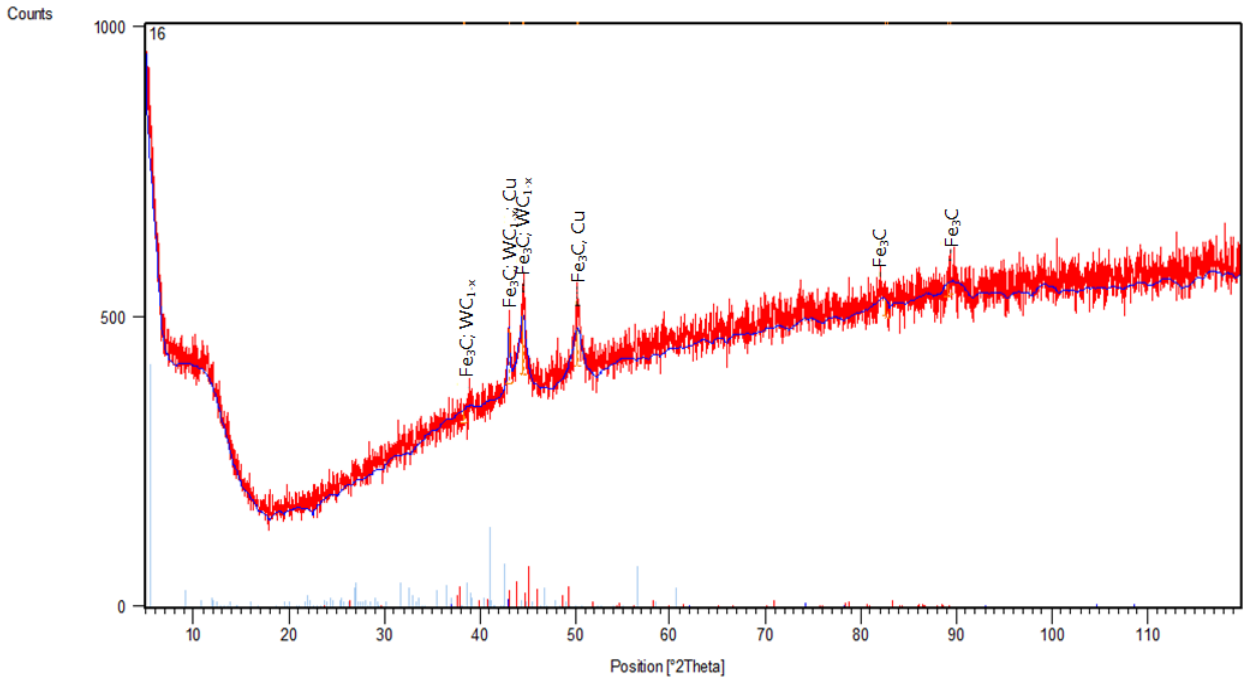

Figure 5.26: XRD pattern for AISI-H13 workpiece machined without powder with tungsten-copper tool without magnet at 8 A current, 200 µs pulse on time

XRD pattern for AISI H13 workpiece machined with tungsten-copper tool without magnet at 8 A current and 200 µs pulse on time without powder being mixed in the dielectric is shown in Figure 5.26. From XRD analysis, it is observed that cohenite synthetic (Fe_3C), tungsten carbide (WC_{1-x}) and copper synthetic is observed on the machined surface. Even though the base material is not so hard, the hardness of the machined sample (213.63 VHN) is good with the presence of tungsten carbide and copper particles. As current is high, more carbon (from dielectric) and tungsten, copper (extracts from tool) are added to the surface. Pattern list for this pattern is given in Table 5.10.

Table 5.10: Pattern list (AISI-H13 workpiece machined with tungsten-copper tool without powder at 8 A current, 200 µs pulse on time without magnetic field)

S. No.	Ref. Code	Score	Compound Name	Scale Factor	Chemical Formula
1	01-075-0910	11	Cohenite, synthetic	0.070	Fe_3C
2	00-020-1316	7	Tungsten Carbide	0.013	WC_{1-x}
3	00-004-0836	0	Copper, synthetic	0.005	Cu

5.4 Crater Analysis

Crater analysis is done with single spark discharge in EDM. It is mainly performed to differentiate in crater shape and size formed with and without magnetic field assistance. Crater is the shape that is formed on the workpiece after a single discharge takes place at a point. Melting/Evaporation phenomenon is used for defining material removal in EDM, evaporated material is removed completely, while melted material deposits itself on the periphery. To distinguish between the shape and depth of the crater formed, with or without magnetic field, Leica metallurgical microscope is used. Samples are prepared by cleaning the machined part with acetone. Parameters used for crater analysis are tabulated in Table 5.11. Crater images are segregated on the basis of current.

Table 5.11: Parameters used for crater analysis

S. No.	Parameters	Levels	
1	Current (A)	6	8
2	Magnetic field	No field	0.36 T bar magnets
3	Workpiece	AISI D3	
4	Tool	Copper	
5	Dielectric	EDM oil	
6	Powder	No powder	
7	Pulse on Time (µs)	20	
8	Pulse off Time (µs)	57	
9	Magnification	20×	

5.4.1 Crater images at 6 A current

Crater images at 6 A current are shown in Figure 5.27. Crater images with and without magnetic field has one significant difference that craters without magnetic field form complete rim of resolidified metal outside the crater while in case of craters with 0.36 T bar magnets, craters don't complete rim formation. In case of magnetic field assisted EDM, melted metal is supposed to be pulled in one particular direction, because of the magnetic force in that particular direction. It is studied in some studies that molten metal is affected by magnetic force [Oldenburg et al., 2000], which leads in better removal of material from the gap. But one more thing is noticed that craters are found somewhat shallower in case of craters with magnet as compared to without magnetic field. Lorentz force direction $\vec{F}$, applied magnetic field direction $\vec{B}$ and current direction $\vec{I}$ are shown in all the craters with magnetic field assistance.

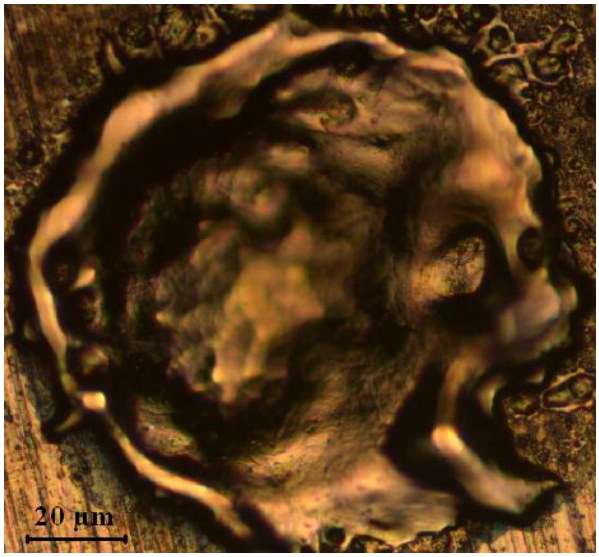

(a)

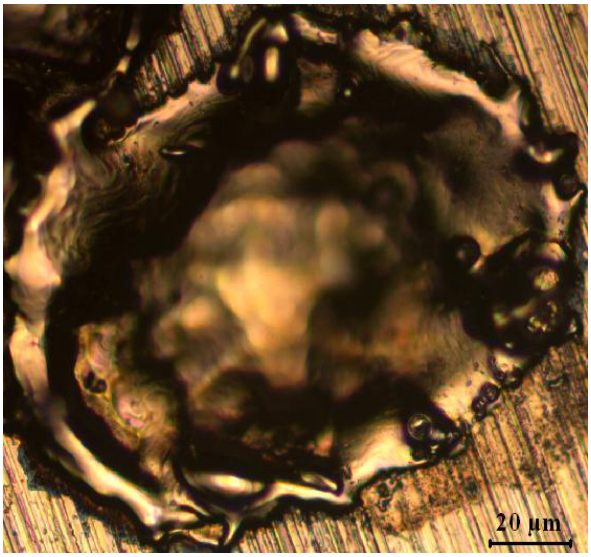

(b)

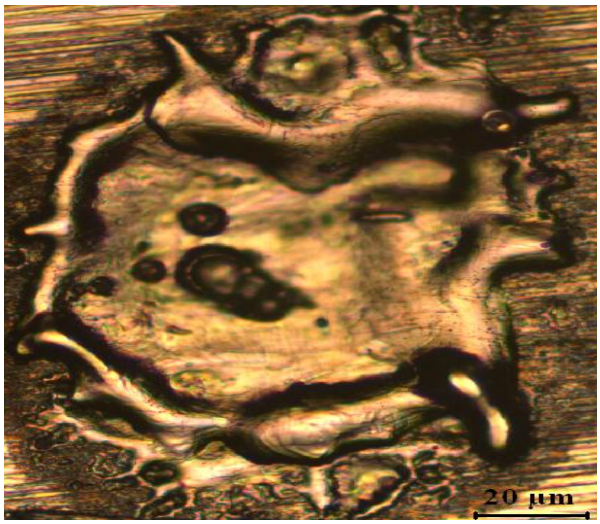

(c)

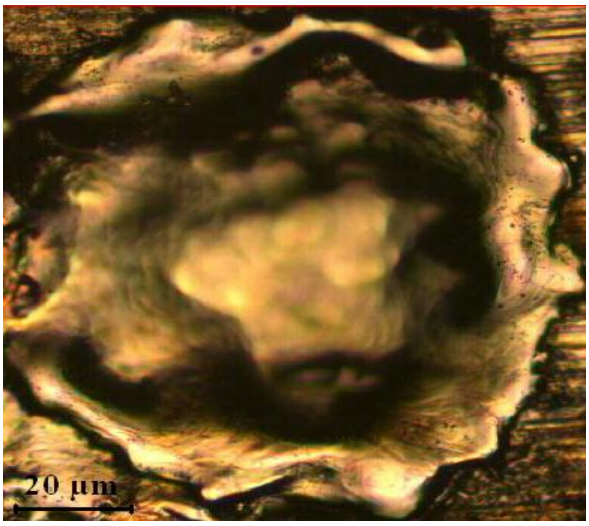

(d)

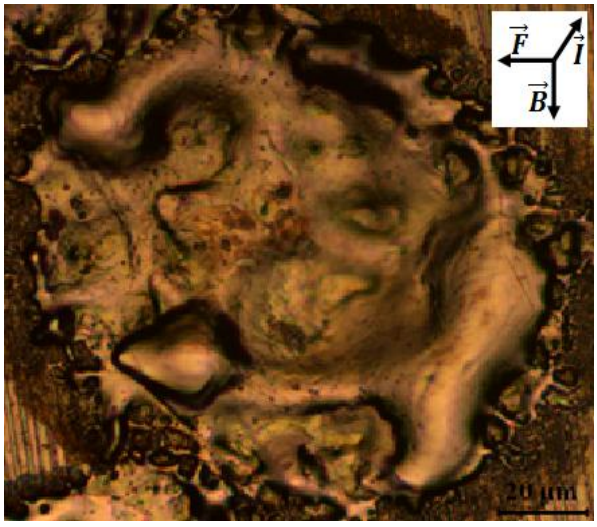

(e)

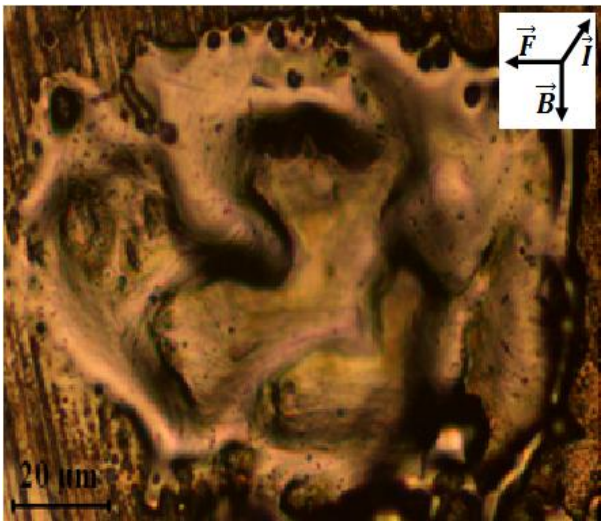

(f)

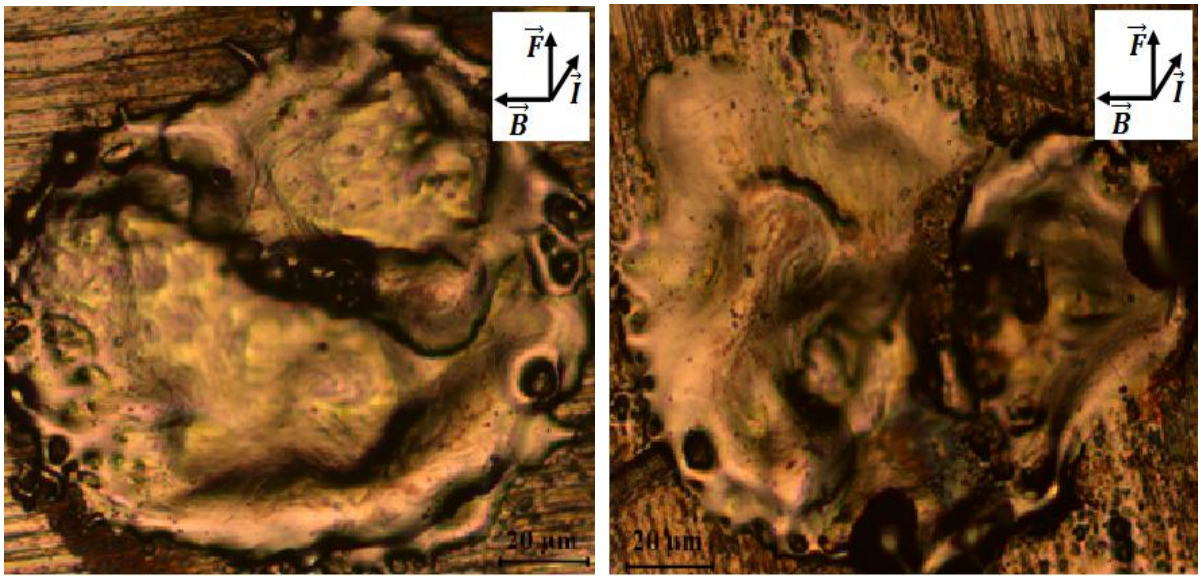

(g) (h)

Figure 5.27: Craters at 6 A current (a), (b), (c), (d) Without magnet; (e), (f), (g), (h) With 0.36 T bar magnets

5.4.2 Crater images at 8 A current

Crater images at 8 A current are shown in Figure 5.28. In general crater size for higher current should be larger than that of the crater size formed because of lower current, but there is very less difference in size of crater because of different time for spark/discharge. But the magnetic force (Lorentz force) effect is observed to act in the same way for both the current value. Molten metal will be more in case of higher current, so larger molten metal portion should be extracted under the effect of magnetic field for higher current value.

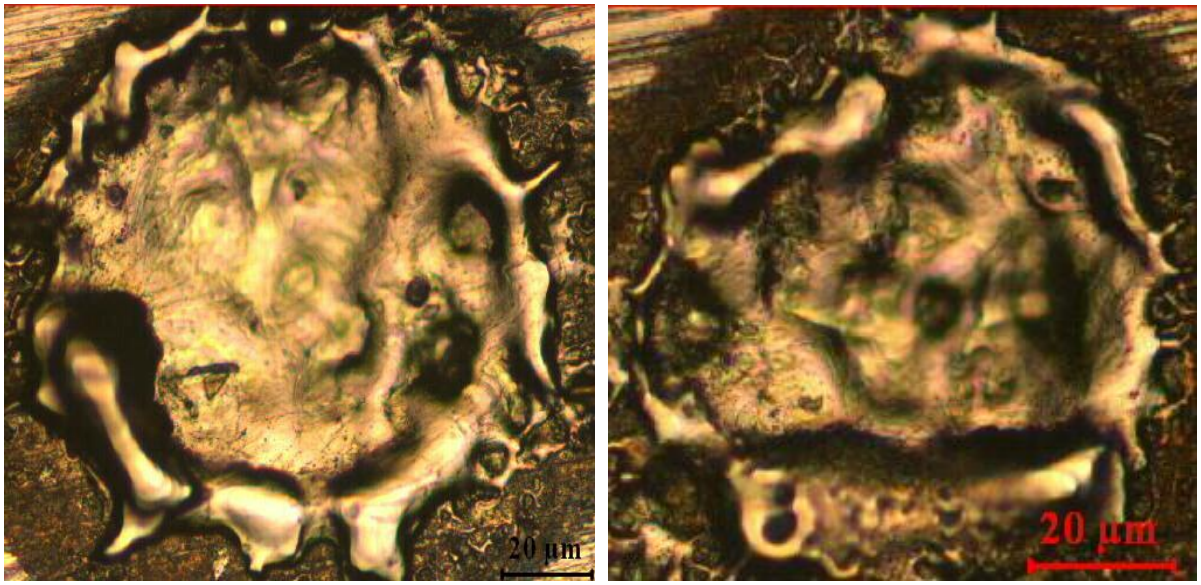

(a) (b)

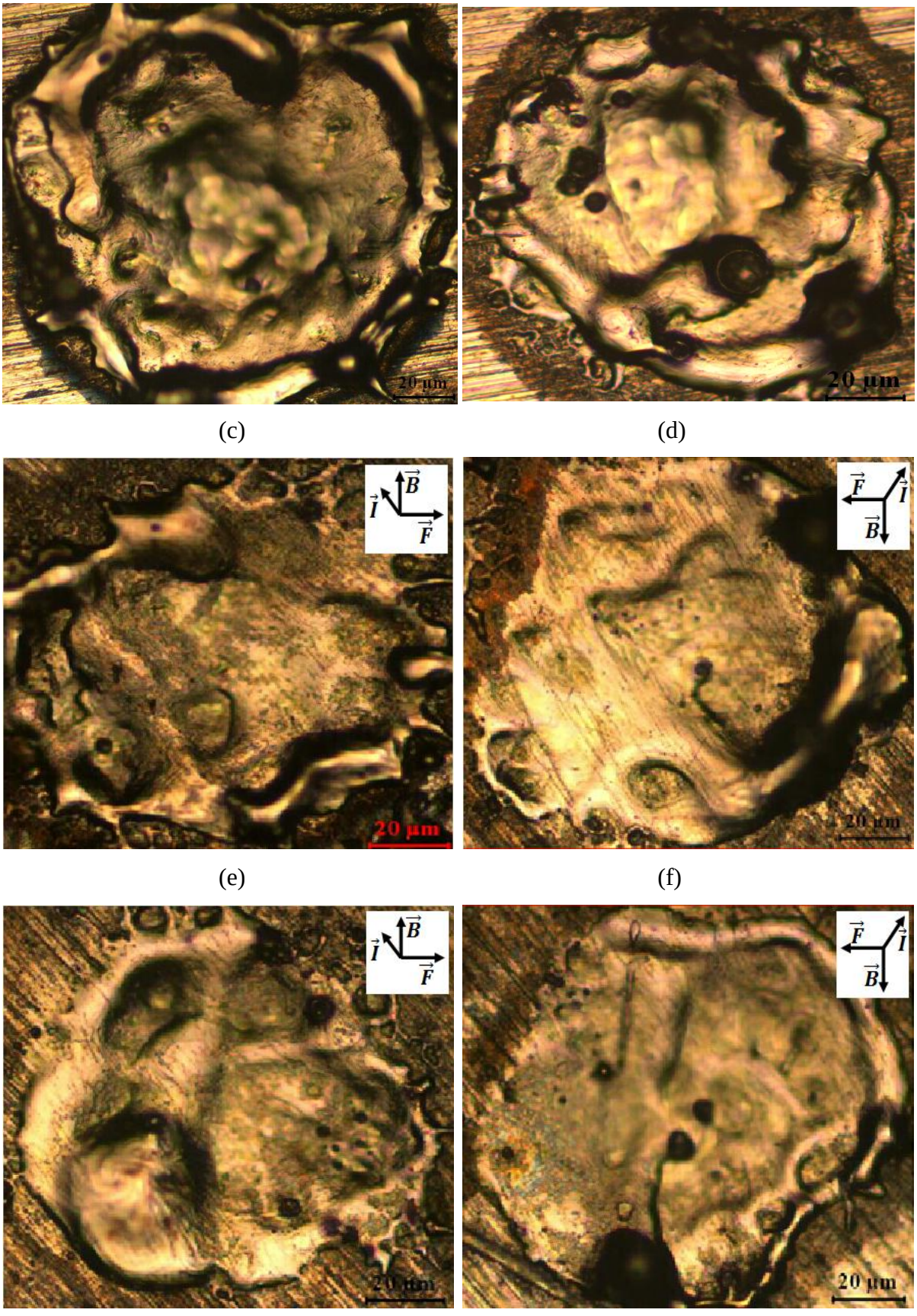

(c) (d)

(e) (f)

(g) (h)

Figure 5.28: Craters at 8 A current (a), (b), (c), (d) Without magnet; (e), (f), (g), (h) With 0.36 T bar magnets

CHAPTER 6

CONCLUSION

6.1 CONCLUSION

This study was mainly aimed at making comparison of magnetic field assisted conventional EDM and magnetic field assisted PMEDM using permanent magnets of different configuration and strength. Different process parameters like current, pulse on time, workpiece (AISI D2, AISI D3 and AISI H13), tool electrodes (copper, tungsten-copper and C18000), magnetic strengths and type of powders (graphite, tungsten and titanium) varied at different concentrations are used. Different response characteristics considered are MRR, TWR, OC, SR and MH including metallurgical analysis of some selected machined samples. Some important conclusions that are drawn on the basis of analysis of results (using ANOVA) and metallurgical study are:

- Current is observed to be the most significant parameter in case of all the response characteristics resulting in increase of all the response characteristics namely MRR, TWR, OC, SR and MH.
- AISI D3 as workpiece has offered better response in terms of MRR, MH and SR in spite of being the hardest workpiece material amongst all the used workpiece materials.
- Under the effect of magnetic field, MRR increases but for PMEDM, the increase is observed at lower current values.
- C18000 as a tool was a new tool material explored and it has reported in significantly good results in terms of high MRR and high MH at the expense of higher TWR and OC.
- Tungsten-copper being the hardest tool has contributed towards low TWR, low OC and high MH results.
- Tungsten powder has reported better MRR and better MH results with higher TWR.
- With magnetic field assistance, TWR decreases, while OC and MH increase in conventional as well as powder mixed EDM, while contrary results are seen for SR in case of conventional and PMEDM, it increases for conventional EDM while decreases for PMEDM at lower current values with the increase in field strength.

- Powder concentration up to a certain limit compliments EDM while opposite effects are seen at further high concentration.
- In terms of metallurgical aspects, it is observed that multilayer formation due to uniform sparks in presence of powder compliments MRR and increases SR as well.
- XRD analysis has reported that the high MH is mainly the result of carbide formation that is reported by XRD patterns.
- Analysis of single discharge craters with and without magnetic field has shown that in case of magnetic field, no complete rim formation is there, instead material is supposed to be pulled in one particular direction as a result of acting Lorentz force.
- Magnet shape has not shown any drastic difference in response characteristics.

6.2 FUTURE RECOMMENDATION

Some more workpiece materials can be explored to study with some more tool materials. Magnetic field although being insignificant has shown some improvement in response characteristics, hence some higher strength magnets can be explored to study with some new dielectrics.

CHAPTER 7
REFERENCES

ASTM B432 - 09a, Standard Specification for Copper and Copper Alloy Clad Steel Plate, ASTM standards.

Batish, A., Bhattacharya, A., Singla, V.K., Singh, G. (2012) Study of Material Transfer mechanism in Die Steels Using Powder Mixed Electric Discharge Machining, Materials and Manufacturing Processes, 27: 449–456.

Batish, A. and Bhattacharya, A. (2012) Mechanism of material deposition from powder, electrode and dielectric for surface modification of H11and H13 die steels in EDM process, Materials Science Forum, 701: 61–75.

Bhattacharya, A., Batish, A. and Kumar, N. (2013) Surface characterization and material migration during surface modification of die steels with silicon, graphite and tungsten powder in EDM process, Journal of Mechanical Science and Technology, 27 (1): 133–140.

Bhattacharya, A. and Batish, A. (2012) Effect of process variables on microhardness, grain size and strain during machining of various die steels with powder-mixed electric-discharge machining using dummy treated experimental design, Proceedings of IMechE Part B: Journal of Engineering Manufacture, 226(7): 1192–1204.

Bhattacharya, A., Batish, A., Singh, G. and Singla, V.K. (2011a) Optimal parameter settings for rough and finish machining of die steels in powder-mixed EDM, International Journal of Advanced Manufacturing Technology, 61: 537–548.

Bhattacharya, A., Batish, A. and Singh, G. (2011b) Optimization of powder mixed electric discharge machining using dummy treated experimental design with analytic hierarchy process, Proceedings of IMechE Part B: Journal of Engineering Manufacture, 226 (1): 103–116.

Bhattacharya, A., Batish, A. and Singh G. (2012) Surface Modification of High Carbon High Chromium, EN31 and Hot Die Steel using powder mixed EDM process, Materials Science Forum, 701: 43–59.

Brujin, H.E.D., Delft, T.H. and Pekelhang, A.J. (1978) Effect of magnetic field on the gap cleaning in EDM, Annals of the CIRP, 27 (1): 93–95.

Bruyn and De, H.E. (1968) Slope control: A great improvement in spark erosion, Annals of the CIRP, 16: 183–186.

Chattopadhyay, K.D., Satsangi, P.S., Verma, S. and Sharma, P.C. (2008) Analysis of rotary electrical discharge machining characteristics in reversal magnetic field for copper-EN8 steel system, International Journal of Advance Manufacturing Technology, 38: 925–937

Data Handbook, Cohenite, Mineral Data Publishing, version 1.

Erden, A. and Bilgin, S. (1980) Role of impurities in electric discharge machining, In: Proceedings of 21st International Machine Tool Design and Research Conference, Macmillan, London, 345–350.

Fuller and John, E. (1996) Electrical Discharge Machining, ASM Machining Handbook, 16: 557–564.

Govindan, P., Gupta, A., Joshi, S.S., Malshe, A. and Rajurkar, K.P. (2013) Single-spark analysis of removal phenomenon in magnetic field assisted dry EDM, Journal of Materials Processing Technology, 213: 1048–1058.

Heinz, K., Kapoor, S.G., DeVor, R.E. and Surla V. (2011) An Investigation of Magnetic-Field-Assisted Material Removal in Micro-EDM for Nonmagnetic Materials, Journal of Manufacturing Science and Engineering, doi: 10.1115/1.4003488.

Hintermann, H.E., Boving, H. And Hanni, W. (1978) Wear-resistant coatings for bearing applications, Wear, 48 (2): 225–236.

Jahan, M.P., Rahman, M. and Wong, Y.S. (2011) Study on the nano-powder-mixed sinking and milling micro-EDM of WC-Co, International Journal of Advance Manufacturing Technology, 53: 167–180.

Jeswani, M.L. (1981) Effects of the addition of graphite powder to kerosene used as the dielectric fluid in electrical discharge machining, Wear, 70: 133–139.

Joshi, S., Govindan, P., Malshe, A. and Rajurkar, K. (2011) Experimental characterization of dry EDM performed in a pulsating magnetic field, CIRP Annals - Manufacturing Technology, 60: 239–242.

Kansal, H.K., Singh, S. and Kumar, P. (2005a) Parametric optimization of powder mixed electrical discharge machining by response surface methodology, Journal of Materials Processing Technology, 169: 427–436.

Kansal, H.K., Singh, S. and Kumar, P. (2005b) Application of Taguchi method for optimization of powder mixed electric discharge machining, International Journal of Management and Manufacturing Technology, 7(2-4): 329–341.

Kansal, H.K., Singh, S. and Kumar, P. (2007) Technology and research developments in powder mixed electric discharge machining (PMEDM), Journal of Materials Processing Technology, 184: 32–41.

Kim, J.D., Jin, D.X. and Choi, M.S. (1997) Study on the effect of a magnetic field on an electrolytic finishing process, International Journal of Machine Tools and Manufacture, 37: 401–408.

Koutsomichalis, A., Vaxevanidis, N.M., Petropoulos, G., Mourlas, A. and Antoniou, S.S. (2008) Friction, wear and mechanical behaviour of plasma sprayed WC-12% Co coatings on mild steel, In: Proceedings of the 7th International Conference Coatings in Manufacturing Engineering, Chalkidiki, Greece, 1-3 October 2008: 259–268.

Kumar, S. and Batra, U. (2012) Surface modification of die steel materials by EDM method using tungsten powder-mixed dielectric, Journal of Manufacturing Processes, 14: 35–40.

Kumar, S., Singh, R., Singh, T.P. and Sethi, B.L. (2009) Surface modification by electrical discharge machining: A review, Journal of Materials Processing Technology, 209: 3675–3687.

Kung, K.Y., Horng, J.T. and Chiang, K.T. (2009) Material removal rate and electrode wear ratio study on the powder mixed electrical discharge machining of cobalt-bonded tungsten carbide, International Journal of Advance Manufacturing Technology, 40: 95–104.

Kuneida, M., Lauwers, B., Rajurkar, K.P. and Schumacher, B.M. (2005) Advancing EDM through fundamental insight into the process, Annals of CIRP, 54(2): 599–622.

Lin, Y.C., Chen, Y.F., Wang, D.A. and Lee, H.S. (2009) Optimization of machining parameters in magnetic force assisted EDM based on Taguchi method, Journal of Materials Processing Technology, 209: 3374–3383.

Lin, Y.C. and Lee, H.S. (2008) Machining characteristics of magnetic force-assisted EDM, International Journal of Machine Tools & Manufacture, 48: 1179–1186.

Lin, Y.C. and Lee, H.S. (2009) Optimization of machining parameters using magnetic-force-assisted EDM based on gray relational analysis, International Journal of Advanced Manufacturing Technology, 42: 1052–1064.

Oldenburg, C., Borglin, S.E. and Moridis, G.J. (2000) Numerical Simulation of Ferrofluid Flow for Subsurface Environmental Engineering Applications, Transport in Porous Media, 38: 319–344.

Pecas, P. and Henriques, E. (2008) Electrical discharge machining using simple and powder-mixed dielectric: The effect of the electrode area in the surface roughness and topography, Journal of Materials Processing Technology, 200: 250–258.

Prihandana, G.S., Mahardika, M., Hamdi, M., Wong, Y.S. and Mitsui, K. (2009) Effect of micro-powder suspension and ultrasonic vibration of dielectric fluid in micro-EDM

processes- Taguchi Approach, International Journal of Machine tool and manufacture, 49: 1035–1041.

Prihandana, G.S., Mahardika, M., Hamdi, M., Wong, Y.S. and Mitsui, K. (2011) Accuracy improvement in nanographite powder-suspended dielectric fluid for micro-electrical discharge machining processes, International Journal of Advance Manufacturing Technology, 56: 143–149.

Syed, K.H. and Kuppan, P. (2013) Studies on Recast-layer in EDM using Aluminium Powder Mixed Distilled Water Dielectric Fluid, International Journal of Engineering and Technology, 5 (2): 1775–1780.

Teimouri, R. and Baseri, H. (2012a) Effects of magnetic field and rotary tool on EDM performance, Journal of Manufacturing Processes, 14(3): 316–322.

Teimouri, R. and Baseri, H. (2012b) Study of tool wear and overcut in EDM process with rotary tool and magnetic field, Advances in Tribology, Volume 2012, Article ID 895918, 8 pages, doi: 10.1155/2012/895918.

Teimouri, R. and Baseri, H. (2012c) Experimental study of rotary magnetic field-assisted dry EDM with ultrasonic vibration of work piece, International Journal of Advance Manufacturing Technology, doi: 10.1007/s00170-012-4573-6.

Tsai, K.M. and Wang, P.J. (2001) Predictions on surface finish in electrical discharge machining based upon neural network models, International Journal of Machine Tools & Manufacture, 41(10): 1385–1403.

Wong, Y.S., Lim, L.C. and Lee, L.C. (1995) Effect of flushing on electro-discharge machined surfaces, Journal of Materials Processing Technology, 48: 299–305.

Wu, K.L., Yan, B.H., Huang, F.Y. and Chen, S.C. (2005) Improvement of surface finish on SKD steel using electro-discharge machining with aluminium and surfactant added dielectric, International Journal of Machine Tools & Manufacturing, 45: 1195–1201.

Yeo, S.H., Murali, M. and Cheah, H.T. (2004) Magnetic field assisted micro electro-discharge machining, Journal of Micromechanics and Micro engineering, 14: 1526–1529.

Zhao, W. (2011) Discussion on polarity effect on EDM, Advanced materials research, 154–155: 429–432.

Zhao, W.S., Meng, Q.G. and Wang, Z.L. (2002) The application of research on powder mixed EDM in rough machining, Journal of Materials Processing Technology, 129: 30–33.

WEB REFERENCES:

http://nptel.iitm.ac.in (downloaded on 8th April, 2012)

http://technoccult.net (downloaded on 31st October, 2012)

APPENDIX-A

TECHNICAL SPECIFICATION OF EDM MACHINE

The experiments has been conducted on Electrical Discharge Machine (Model: T-3822M), Victory Electromech, India. Technical data of machine is as under:

Electrical Data

Supply voltage	415 V, 3 Φ, 50 Hz
Connected load	3 KVA
Open gap voltage output	(135 ± 5) % V
Maximum machine current	12 A
Current range	3 ranges of 4 A each

SPECIFICATION OF DIELECTRIC MEDIUM

EDM oil

Appearance	Clear, light
Density (kg/m^3)	835
Flash point (^oC)	130
Viscosity	3.12
Specific gravity (cSt)	0.78 ± 0.02
Dielectric strength	45 kV

APPENDIX-B

SPECIFICATIONS OF MEASURING INSTRUMENTS

1. PROFILE PROJECTOR

Model and make	V-10A, Japan
Voltage requirement	220 V / 230 V / 240 V
Current requirement	0.6 A
Least count	0.001 mm

2. SURFACE ROUGHNESS TESTER

Model and make	Surftest, SJ-400, Mitutoyo
Measurement method	Stylus probe
Profile resolution	100 nm
Cut off length	0.8 mm
Tracing length	4.8 mm

3. DIGITAL GAUSS METER

Model and make	ESC18B, Eastwest Engineering Electronics Pvt. Ltd., India
Mesurement range	2000 Gauss on ×1 range
	20000 Gauss on ×10 range

4. OPTICAL EMISSION SPECTROMETER

Model and make	DV-6, Baird, USA
Base	Iron, Aluminium, Copper
Medium	Argon gas
Accuracy	0.0001 %

3. MICROHARDNESS TESTER

Model and make	MVH-2, Metatech, India
Software Used	Quantimet
Load applied	1 kg
Dwell time	20 s

4. SCANNING ELECTRON MICROSCOPE

Model and make	LEO 435 VP, SEMTech Solutions, USA
Magnification range	up to 240,000
Magnification range used	200×, 500×

5. X-RAY DIFFRACTION MACHINE

Model and make	D8 ADVANCE, Bruker Corporation, USA
Scan speed	5^{o}/minute
2θ range	5^{o} - 120^{o}